# SANDIA REPORT

SAND2015-2369
Unlimited Release
Printed March, 2015

# Intermediate-scale Fire Performance of Composite Panels under Varying Loads

Alexander L. Brown, Dann A. Jernigan, Amanda B. Dodd

Prepared by
Sandia National Laboratories
Albuquerque, New Mexico 87185 and Livermore, California 94550

Sandia National Laboratories is a multi-program laboratory managed and operated by Sandia Corporation, a wholly owned subsidiary of Lockheed Martin Corporation, for the U.S. Department of Energy's National Nuclear Security Administration under contract DE-AC04-94AL85000.



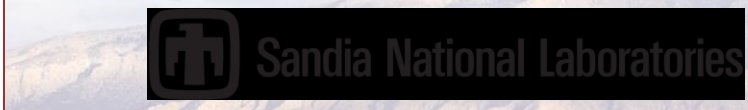

Issued by Sandia National Laboratories, operated for the United States Department of Energy by Sandia Corporation.



Available to DOE and DOE contractors from
U.S. Department of Energy
Office of Scientific and Technical Information
P.O. Box 62
Oak Ridge, TN 37831

Telephone: (865) 576-8401
Facsimile: (865) 576-5728
E-Mail: reports@adonis.osti.gov
Online ordering: http://www.osti.gov/bridge

Available to the public from
U.S. Department of Commerce
National Technical Information Service
5285 Port Royal Rd.
Springfield, VA 22161

Telephone: (800) 553-6847
Facsimile: (703) 605-6900
E-Mail: orders@ntis.fedworld.gov
Online order: http://www.ntis.gov/help/ordermethods.asp?loc=7-4-0#online

SAND2015-2369
Printed March, 2015

# Intermediate-scale Fire Performance of Composite Panels under Varying Loads

Alexander L. Brown, Dann Jernigan
Fire Science and Technology

Amanda B. Dodd
Thermal/Fluid Science & Engr

Sandia National Laboratories
P. O. Box 5800
Albuquerque, NM 87185

## Abstract

New aircraft are being designed with increasing quantities of composite materials used in their construction. Different from the more traditional metals, composites have a higher propensity to burn. This presents a challenge to transportation safety analyses, as the aircraft structure now represents an additional fuel source involved in the fire scenario. Most of the historical fire testing of composite materials is aimed at studying kinetics, flammability or yield strength under fire conditions. Most of this testing is small-scale. Heterogeneous reactions are often length-scale dependent, and this is thought to be particularly true for composites which exhibit significant microscopic dynamics that can affect macro-scale behavior. We have designed a series of tests to evaluate composite materials under various structural loading conditions with a consistent thermal condition. We have measured mass-loss, heat flux, and temperature throughout the experiments. Several types of panels have been tested, including simple composite panels, and sandwich panels. The main objective of the testing was to understand the importance of the structural loading on a composite to its behavior in response to fire-like conditions. During flaming combustion at early times, there are some features of the panel decomposition that are unique to the type of loading imposed on the panels. At load levels tested, fiber reaction rates at later times appear to be independent of the initial structural loading.

## Acknowledgements

The authors would like to acknowledge the contributions of the technologists who conducted the tests, including Jerry Koenig, Shane Adee, and Jessie Fowler. Shea Loges and Richard Simpson provided video editing services. The design and construction of the test structure was overseen by Pat Brady. Bennie Belone and Randy Foster helped with test rig assembly.

The authors would also like to recognize the contributions of Sean Kearney, Anay Luketa, Brian Lattimer, and Scott Case, who helped early in the discussion and design of these experiments.

ABDR and 18x24 thick panels were donated by the Air Force Advanced Composite Office, Hill AFB. Input and programmatic support from Capt. Ownby and Frank Bruce is appreciated. Hill's contributions to this testing were invaluable. The remaining materials were acquired from Composite Tooling Corporation, fabricated for this test series.

# Contents

# List of Figures

# List of Tables

This page intentionally left blank

# 1 Introduction

Composites are being used increasingly in the design and construction of aircraft. As Sandia has a need to assess the safety of various types of hazardous aircraft cargo for adverse environments, the transportation fire environment created by composite aircraft is important. Safety analyses in more recent years have increasingly involved modeling and simulation. It is less expensive for parametric assessments than experiments. New needs for safety assessments occasioned by increasing use of composites include models to characterize the fire environment, and an understanding of the effect of composites on the thermal and mechanical environment. Modeling capabilities for composite fires exist, but at present are immature, not having been proven accurate for fire applications.

There is a significant lack of data on the performance of composite materials in fire. We expect to have a need to test the response of aircraft cargo under a fire test condition for a safety assessment in the coming years. Several projects have already been reported that help describe the behavior of composite materials in a fire-like environment (Brown et al., 2011; Hubbard et al., 2011). Significant findings from these tests suggest the behavior of composite decomposition under 20-30 $kW/m^2$ radiant heat flux (Hubbard et al., 2011). Spontaneous flaming was not assured at any of the conditions tested without a pilot. Also, the 25-40 kg bulk burn tests suggest that peak heat fluxes from the burning composite are not higher than those achieved from wood or hydrocarbon fuel burns (Brown et al., 2011). The duration of the burns is found to be very long, lasting 5-8 hours under controlled conditions. This test series also found that the decomposition of bulk materials is not dissimilar from that found from thermo-gravimetric analysis (TGA) in that the pyrolysis occurs chronologically first, followed by a long-term glowing oxidation phase.

In addition to these ongoing efforts, there are some instances of relevant data in the literature. Keller and Bai (2010) reviewed this very topic, which cites many of the articles indicated herein. Notably missing from the Keller and Bai review was highly relevant work to our interests by Elmughrabi et al. (2008), who converted a cone calorimeter to accept a loaded test article of vinyl ester and polyester glass laminates. Test articles were stressed in compression and tension and heated at several thermal flux levels. They found a small effect of the stress on the decomposition heat release rate, smoke generation, and time to ignition. Tension tends to enhance decomposition rate, while compression has the opposite effect (i.e. reduces the decomposition rate). Their test design prohibited simultaneous mass loss measurements, although they were able to evaluate heat release rates in the calorimeter apparatus. Another review by Mouritz et al. (2009), while focused on modeling, includes many relevant experimental citations and information pertinent to this work.

There is a moderate amount of work on the behavior composites in a fire-like environment. Less is found for materials that are pre-stressed. Included in this sub-category is Feih et al. (2008, 2008a) Bai and Keller (2009), Boyd et al. (2007, 2007a), Burns et al. (2010) Kwon et al. (2006) La Delfa et al. (2009), Liu and Holmes (2007), and Liu et al. (2011). Liu et al. (2011) examined compressively stressed composites under a thermal environment (60-260°C) with experimental testing. Bai and Keller (2009a), Cao et al. (2009) and Feih et al., (2007) looked at tensile strength under similar conditions. Gibson et al (2004) looked at both tension, compression, and unloaded samples. Sorathia et al (1993) did thermal post-test stress analysis. Of all the above, Cao et al. (2009), Burns et al. (2010), Kwon et al. (2006), La Delfa et al (2009), Liu et al. (2011) and Sorathia (1993) evaluated composites with carbon fibers of varying types. Kawai et al., (2001, 2009) also examined carbon fiber epoxy materials, but they were unidirectional layers not rotated in the matrix, but rotated on the structural rig. This lay-up is not as is normally the practice in aviation composites. High temperature in these studies is considered 100°C. Kandare et al. (2010) tested custom glass based samples and afterwards measured structural integrity. A significant finding from the work is that char formation enhances strength after fire damage. Indeed, much of the material science literature (not all cited here) is focused on finding additives to enhance charring of the binder to reduce volatile emissions and retain strength. Feih et al. (2008), La Delfa et al. (2009), Liu et al. (2011), and Lua (2011) looked at sandwich materials.

In the above work, the experiments did not focus on long duration material behavior while exposed to fire-like heat fluxes except in our recent tests (Brown et al., 2011). Testing was often performed at fluxes as high as 75 $kW/m^2$, which should be high enough to induce oxidative reactions. Generally, the tests were concluded once structural strength was lost in the materials.

Carbon fiber epoxy composites are very expensive. Aircraft contain large quantities of composite materials. In bulk, the decomposition behavior is not expected to be governed by the same physical mechanisms as with small samples. We are fortunate to have a supply of size appropriate materials supplied from Hill AFB. Based on previously discussed work, we anticipate finding the bulk decomposition behavior to be influenced by the types of stresses imposed on the panel. This work hopes to quantify this effect on larger panels. We also hope to simultaneously measure time-dependent mass loss for the panels to characterize the behavior of large panels in fire conditions. Fiber and char oxidative reactions were demonstrated in an extreme fire environment (Brown et al. 2011), but have not been widely examined in other testing. The conditions under which this type of reaction is initiated and sustained is not well described, and will be explored in this test series.

This effort is motivated by the need to design a representative fire test for an aircraft safety analysis. We do not anticipate being able to requisition an aircraft for the test, so the hope is to be able to design an appropriate surrogate. Never having done this for an aircraft with composite materials, there are design issues that need to be explored to make appropriate surrogate assumptions. In the literature review above, very few fire tests have been performed on large-scale panels. Fire and structural performance is often performed on very small (a few centimeters) samples. This is in part because traditional structural testing facilities are typically designed to accommodate small samples. It may also be due to the cost of larger-scale materials and the lack of test apparatus to perform this type of testing. We have observed that the decomposition behavior of the composite is closely related to the proximity to the edge of the composite. It therefore may be important to test materials in the appropriate scale range to be able to correctly replicate the large-scale environment. The findings of Elmughrabi et al. (2008) are also a motivating factor. They found structural loading to be related to decomposition rate during the pyrolysis phase. To our knowledge nobody has tested the decomposition rate under loading for full-scale panels as are found on the skins of aircraft. Further, the propensity for glowing combustion exists in an unmitigated fire scenario. The Elmughrabi et al. (2008) dataset does not address fiber decomposition behavior (they were using glass fibers), the rate of which might potentially be augmented if structural forces cause dramatic changes in the surface area available for oxidative reactions.

There is also a lack of data for sandwich composites, as described above in the literature review. At the inception of the project, we had little data on the extent of the use of this type of material in aircraft. Believing such materials to be commonplace, we seek to better understand their behavior in fire environment conditions.

## *1.1 Objectives*

This test series is evaluating intermediate-scale composite panels under fire conditions. The main objectives of this work are as follows:

1. To *resolve the mass loss* from panels during decomposition with structural loading at a larger scale. This work is distinguished from previous work found in the literature because the materials will be closer in size to materials as they are believed to be found on aircraft. In addition, we intend to test well beyond the point in time when typical structural thermal tests are concluded to assess surface oxidation reactions.
2. To *impose higher heat fluxes* on the test panels than in the previous radiant heat tests, which provided peak fluxes of 20-30 $kW/m^2$. To do this, a more intimate heat source will be used. The intent of the tests

in this regard will be to explore the behavior of composite panels under conditions that transition from pyrolysis reactions to surface oxidative burning.

3. To evaluate the behavior of the materials under structural loading. Specifically, these tests aim to induce multiple modes of loading to test a range of potential responses that could be created based on the varying compression, tension, and torsion loading on an aircraft panel.

# 2 Methods

A hardware test apparatus was constructed for measuring mass loss while imposing structural loading. Several types of panels were obtained for testing. A custom oven was constructed to impose a repeatable thermal flux. The oven was characterized using a numerical model, and experimentally. A test matrix was devised that was expected to provide good comparative data for the various panels. These aspects of the test are all described below.

## *2.1 Test Apparatus*

The test apparatus as designed is illustrated in Figure 1. A beam balance is placed on a stand structure (green). The composite holder frame (gray) is hung from one end. A counter-balance (illustrated by the gray cylinders) on the opposite end is used to zero the weight measurement, which is taken by a load cell at that same end of the frame. The load cell had a range of +/- 2.27 kg, and is positioned far enough away from the test to remain cool and to provide a consistent reading throughout the test. It is a Omegadyne Inc. model LC601-5 sensor, and was factory pre-calibrated. It was generally capable of reading mass changes of approximately 4 grams. The location of the load cell is obscured in the view of Figure 1. The test apparatus is illustrated with an oven box heater that is described in detail in a later section.

The load and load cell were designed to be equal distance from the pivot point in opposite directions. Consequently, the data reading on the load cell can be taken as the direct mass reading for the panel in the holder.

In pre-test analysis, a metal (inert) panel was heated and weighed with an applied heat flux of approximately the same magnitude and duration of the actual tests. Mass change was seen to be small, gradual, and on the order of tens of grams 'lost' weight (~50 g maximum; compare this to the panel masses quantified in Table 1). This is believed to be the effect of buoyancy and viscous sheer on the mass reading, ultimately a small bias on the overall test. This bias is expected to be similar during composite tests as it was with the metal panel.

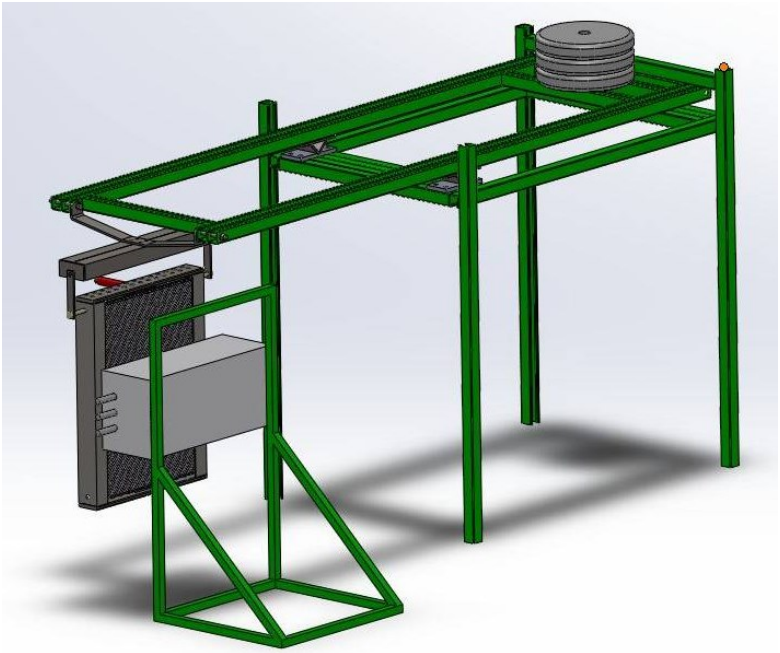

**Figure 1. An illustration of the test apparatus for measuring mass loss.**

Figure 2 shows two photographs of the final assembly. The assembly was elevated using cinder blocks to provide clearance above the ground level for several of the tension tests. Upon release of the spring energy (in tension only), the rods would impact the ground and influence the mass reading. For these tests only, the cinder blocks were used to assure good mass loss data through the full series of tests. The final assembly was located in the FLAME facility at Sandia National Lab's Thermal Test Complex, about 5 meters from the center of the cylindrical enclosure. During the test, the facility fans were on at a very low level (~75,000 cfm), producing some ambient flows below 1 m/s. The effluent was routed through the facility electrostatic precipitator.

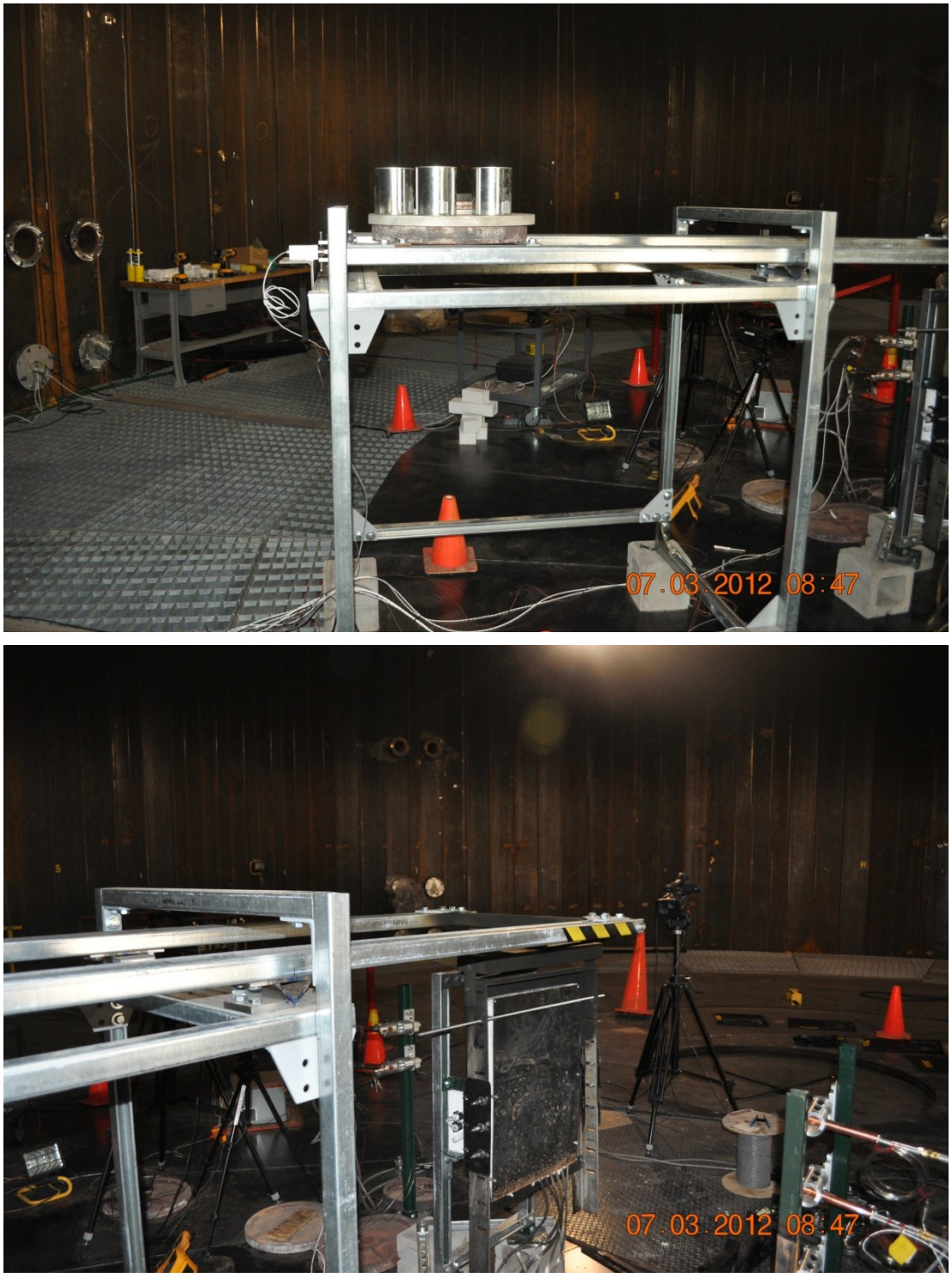


**Figure 2. Photographs of the final test assembly.**

## *2.2 Composite Holders*

Three structural apparatus configurations were designed, and are illustrated below for one of the composite panel configurations that was 45.7 cm by 61.0

cm by 0.8 cm thick. In each case, retaining bolts were used to compress springs, which provided a measured load and a linear decrease in the load over several centimeters. Oblique views for all three of the designs are shown in Figure 3, with a free-body diagram illustrating imposed forces for the torsion case.

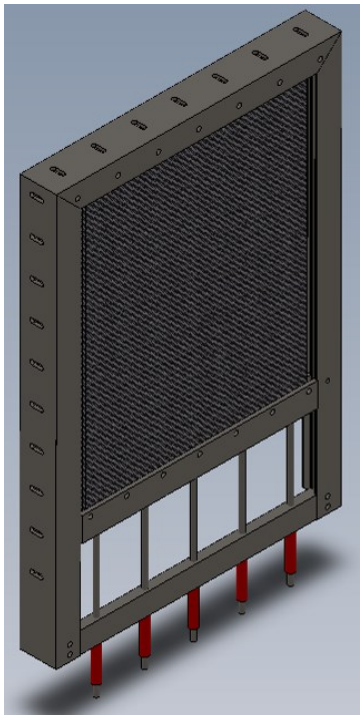

Tension Configuration

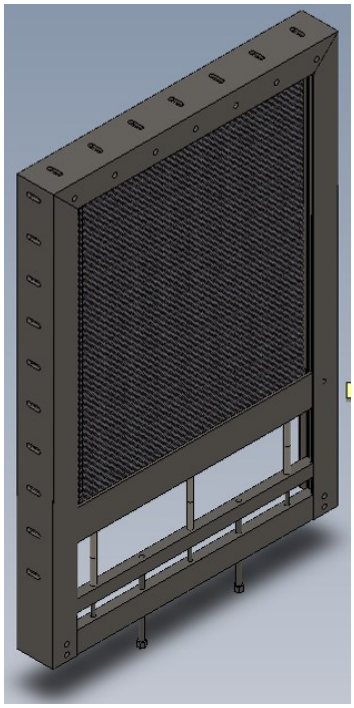

Compression Configuration

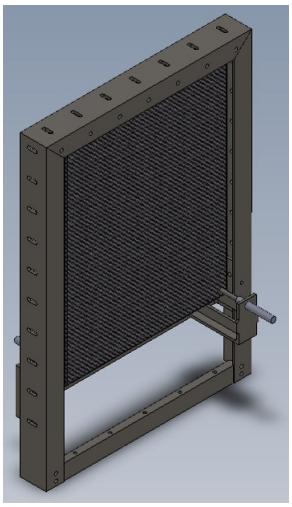

Torsion Configuration

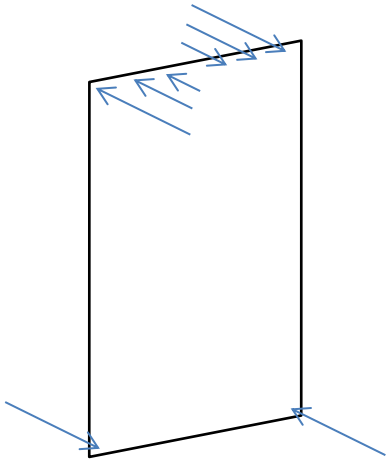

**Figure 3. The structural test rigs.**

The first configuration used in testing was designed to put the panel in compression as it was subjected to the fire-like conditions. Drawings of this configuration are illustrated in Figure 4.

The second configuration used in testing was in tension, configured with the panel being compressed between two plates on the top and bottom to secure the panels in the frame. The test rig and set-up is illustrated in Figure 5. For these tests, holes were drilled in the panels, and the panels were bolted to the upper and lower structural members.

The third configuration used was the bending configuration, which was designed to impose a torsional loading on the panels. It is illustrated in Figure 6.

A fourth configuration existed, which was a panel in the support with no force imposed. This condition served as a control, providing data for the decomposition of a panel under no external loading other than what naturally exists in the support of its own weight.

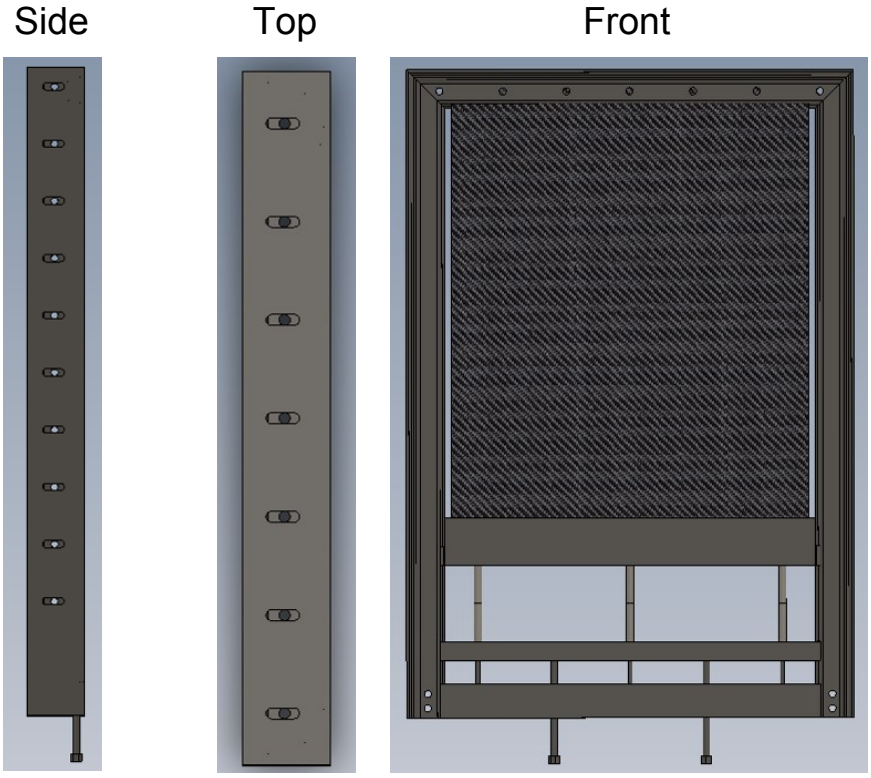


**Figure 4. Three views of the compression structural test rig.**

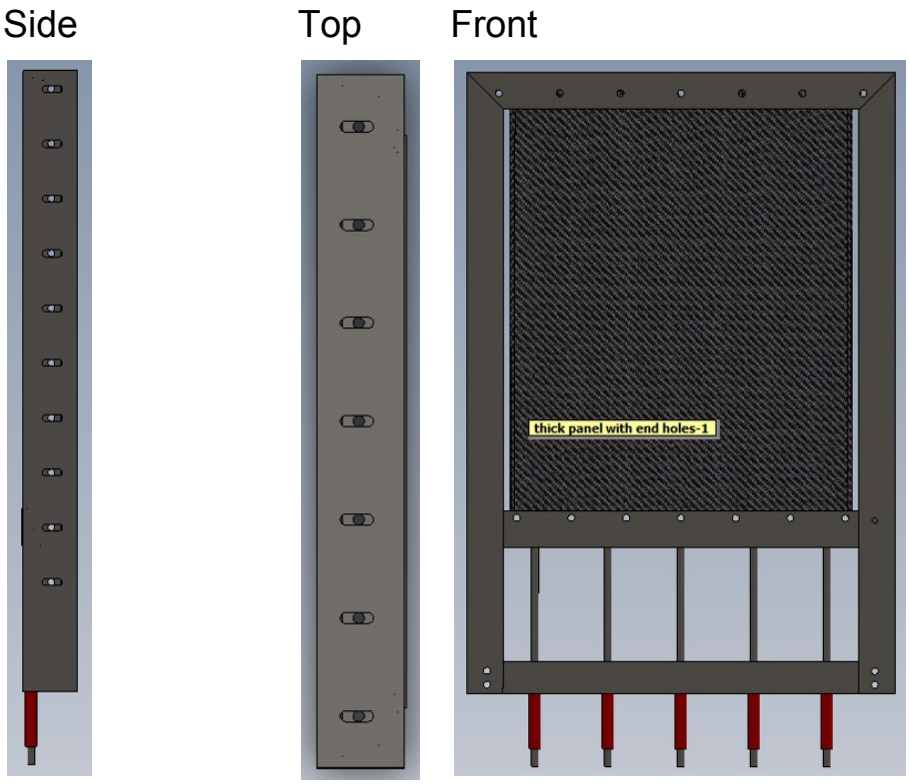


**Figure 5. Three views of the tension structural test rig.**

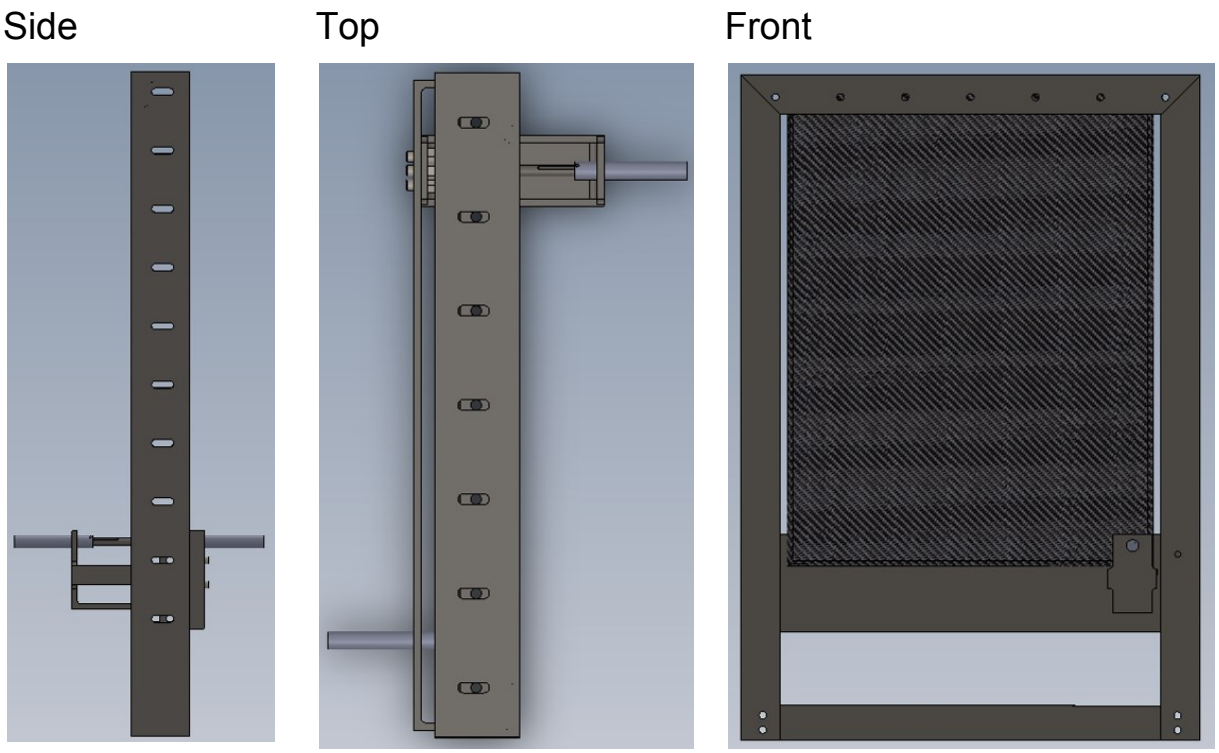


**Figure 6. Three views of the torsional structural test rig.**

Springs were acquired with linear spring constants. Typically, 222 N (50 lbs) springs were used, which when compressed a full 2.54 cm (1 inch) imparted the full force. In compression, four springs were normally used on two bolts, so the full force of 889 N (200 lbs) was imposed over that distance. In compression tests, the springs were slightly relaxed (about 10%) from full compressive force to allow for a small amount of thermal expansion in the early test. In tension, four springs on four rods were used, meaning the full force was imposed over half the distance (889 N, or 200 lbs over 2.54 cm or 1 inch). In torsion, only one spring was used, so the total force was ¼ that of the other tests. Panels were rigidly fixed at the top, and forces imposed from the bottom.

The force applied to the panels is relatively small. For comparison, the work of Elmughrabi et al. (2008) typically tested panel stress levels of 10-100 MPa, whereas the peak stress initially imposed on the panels in this test series is less than 1 MPa. The stress is difficult to quantify for the sandwich panel, as the physical cross-section is not easily extracted through the honeycomb sandwich material. These force levels were selected to be representative of normal operation stresses, not performance level. Thus, the stresses are believed to be more in line with structural loading of an aircraft composite as it rests on the runway, and not near peak design threshold levels as might be obtained during flight.

## *2.3 Materials*

Three principal materials are the subject of this testing. The **first** material is a sandwich board composed of unidirectional layers of Cytec 5208/T-300-12 with a +45, -45, 0, 90, 90, 0, -45 +45 lay-up (about 1.5 mm thick), a HRP-3/16 core (NOMEX, about 25 mm thick), and an 8-layer fabric Kevlar epoxy fabricated in a 0/90 x 4 lay-up (about 1 mm thick). The layers are adhered with HYSOL EA 9628 adhesive. The sandwich boards are termed Advanced Battle Damage Repair panels (henceforth abbreviated as ABDR panels or ABDR sandwich panels), and they are nominally 30.5 cm by 45.7 cm (12" x 18") in dimension. They were acquired from the US Air Force, and are understood to be used to train students on the repair of composite airframes. These weigh about 0.45 kg (1 lb) each. Figure 7 and Figure 8 show photographs of an example part. These materials were contributed to the study by the Hill AFB Advanced Composite office. The **second** material was obtained from Composite Tooling Corporation, and consisted of 16 layers of a unidirectional IM7G/8551-7A Hercules carbon fiber prepared with varying rotations. The exact lay-up is (0/90/-45/+45/-45/+45/90/0/0/90/+45/-45/+45/-45/90/0), with two of these being placed together to get the thickness to where they were tested. These are 3.2 mm thick, and 48.7 cm x 61.0 cm in dimension (1/8" thick, and 19 3/16" x 24"). These panels are henceforth called 19x24 thin panels. They weigh approximately 1.4 kg (3 lbs). These were cut from a single 1.22 x 2.44 m (4 x 8 foot) panel, and there

were nine ostensibly identical panels. The last panel from the larger original piece was further cut for testing in another test series. The **third** material is a 45.7 cm by 61.0 cm (18" x 24") panel, approximately 8 mm thick. The precise lay-up of these panels was not available, but they consisted of rotated layers of carbon fiber fabric, much like the other two panels in this test series. These will be henceforth described as the 18x24 thick panels. These weigh approximately 4.1 kg (9 lbs), and are believed to be Cytec 5208/T-300-12 carbon fiber epoxy woven fabric (based on verbal indication from Hill AFB, the point of manufacture). A photograph of one of these is found in Figure 9. These panels had rounded edges with a radius on the order of 1 cm, suggestive that they were pressed in a mold when they were manufactured. There were 27 inventoried 18x24 panels and 46 ABDR panels. However an earlier test series consumed 3-4 of each.

There is some variation among the materials in their quality. Specifically, the edges of the 18x24 panels and their surfaces show light signs of wear or age with fraying and abrasion marks. ABDR panels were made from two different types of honeycomb sandwich materials, a hex core being the most common, with a rectangular core also being found in some instances. We did not record any instances of using the rectangular core material for this series, although these were found in a previous series. The ABDR panels may also have some signs of wear. The adhesive was manually applied, and therefore not uniform in distribution or total weight. The higher quality (more uniform) pieces were generally selected for this test series.


**Figure 7. A photograph of an ABDR panel, the Kevlar (back) side.**

**Figure 8. A photograph of an ABDR panel, the carbon fiber (front) side.**

**Figure 9. A photograph of an 18x24 panel.**

Each panel was weighed before and after testing. A Mettler 1D1 lab scale with 0.0091 kg (0.02 lbs) resolution was used to weigh pre- and post-test samples. Table 1 shows a summary of the panel mass for the panels tested in this series.

**Table 1. A summary of panel mass.**

| Panel | Average Mass *[kg]* | Standard Deviation *[kg]* |
|---|---|---|
| ABDR sandwich | 0.753 | .0325 |
| 18x24 thick | 4.070 | .00377 |
| 19x24 thin | 1.354 | .00835 |

The ABDR sandwich panels have the largest standard deviation in mass and are also the lightest panels. The large variability in mass is most likely due to manual application of the adhesive and a lack of control on the amount of adhesive used when fabricating these parts.

## *2.4 Heat Source*

### 2.4.1 Oven Design

The heat source for this test series was a critical aspect of the tests. The intent was to generate a severe environment representative of a moderate to long-term fire. Under previous radiative testing (e.g. Hubbard et al., 2011), spontaneous ignition of the panels was not particularly reproducible, and this feature inhibits good post-test characterization of the material behavior. Also, carbon fiber composites require a significant sustained incident flux to assure transition from flaming to glowing combustion. A sustained flux of at least 50 $kW/m^2$ is desirable to assure transition to glowing combustion, as per data from Brown et al. (2011).

An oven was constructed to impose a repeatable thermal environment on the panels. The original intent was to use a flame or torch, but preliminary testing with such a heat source was unsuccessful in creating a desirable environment. More information regarding some of the preliminary testing is found in the appendix. The oven box was constructed from Pyrotherm I-14 insulation board from Pyrotek™. Manufacturer specifications suggest a density of 288 $kg/m^3$, heat capacity of 1.09 kJ/kg-K, and conductivity at 204 ºC of 0.088 W/m-K, with the conductivity varying from 0.078 to 0.105 W/m-K for the range of 93-427 ºC.

Three silicon carbide rod heating elements were electrically powered to provide the heat source. These are Starbar® brand 10 inch rods. Their diameter is 19 mm, and advertised heated length was 254 mm. Due to manufacturing variability, the peak heated length could be as much as 20% lower than the total advertised heated length. According to the manufacturer specifications, the heated zone has a resistance of 0.00341 ohms/mm, while the remaining rod is about two orders of magnitude below that. Rods were wired in serial, and electrically powered from a 480 volt AC wall outlet through a Silicon Controlled Rectifier (SCR) where current was controlled by

a 4-20 mA control box. Separate instrumentation was used to record the current and voltage. The average power thus calculated for the tests was 6,700 Watts, with a standard deviation of 366 W. Even though the nominal setting for each test was identical, the test to test variation in the configuration resulted in different power delivery to the heater rods.

A drawing of the oven box assembly is found in Figure 10. It was constructed by screwing together various cuts of the insulation board with standard iron based board screws.

To understand the repeatability of each test, two thermocouples were placed at fixed locations within each oven as illustrated in Figure 10. These monitored the temperature of the oven, and provided the control room with a good indicator of repeatability and of abnormalities in tests. Both ovens and rods had a finite lifetime. A total of 8 oven boxes were constructed, and seven rods were used (three at a time). Test 38 is omitted because a rod exploded early in the test, rendering the data and panel less useful. The thermal environment was controlled by the electrical supply settings, which were actively measured and shown to be consistent from test to test to within two decimal places.

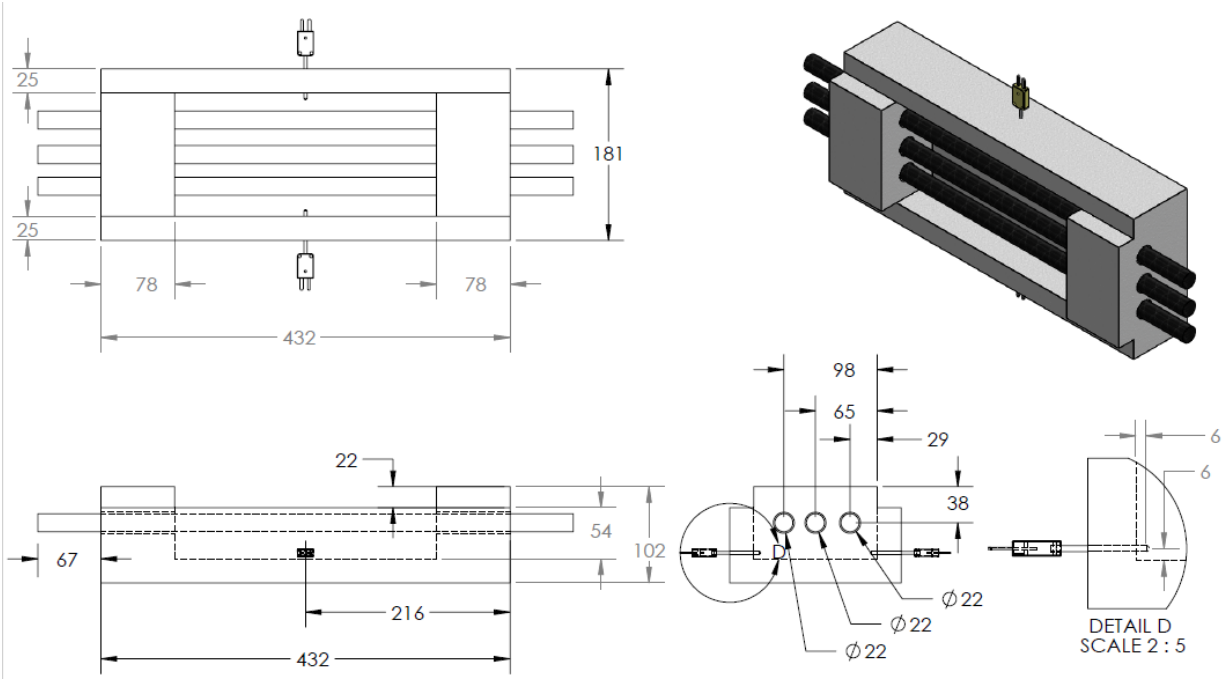


**Figure 10. Engineering drawings of the insulated box (units in mm).**

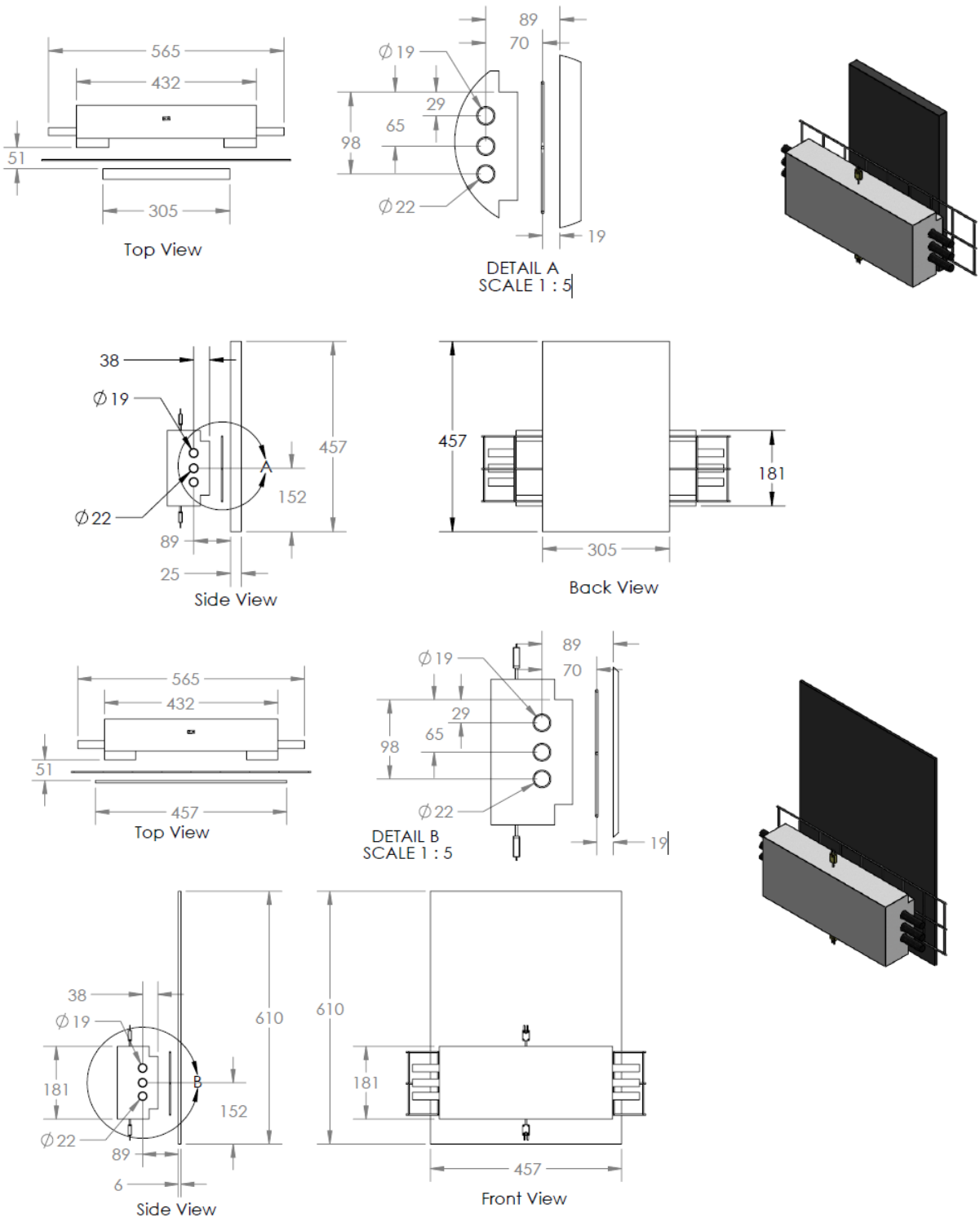


**Figure 11. Engineering drawings of the assembly for the ABDR (top) and 18x24 thick (bottom) panel tests (units in mm).**

Figure 11 shows an engineering drawing of the assembly including the rods, metal cage, and two of the panels. The cage was mounted to the structural

assembly and located at a fixed position between the oven and composite panel as illustrated in Figure 11. The oven and the cage were not ever in contact, although we have reason to believe that some of the panels did periodically come in contact with the cage depending on the way they deformed during the thermal decomposition while exposed to the hot oven. The oven center was vertically located 152 mm from the bottom of the panels, which is 1/4 the distance from the bottom for the two large panels and 1/3 the distance from the bottom for the ABDR panels.

The metal cage was mounted on the composite mounting frame to prevent distortions in the panel during decomposition from reaching the oven and affecting the mass loss measurements. The cage was made of 1.59 mm thick stainless steel wires which were arranged in a square pattern with 76.2 mm between the wires. Three horizontal wires spaced vertically were used, and the cage was centered with the oven. The cage was spring mounted to be in tension to prevent a similar problem due to thermal distortions in the cage during tests. Because of the presence of the cage, the thermal conditions are moderately complicated. An attempt has been made to describe the thermal conditions at the panel surface both in terms of a computational model for radiating bodies, and in terms of a surface total flux characterization using a thin plate radiometer.

Reflectivity of the oven insulation material was measured with the reflectometer (described later in this chapter). This helps characterize the spectral emissivity, suggesting low emissivity at visible and near IR ranges, but a very high emissivity in the deep IR. These data are found in Figure 12. Error bars are mostly quite small, and are a single standard deviation in magnitude from three measurements.

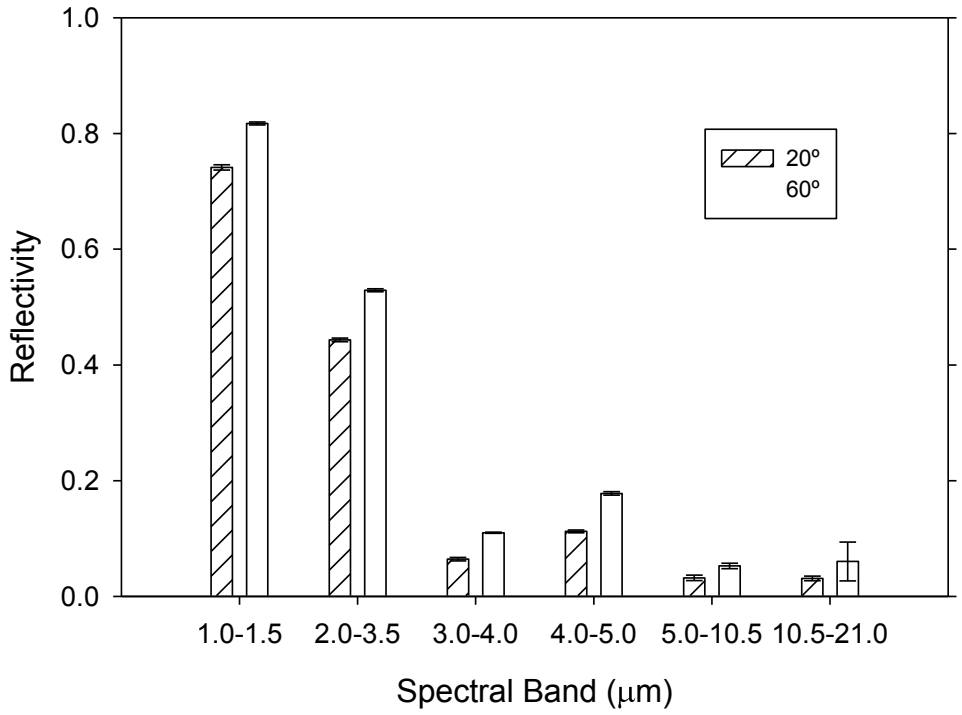


**Figure 12. Measured reflectivity of the oven insulation.**

### 2.4.2 Environment Estimates

To design an appropriate oven box, a radiation prediction was made for transport of radiative energy from the oven to the panel. This was necessary to select the number of rods for the test, as well as to determine the flux available given the distance from the object. Radiation is expected to be the dominant mode of heat transfer, and make the most significant contribution to the total heat flux to the panel. A model was constructed for the heating elements that allowed for general prediction of the heat flux from the rods to a surface. The model used classically determined relationships for view factors, as found in Appendix C of Siegel and Howell (1992). The rod calculation was performed based on assembly of flux relations primarily using the relation found in Figure 13, reproduced from the reference material.

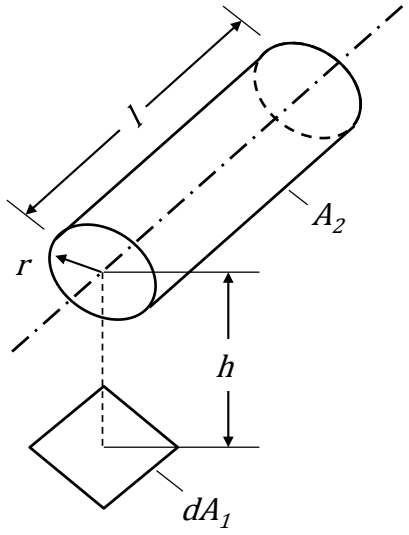


**Figure 13. View factor equation for calculating heat flux from a rod to a surface at a fixed distance from the rod.**

The equation for this view factor is:

$$F_{d1-2} = \frac{1}{\pi H} tan^{-1} \frac{L}{\sqrt{H^2 - 1}} + \frac{L}{\pi} \left[ \frac{X - 2H}{H\sqrt{XY}} tan^{-1} \sqrt{\frac{X(H-1)}{Y(H+1)}} - \frac{1}{H} tan^{-1} \sqrt{\frac{(H-1)}{(H+1)}} \right]$$

where

$$L = \frac{l}{r} \qquad H = \frac{h}{r}$$

$$X = (1 + H)^2 + L^2$$

$$Y = (1 - H)^2 + L^2$$

Relations were found for flux from three 1400°C rods to a surface at a distance from the rods. After gaining operational experience through check-out testing and examinations with the IR camera, the oven thermocouple temperatures were believed to be representative of the oven insulation temperature. The low-emissivity oven is thought to behave like a cavity, reflecting much of the incident radiation from the rods and re-radiating to appear close to a black-body at the thermocouple temperature. Emissivity was assumed to be 0.9 for the rods and for the oven. The oven was modeled using the Siegel and Howell (1992) Appendix C relations found reproduced in Figure 14.

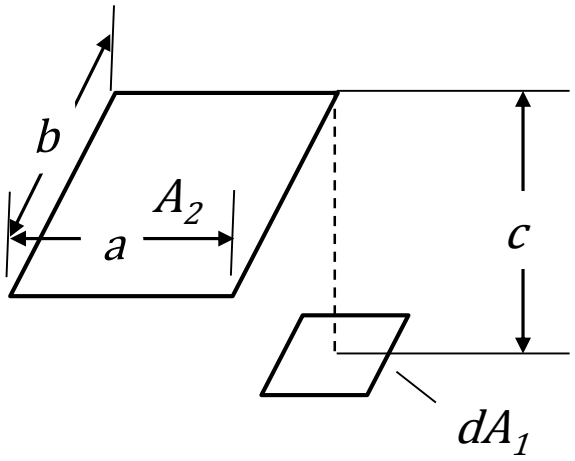


**Figure 14. View factor equations for calculating heat flux from rectangles to surfaces a fixed distance away.**

The view factor for this arrangement is:

$$F_{d1-2} = \frac{1}{\pi Y}\left(\sqrt{1+Y^2}\, tan^{-1}\frac{X}{\sqrt{1+Y^2}} - tan^{-1}X + \frac{XY}{\sqrt{1+X^2}} tan^{-1}\frac{Y}{\sqrt{1+X^2}}\right)$$

where:

$$X = \frac{a}{c} \qquad Y = \frac{b}{c}$$

Geometric math is used to construct the view factors for calculating incident flux to a panel a given distance away. The model was then sampled at many locations over an area, and the plot found in Figure 15 was obtained. The key quantitative finding in this endeavor is that the peak fluxes to the panel will be above 50 kW/m$^2$, which should be sufficient to assure char and fiber oxidation reactions occur once flaming subsides. Having made assumptions about emissivities and temperatures, the quantitative values are not thought to be particularly accurate. However, the qualitative relationships are thought to be reasonably representative. Thus, the model predictions are taken as good indicators of the peak flux location, and the relative drop-off in flux moving away from the peak region.

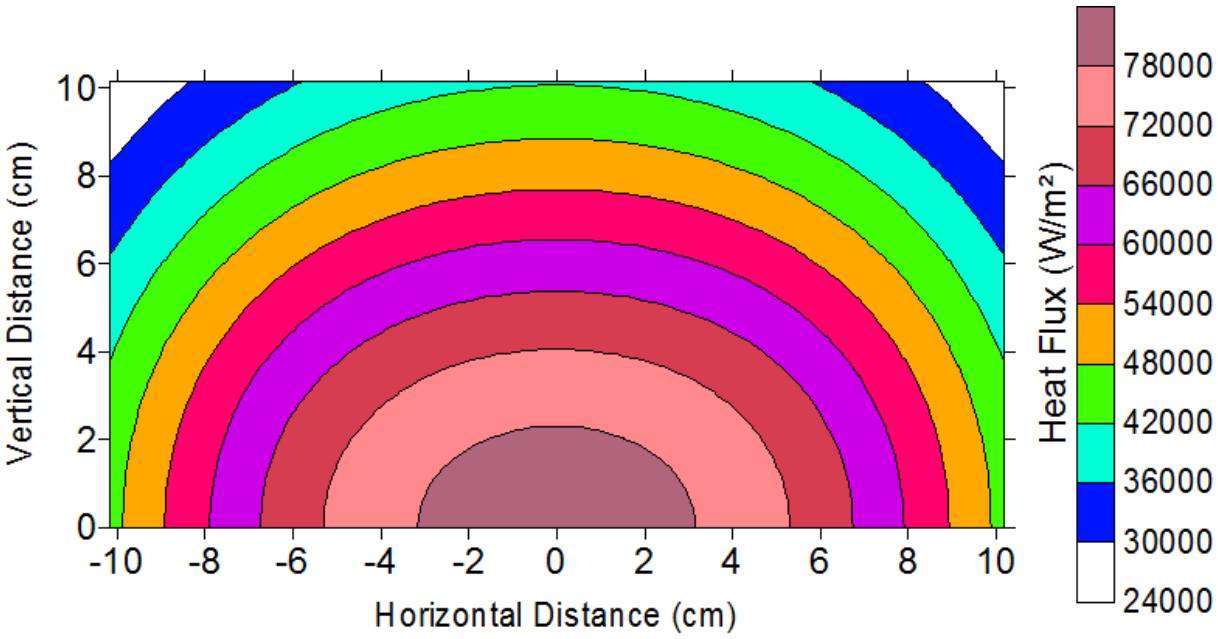


**Figure 15. Predicted radiative heat flux to the objective surface. Axis scales are distance in inches, contours are radiative flux in W/m².**

This model ignores the flux contributions of hot objects other than the core oven around the panel. It also ignores the full width of the oven, only modeling ~20 cm (8 inches) width. It is not expected to be fully accurate, and should give a low-end estimate of the actual flux. It is presented because it gives an estimate of the flux for a complex system that was helpful to the design team to understand the test conditions. The important finding from this was that the imposed radiative flux would be at least 50 kW/m², helping to assure fiber and char combustion once flaming had subsided.

### 2.4.3 Differential Flux Measurements

To further characterize the oven, an instrumented plate was constructed to extract total heat flux to points on the surface of a metal plate. The plate face was designed to be the same size as the 18x24 thick composite materials. It consisted of a 3.2 mm (1/8 inch) thick steel plate with thermocouples press-mounted in a square grid (3.81 cm or 1.5 inch spacing) in one quadrant of the plate. The lay-out is shown in Figure 16 in a view from the back side (hence the negative/positive horizontal axis shift compared to the front side data in other figures). The quadrant of thermocouples allows for symmetry to be assumed when interpreting the full-field of data. The front side of the plate was painted with Pyromark™ paint to help assure a consistent thermal radiative boundary condition of high emissivity. A layer of insulation is placed over the thermocouples, and a backing plate was mounted to create a sandwich instrument. The design of

this plate follows typical construction of differential flame thermometers (DFTs), which are frequently used for probing total heat flux in open flames. The design principle is that the total heat flux can be deduced from an inverse calculation given the thermocouple reading results with an understanding of the heat transfer behavior of the instrument.

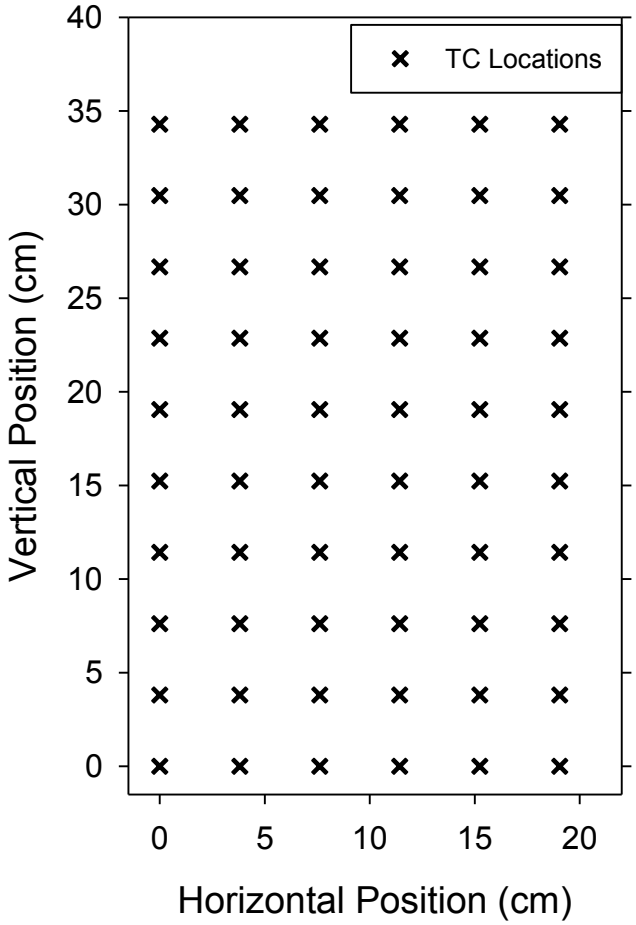


**Figure 16. Positioning of the thermocouples on the panel used to characterize the oven environment.**

Because the plate was used extensively in pre-test characterization of the heat source and it took several iterations to select the source, the plate was well used by the time characterization was performed with the oven box. The paint was removed in areas, and the plate had warped significantly in areas, as suggested by the photograph in Figure 17.


**Figure 17. A photograph of the plate showing the significant distortions and wear of the panel.**

A consequence of the wear on the plate is that the data are not considered particularly accurate after interpretation. It would have been much better to take these data on a new plate. Even with a new plate, some distortion and variability exists using this method to probe the environment created by the oven.

After examining data, the best method for evaluating the plate temperatures was determined not to be an inverse method, rather an energy conservation analysis performed at each time at which data existed. The thermocouple data are interpreted based on a model that assumes conservation of energy. Conservation is solved in terms of the energy flux. The total heat flux is solved for, which is the incident radiation flux plus convective flux. In this case, radiation is expected to be dominant. It is determined from the thermocouple measurements by assuming that all loss or accumulation mechanisms including sensible energy changes, conductive losses, and radiative emission are equal to the total heat flux, as per the following equation:

$$q_{total} = q_{conduct} + q_{sensible} + q_{emit}$$

A 1-d conduction model was evaluated, and it was shown that conduction through the plate was fast compared to other processes. Generally only a

few degrees difference exists between the temperature at either face. The radiation emission term then is simply calculated based on the thermocouple temperature:

$$q_{emit} = \epsilon\sigma T^4$$

Here, $\varepsilon$ is the emissivity, assumed to be 0.9, and $\sigma$ is the Stefan-Boltzmann constant (5.67E-8 W/m$^2$K$^4$).

Taking advantage again of the fact that the temperature is fairly constant across the thickness of the panel, the specific energy flux of the panel can be well approximated by the temperature at the point of the thermocouple:

$$q_{sensible} = \rho C_P \tau \frac{dT}{dt} \cong \rho C_P \tau \frac{T_2 - T_1}{t_2 - t_1}$$

Here, $C_P$ is the specific heat, $\tau$ the thickness, and $\rho$ the density of the panel. The change in temperature with time is extracted at the reporting interval of the test data, over one second. Density was assumed constant at 7854 kg/m$^3$, and the specific heat constant at 685 J/kg-K. These were taken from tables found in heat transfer textbooks, with the specific heat taken at an intermediate average temperature (~800 K) in the hot region. Thermal conductivity is required for the conduction term (k), and is taken at the same temperature to be 40 W/m-K (Incropera and Dewitt, 1990). A finite difference assumption is made for the conduction. Each thermocouple had a neighbor, which was considered a finite difference point. A discretization approximation is made according to Figure 18, such that conductive flux may be calculated:

$$q_{cond} = k\frac{dT}{dx} \cong k\left[\frac{T - T_{up}}{\Delta x} + \frac{T - T_{down}}{\Delta x} + \frac{T - T_{right}}{\Delta x} + \frac{T - T_{left}}{\Delta x}\right]$$

In this equation, $k$ is the thermal conductivity of the metal. This set of equations was shown to give a respectable representation of the total flux in pre-test characterizations as the predicted total flux remained moderately constant as the plate thermocouples were changing significantly. This suggests that the oven was providing a fairly constant heat flux, but the various heat transfer mechanisms balanced such that the consistent nature of the source was reasonably well reproduced. More on this point is found in the appendix.

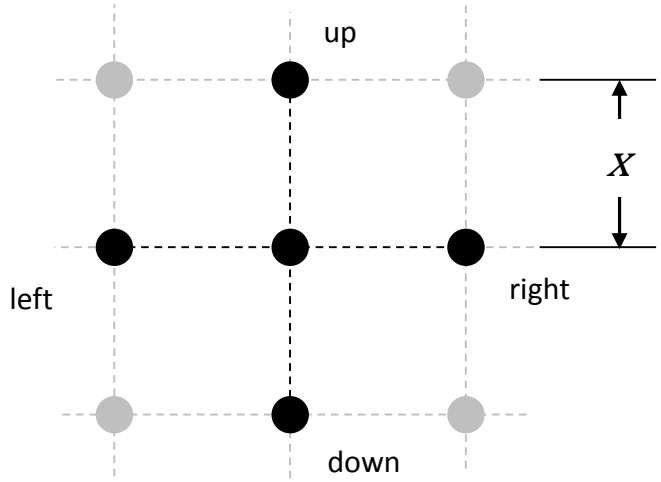


**Figure 18. An illustration of the finite difference convention for the conduction portion of the total heat flux calculation.**

Figure 19 shows measured total flux from the assessment of the panel thermocouple readings. The zero horizontal point is the panel symmetry plane. The total flux was averaged over the main duration of the test. More details are found in the appendix. A surprising feature to this plot is that the peak flux is not located along the centerline. It is rather found about 7 cm in. This is believed to be an artifact of two previously identified issues, namely that the panel was bowed in at the centerline, and that the surface coating had worn off towards the center of the panel. Peak fluxes are also surprisingly high, which may be compensatory for the incorrect emissivity employed in the model to reduce the data. These data might be interpreted to mean that the center of the oven was colder than the edges, however the IR cameras frequently imaged the heated portion of the rods as well as the conduction through the panel, and the IR data do not support this interpretation.

These data are also significantly higher in magnitude than those plotted in Figure 15. Those predictions did not take into account the full extent of the oven or convection. It is therefore not surprising that modeled values are lower than measured values. The magnitude of the difference, however, is somewhat surprising. We consequently expect that the shape of the actual thermal environment contours look more like what is plotted in Figure 15, but the general magnitude to be closer to that found in Figure 19. Vertical scale is also inconsistent between the two figures. The oven was shifted up from the original zero point to resolve data below the horizontal plane of symmetry for the oven.

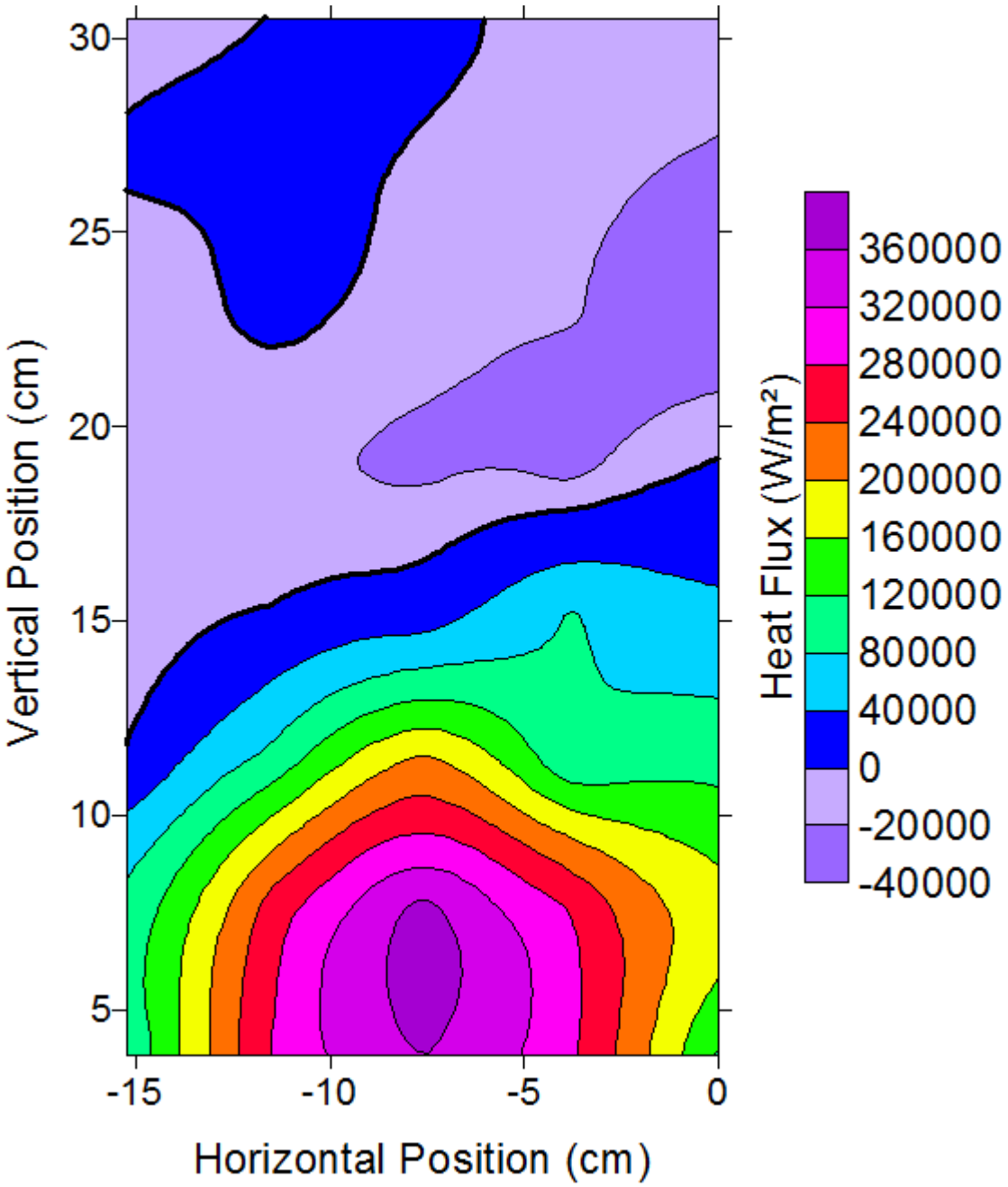


**Figure 19. Quantitative results from analysis of the plate thermocouple data.**

In Figure 19, please note the abrupt change in scaling in the legend at 0 $W/m^2$ (not reflected consistently in the color spacing of the legend) The negative values are indicative of a region where convection and radiation of energy away from the panel are greater than convection to and radiation to the panel.

## *2.5Additional Instrumentation*

Because mass loss was key to the dataset, the test was designed such that no wires were hanging from the panel. Consequently, there are no thermocouple measurements on or around the target. Much of the rest of the instrumentation is designed to provide good environment data.

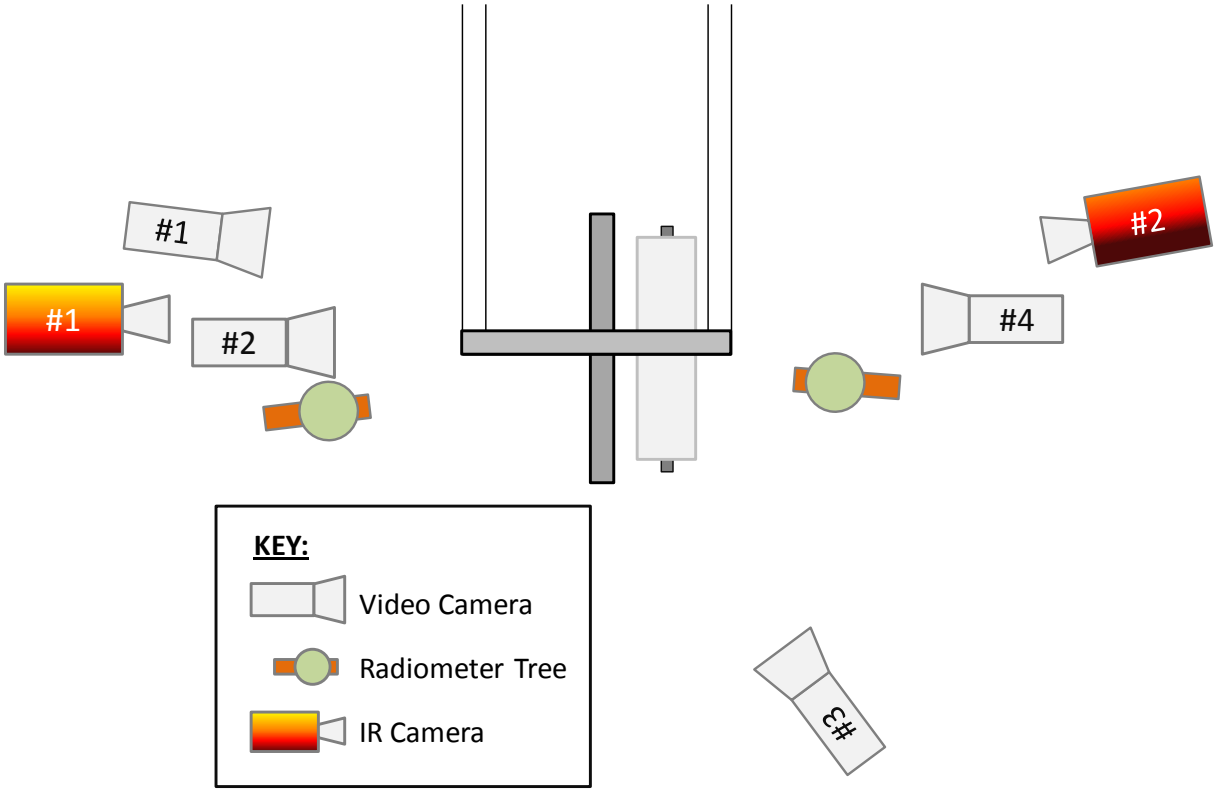


**Figure 20. A general layout of the camera and radiometer instrumentation.**

Figure 20 shows a general layout of the cameras and radiometers. This drawing is not to scale, but roughly representative of the position of the instrumentation. The position of the various instruments was at a given distance from the target and elevation from the center of the panel, as indicated in Table 2. This layout was typical of the layout for the tests, with some minor variations. Video Camera #2 was only used for relevant tests. For torsion tests, Video Camera #3 was zoomed and focused on the springs, which were positioned in good view of this camera as opposed to Video Camera #2.

**Table 2. Camera and radiometer layout details.**

| Instrument | Distance (cm) | Elevation | Target |
|---|---|---|---|
| Video Camera #1 | 123 | Level | Back side center |
| Video Camera #2 | 104 | Low | Back side springs |
| IR Camera #1 | 178 | High | Back side center |
| Back side radiometer tree | 76 | Level | Back side |
| Video Camera #3 | 170 | High | Oblique view |
| Front side radiometer tree | 76 | Level | Front side |
| Video Camera #4 | 118 | Level | Front side center |
| IR Camera #2 | 170 | High | Front side center |

In the actual tests, some variability exists in the positioning of the cameras and instrumentation, as instrumentation was periodically moved to accommodate the new structural rigs, and aimed slightly differently for the various tests. The exact positioning of the cameras is not consequential to any quantitative results in these tests. Details are provided as a reference to aid in interpreting the images that were taken from the cameras.

### 2.5.1 IR cameras

Two FLIR cameras were pointed at the front and back faces of the panel during the test. A ThermaCAM® model S60 was located 178 cm distance from the back-side of the test. It recorded 640 x 480 images examining a spectral range of 7.5 to 13 μm. A FLIR SC660 camera was situated 170 cm from the front side of the test, and recorded images with similar specifications. Images of the two instruments are found in Figure 21.

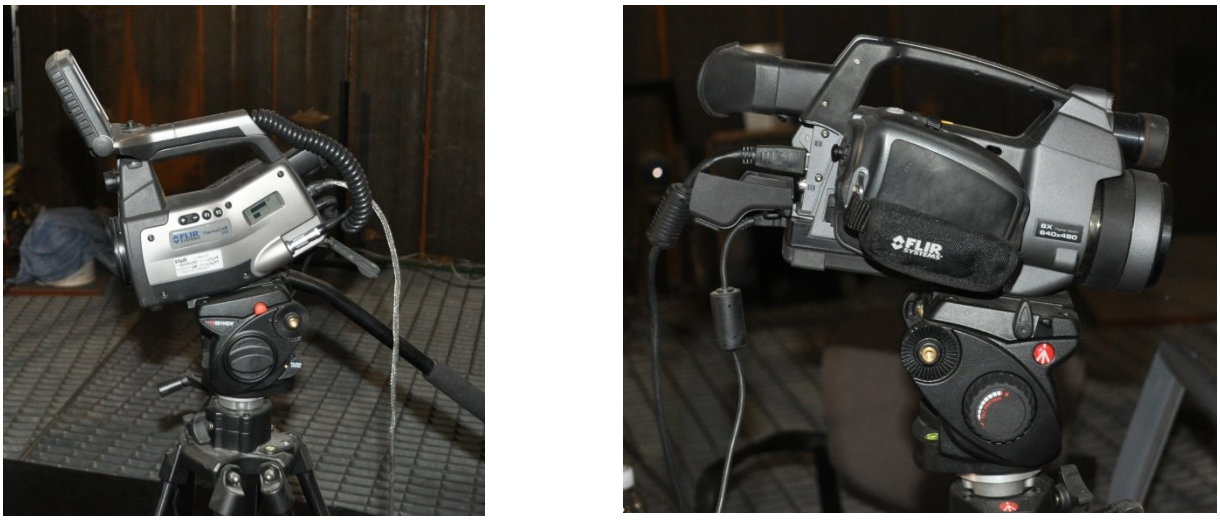


**Figure 21. Images of the IR cameras.**

The IR cameras are limited in range to certain temperature bands. Throughout the tests when the views began to saturate, the recorded range

would be manually adjusted. The data from these instruments are not always in range, and therefore are not always continuous through the test. Radiometers were generally used for point data, and IR cameras to illustrate 2-D thermal images of the panel temperature.

Quantitative temperature results extracted from the IR cameras are dependent on a surface emissivity given to the data acquisition software. Quantitative accuracy is reliant on the values given. At high temperatures, we provide here an estimate of 100°C accuracy on the temperatures. This is based on evaluating constant results as a function of emissivity given over a range of plausible values for the emissivity.

### 2.5.2 Radiometers

Six radiometers were arranged with two viewing the front side of the decomposing panel, and four on the back-side. All radiometers were Medtherm P/N NVRWP(ZnSe)-10-1-20-480-21986K radiometers. These are fast response thermopile water cooled gas purged 1 degree view angle radiometers. These were arranged approximately 76 cm away from the target surface such that two were aimed at the front (heated) side of the panel, while four were aimed at the back side. The target of each radiometer was at regular intervals on the face of each panel. Standard locations were centered horizontally for six instruments, and vertically, 25, 50, 75% of the height of the panel from the bottom. These locations are abbreviated later in this report as ¼, ½ and ¾ height locations. The one offset radiometer was at 25% of the height from the bottom of the panel, and 25% of the width of the panel from one side. Front-side, only the top two heights were visible due to the presence of the oven. Radiometers were factory calibrated before the test series began, and were aimed at small paint spots placed on the panels prior to each test. Because the radiometers were located 76 cm away from the panels, the spot size they are observing is calculated to be 1.4 $cm^2$.

Unistrut® stands were constructed and used to mount the radiometers. Photographs of the front and back radiometer towers are shown in Figure 22.

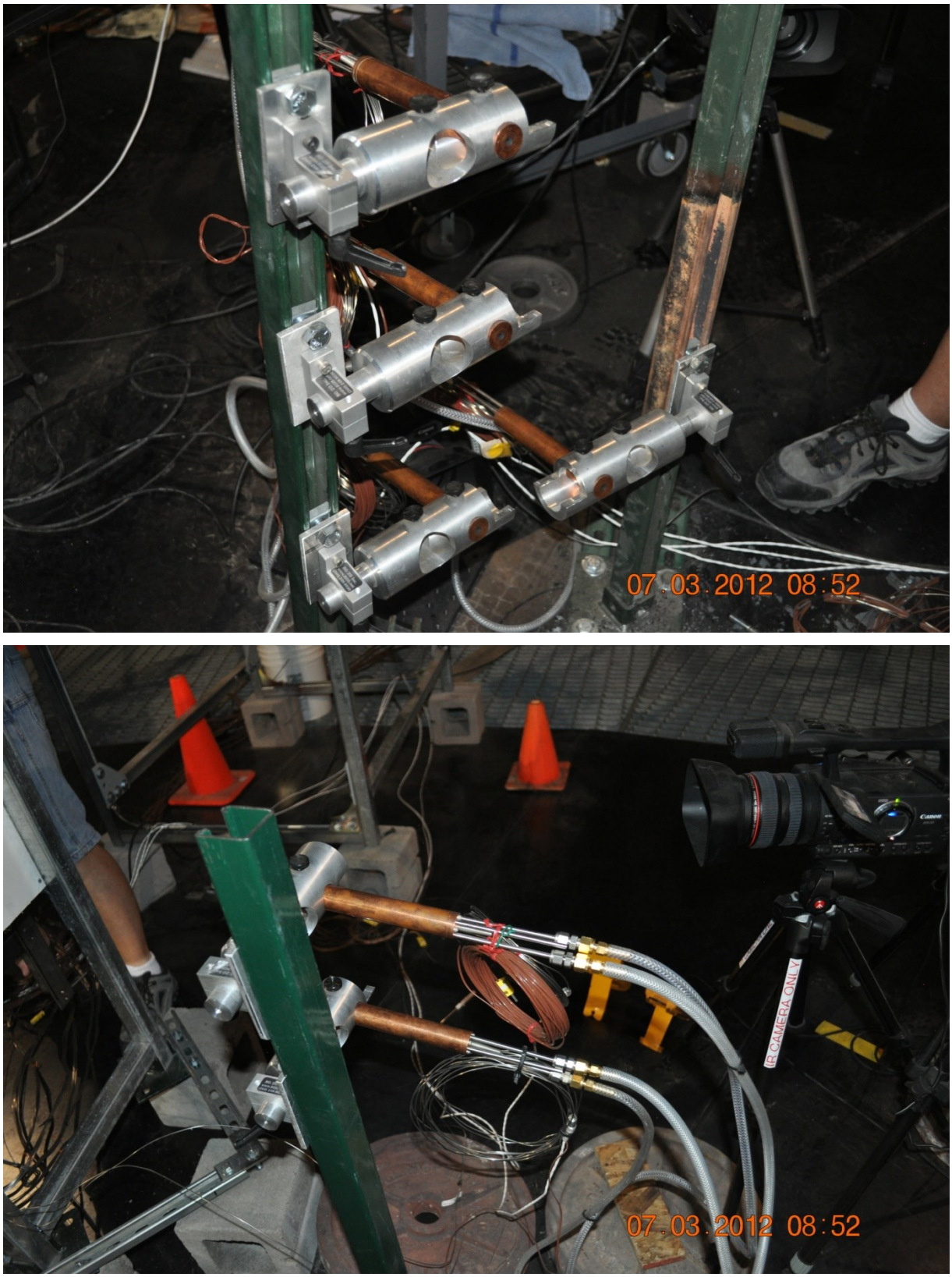


**Figure 22. Photographs of the radiometer towers.**

### 2.5.3 Video Cameras

Video was recorded with a series of Cannon XHA1 video cameras. Between three and four cameras were used, with a front, back, oblique, and spring camera recording the dynamics during the test. Data were recorded to tape media, with a capacity per tape of a little beyond one hour. In six instances, testing went beyond the duration of the tapes. In these cases, technologists would enter the chamber (otherwise vacant of personnel) and change out the tapes as necessary. Two of the video cameras are visible (#1 and #2) in the photograph found in Figure 23. The thermocouple instrumented metal panel is in the test holder in this photograph.

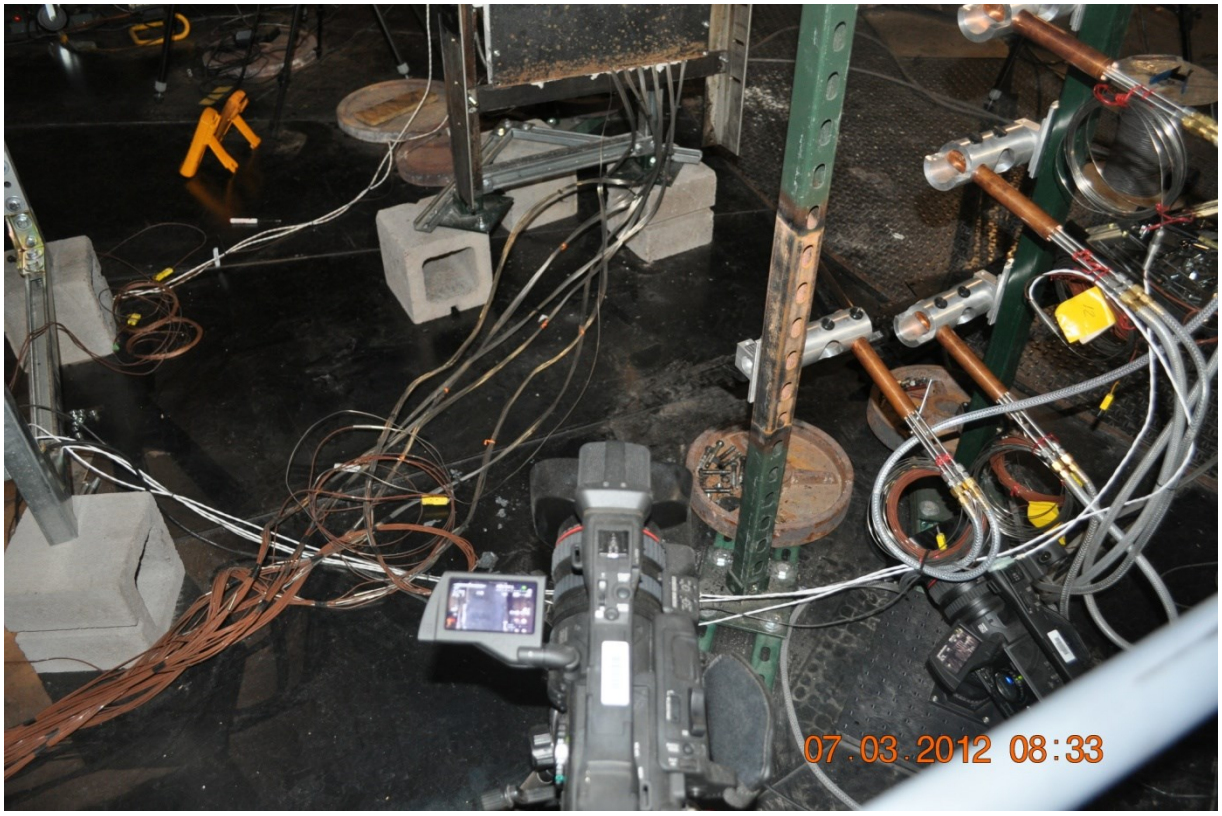


**Figure 23. Photographs of the test set-up for the oven characterization.**

The video results are critical to the interpretation of the force on the panels. Video Camera #2 (except for torsion) was pointed at the springs that were used to monitor the changing load on the panel. Fiducial boards were displayed in front of each camera prior to each test to provide grounds to make quantitative assessments of the motion in each test. Force was deduced by measuring the length of the spring segment as a function of time.

### 2.5.4 Data Acquisition

The data acquisition systems (DAS) for all standard fire and fuel measurements and facility instrumentation consist of a National Instruments PXI-1052 PXI/SCXI chassis with an embedded controller. The chassis has 4 PXI slots and 8 SCXI slots. The DAQ card is a PXI-6052E 16 bit A/D. The temperature channels are monitored with SCXI-1102 32 channel Thermocouple MUX cards connected to TC-2095 TC terminal blocks. The voltage channels are monitored with SCXI-1104 32 channel voltage input modules connected to SCXI-1300 terminal blocks. The chassis have 256 data channels. The systems can be expanded by adding another PXI-6052E connected to an SCXI-1001 12 slot chassis loaded with additional multiplexers.

Signal is sent from the hardware to a PC computer, where digitized data are recorded to log files through a National Instruments LabVIEW custom virtual instrument software interface. For the standard test, the following channels were recorded at roughly one second intervals:

**Table 3. Data acquisition channels.**

| Measurement | Number of Channels |
|---|---|
| Oven Temperature | 2 |
| Load cell temperature | 1 |
| Data acquisition temperature | 1 |
| Heat flux sensor temperature | 1 |
| Heat flux gauges | 6 |
| Load cell mass | 1 |
| Power on fiducial | 1 |
| Data fiducial | 1 |

The data fiducial consisted of power reading to a couple of lamps. The lamps were positioned in view of all of the cameras. These were turned on briefly prior to every test to allow the video and LabVIEW data to be accurately synchronized.

### 2.5.5 Reflectometer

A Surface Optics Corporation model ET100 version 1.0.0.8, with an OS version number 1.2.0.1 was used to evaluate spectral band reflectivity on various calorimeter surfaces. Two angles, 20 and 60 degrees were evaluated. Calorimeter reflectivity was evaluated for pre-test and post-test surfaces. The reflectometer bands were not completely sequential, as the instrument was custom designed for a prior application. This results in IR band overlap in the data, complicating the interpretation of the data when considering integrated reflectivity.

## *2.6 Test Matrix*

A test matrix was constructed with the three types of composite materials used in this study. Two other materials were tested, which were wood mock panels. They were made from oriented strand board (OSB) acquired from a local hardware store. They were principally mass mocks, and their thicknesses were allowed to vary to meet the mass mock goal since the density of the lumber is approximately 1/3 that of the composite material of interest. The ABDR mock panels were 6.35 mm thick, and the larger panel mock OSB panels were 19 mm thick.

Tests were consecutively numbered according to the sequence at which they were performed, as found in Table 4. They were not ordered before beginning testing to allow the facility schedule to be optimized with the tests being performed; the sequence was not randomly selected. Notably, torsion tests were performed late in the test series because they were considered non-essential tests and were optional at the start of the testing. Also, the 19x24 thin panels were tested later in the series because they were not part of the initial test plan. After testing the 18x24 thick panels under burn conditions and seeing that they did not readily burn through, it was decided to test the other panels to obtain a more complete dataset. The DFT (directional flame thermometer) test was not a reacting panel, but the characterization test detailed in section 2.4.3.

**Table 4. A summary of the various tests from this test series.**

| PANEL TYPE | COMPRESSION | TENSION | NO FORCE | TORSION |
|---|---|---|---|---|
| WOOD ABDR MOCK | 23 | 28 | 22 | |
| ABDR SANDWICH COMPOSITE | 24,27 | 31,32 | 25,33 | 43 |
| WOOD 18x24 MOCK | | | | 36 |
| 18x24 THICK COMPOSTE | 26,34 | 29,35 | 30 | |
| 19x24 THIN COMPOSITE | (38) 39,45 | 41 | 37,40 | 42 |
| DAMAGED 19x24 COMPOSITE | | | 44 | |
| DFT | | | 46 | |

A limited number of repeat tests were performed to provide an indication of test to test variability. Some tests were repeated due to irregularities in the baseline test. This is the case with test 38, which was aborted when a rod exploded. Other irregularities are described in more detail in the results section.

# 3 Results and Discussion

There are several ways to present the data from this test series. Since the performance of the three main types of panels studied varied significantly compared to other parameters, the results are organized by grouping tests of similar materials. These results will later be brought together for a general discussion calling out the effects of type of force imposed on the panel for each test.

An effort has been made to plot the data so it will be easy to interpret. In addition to textual labeling, results are color-coded. Compression results are black or a shade of gray. Tension tests are shades of green. Torsion is red, and 'NoForce' indicating panels without any imposed forces are colored blue. The single test with no force and a broken panel is colored yellow. In addition to color, symbols are also used to represent the type of forcing imposed. Tests are consistently colored this way from plot to plot and section to section. Tests are often abbreviated with their number and a few letters to indicate the type of force imposed on the panel during decomposition.

## *3.1 ABDR Sandwich Panels*

This section presents summary data for the ABDR sandwich panel tests. Pre- and post-test weight of the panels suggests the extent of the decomposition. They were also the lightest panels, with an average initial mass of 753 g.

The front-view videos were used to extract flaming times from the tests. These are shown in Table 5. The end of flaming was the most subjective to extract, as the flames could have been hidden behind the oven and smoke looks similar to flames in the video at late times.

**Table 5. ABDR sandwich panel flaming times.**

| Test | First Flaming | End Front Side Flaming | End Flaming |
|---|---|---|---|
| Comp-24 | 2 min 25 sec | 3 min 6 sec | 10 min 41 sec |
| NoForce-25 | 1 min 5 sec | 3 min 0 sec | 16 min 20 sec |
| Comp-27 | 1 min 24 sec | 3 min 2 sec | 10 min 1 sec |
| Tens-31 | 1 min 24 sec | 3 min 3 sec | 14 min 40 sec |
| Tens-32 | 1 min 25 sec | 2 min 50 sec | 15 min 17 sec |
| NoForce-33 | 1 min 29 sec | 2 min 43 sec | 15 min 49 sec |
| Tors-43 | 1 min 11 sec | 2 min 50 sec | 15 min 3 sec |

In general, between the first 1-3 minutes first visible flaming started. Between 30 to 120 seconds later, flaming on the front face subsided. The edges burned for around 7-14 minutes longer. Flaming had finished for all tests by 17 minutes, and in some cases well before that time. Flaming on the front face was typically seen to be initially engulfing, but at later times

periodically moving across the face, or at isolated locations along a fiber. A series of stills have been extracted during smoking, front face burning, and burning on the sides for each test. These are found in Figure 24 through Figure 30.

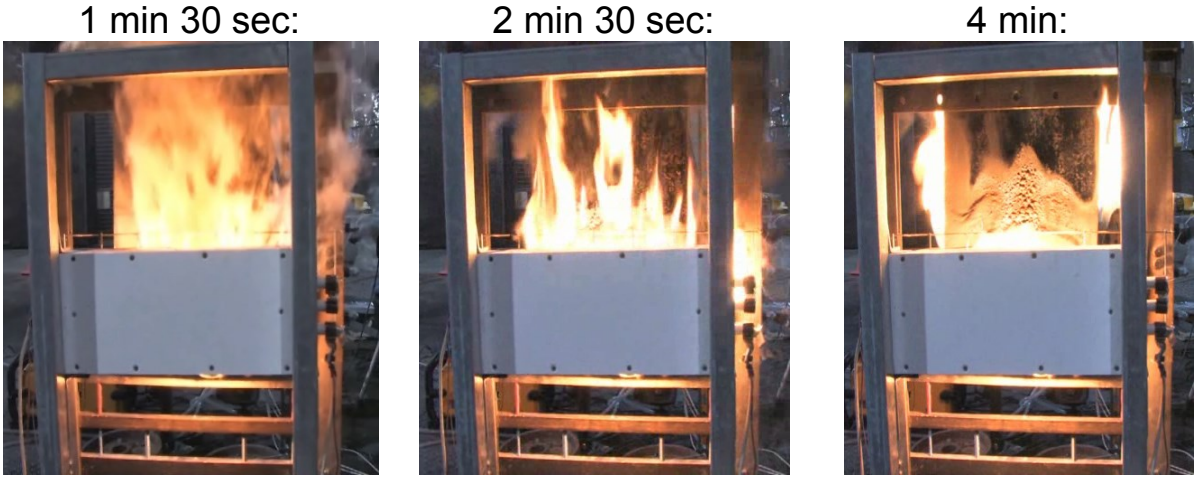


**Figure 24. Front side images for ABDR compression Test 24.**

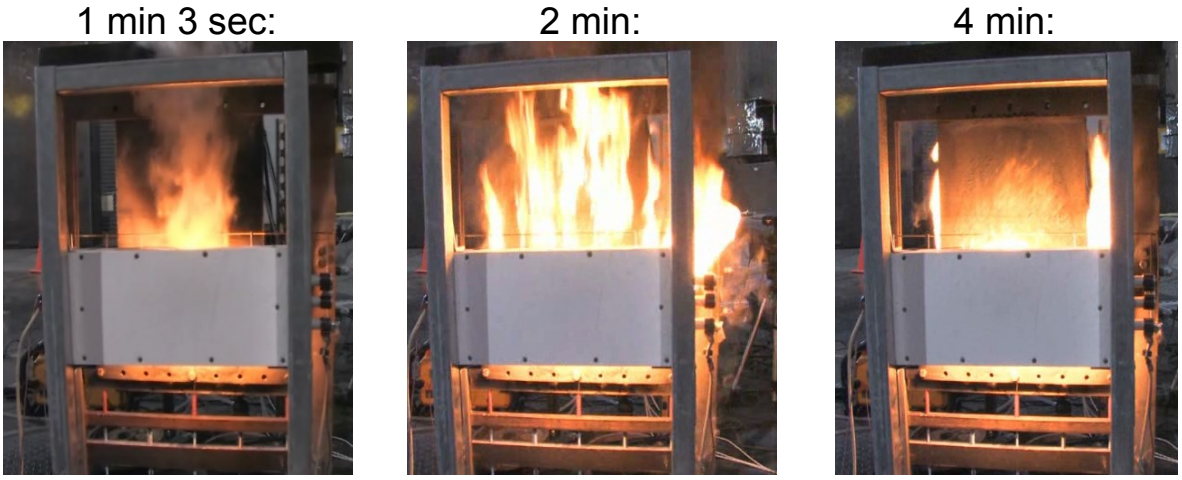


**Figure 25. Front side images for ABDR No-Force Test 25.**


**Figure 26. Front side images for ABDR compression Test 27.**

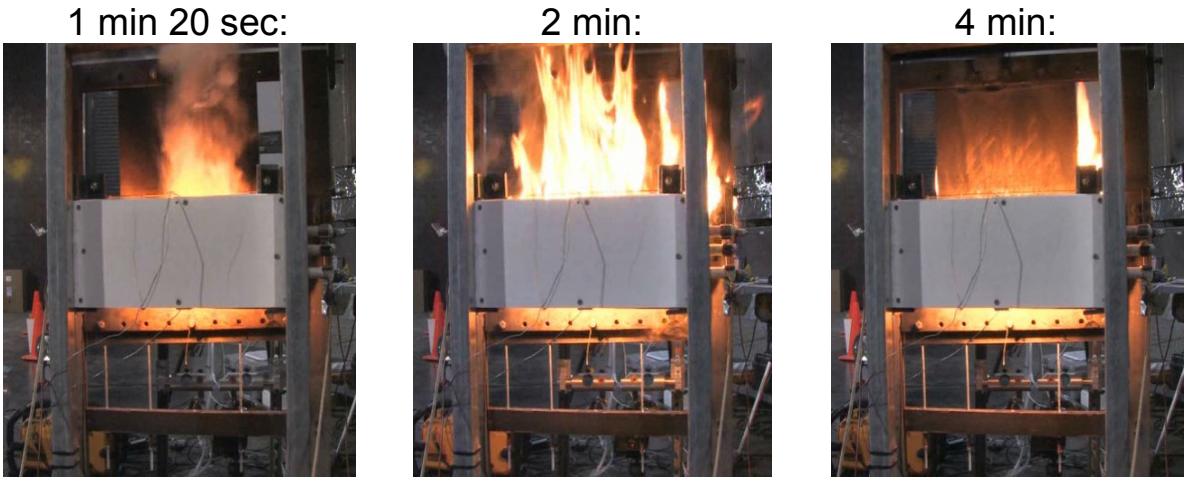


**Figure 27. Front side images for ABDR tension Test 31.**

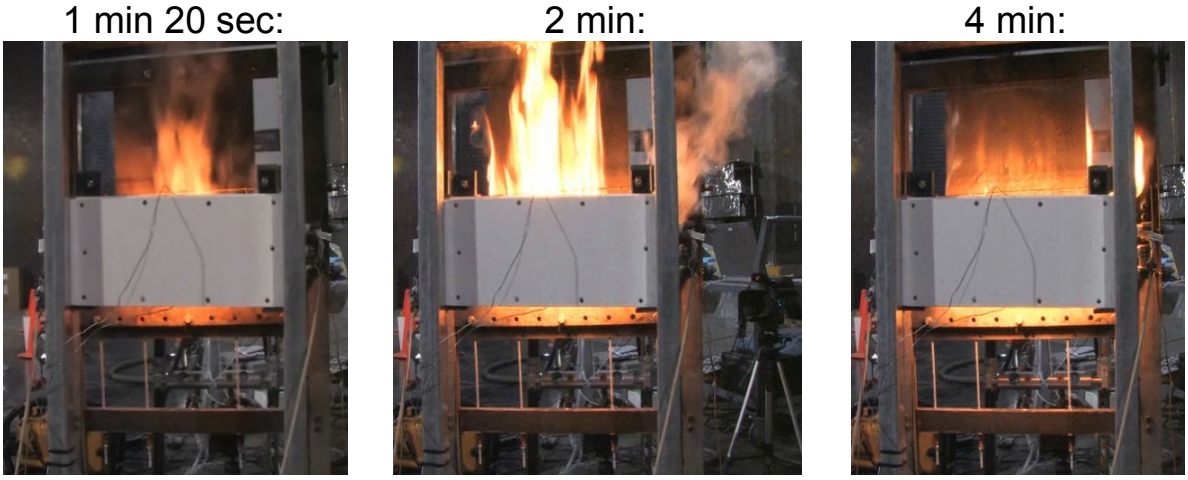


**Figure 28. Front side images for ABDR tension Test 32.**

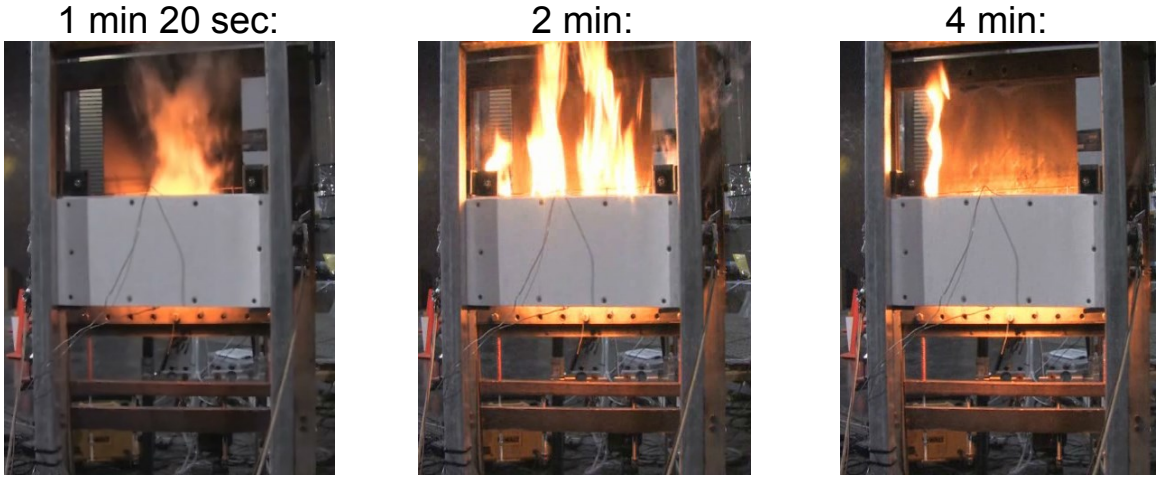


**Figure 29. Front side images for ABDR No-Force Test 33.**

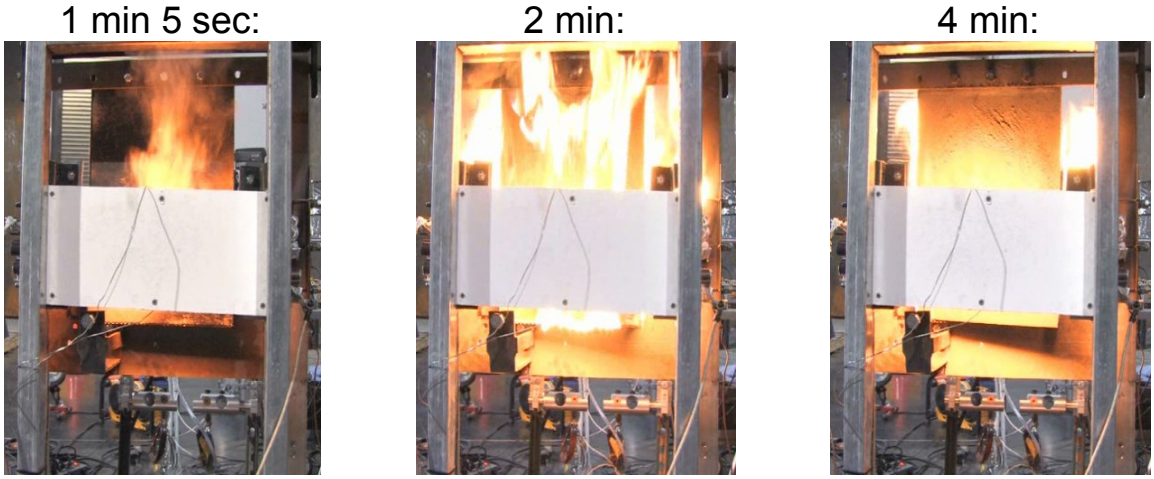


**Figure 30. Front side images for ABDR torsion Test 43.**

### 3.1.1 Mass loss data

ABDR panels lost the most mass on a percentage basis, an average of 63.1% mass remaining with a variability between 51% and 69% mass remaining. Figure 31 shows the percentage of mass remaining for the ABDR panel tests. The torsion test had the most mass lost, compared to compression and tension tests. The total mass lost varied widely for these tests. This is perhaps partly reflective of the variation in the amount of adhesive applied from panel to panel.

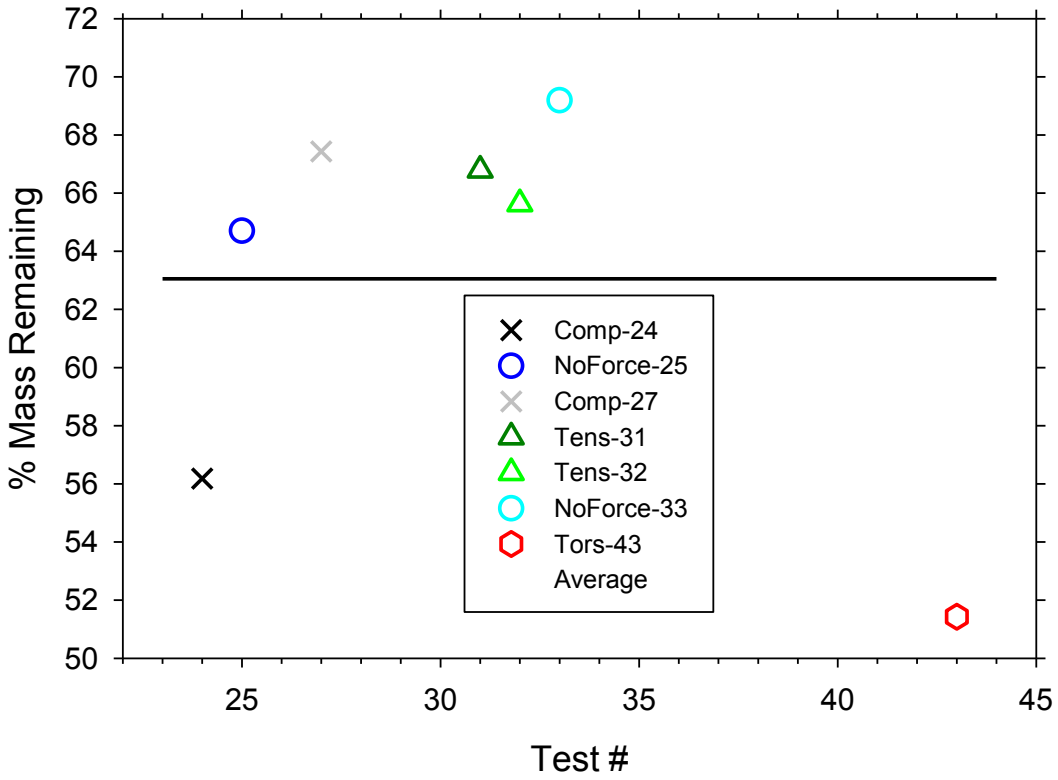


**Figure 31. Total mass loss summary for the ABDR panels.**

Example mass loss curves are shown in Figure 32 to illustrate typical raw data. Some amount of noise is found in the data, more so in the tests with structural loading.

The rate of mass change was computed from the differential change in mass with respect to time, and results are shown in Figure 33. Because of the noise in the mass readings, the data were interpreted based on an average over five minute intervals. In some of the tests, specifically the compression tests, the mass loss readings exhibit large perturbations, which were coincident with significant movement in the structural frame. These are characterized by large oscillations about the mean, as would be expected in such a scenario. To ameliorate against the improper (inadvertent) selection of one of the oscillation peaks while interpreting the mass loss data, point data were smoothed by taking a 10 second average before computing the differential change over the 5 minute interval.

Figure 33 shows computed mass loss reported at the time-center of the differential interval. Because the ABDR panels were the lightest panels, they were most susceptible to the noise in the system. From Figure 32, it can be seen that significant mass loss occurring within the first 10 minutes during flaming combustion, followed by at least 20 minutes of fairly constant rate mass loss due to oxidative reactions of the char and carbon fibers.

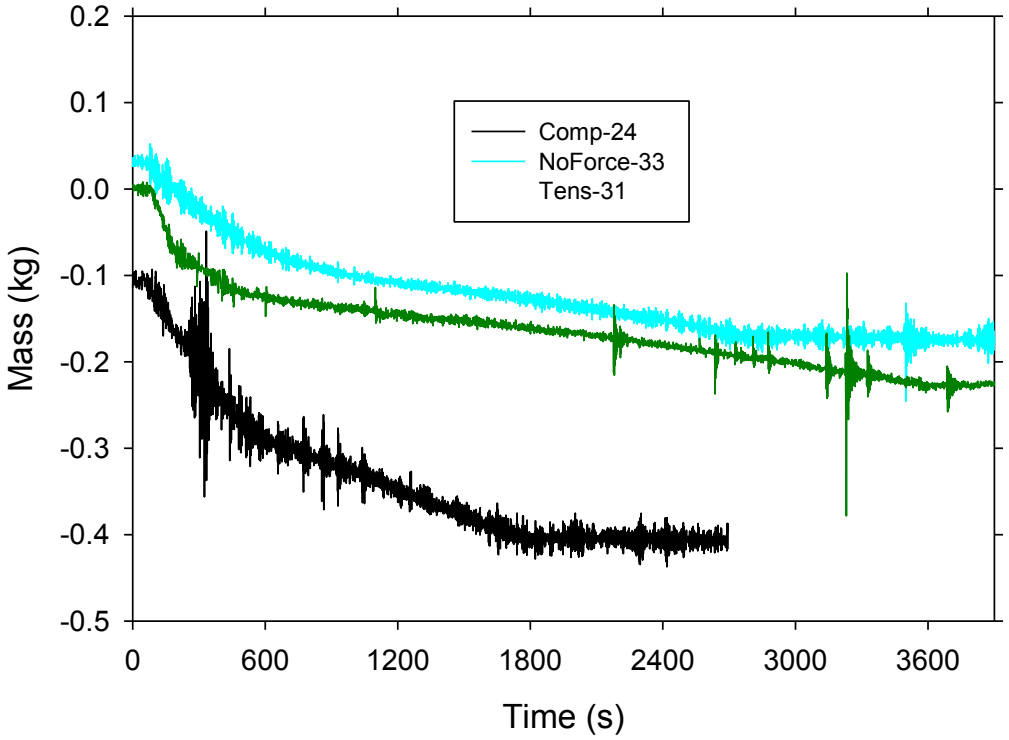


**Figure 32. Typical mass loss raw data for the ABDR panels.**

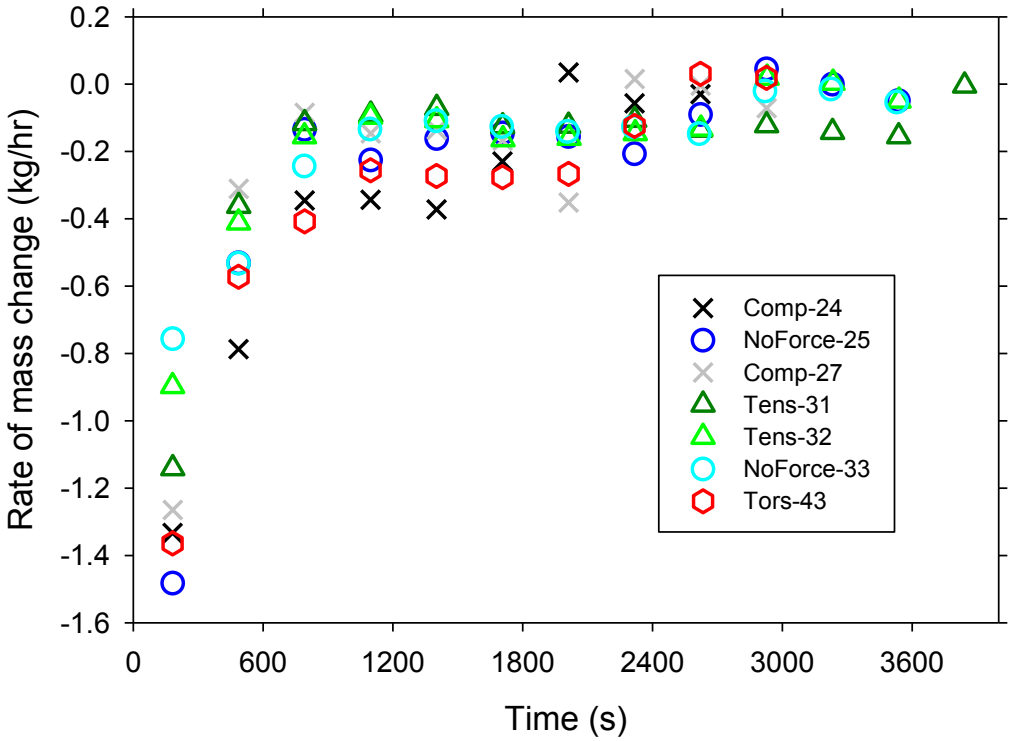


**Figure 33. Rate of mass change summary data for the ABDR sandwich panels.**

Several features of Figure 33 are indicative of the typical test of the ABDR panels. First, notice that the first data points in time are all the highest mass loss rate data points. This is because in the first minute or so the panel face subject to the oven heat flux would begin to smoke. Then between 2.5 and 4.5 minutes, active flaming on the front face of the panel would begin. In a few minutes time, the flaming would transition to the sides of the panel as it decreased on the carbon fiber face. The second data point is the second highest mass loss rate in all cases, and reflects the diminishing flame. After about ten minutes, flames had extinguished and visible smoking had mostly ceased. The panels continued to lose mass, at this point presumably due to oxidative reactions.

The fact that the flaming was significant on the sides of the panels represents a non-ideal feature of these tests. Real aircraft designs are understood to have closed edges where sandwich materials are present. The behavior of an intact aircraft in this regard might consequently be expected to differ from the behavior of the materials used for the present tests.

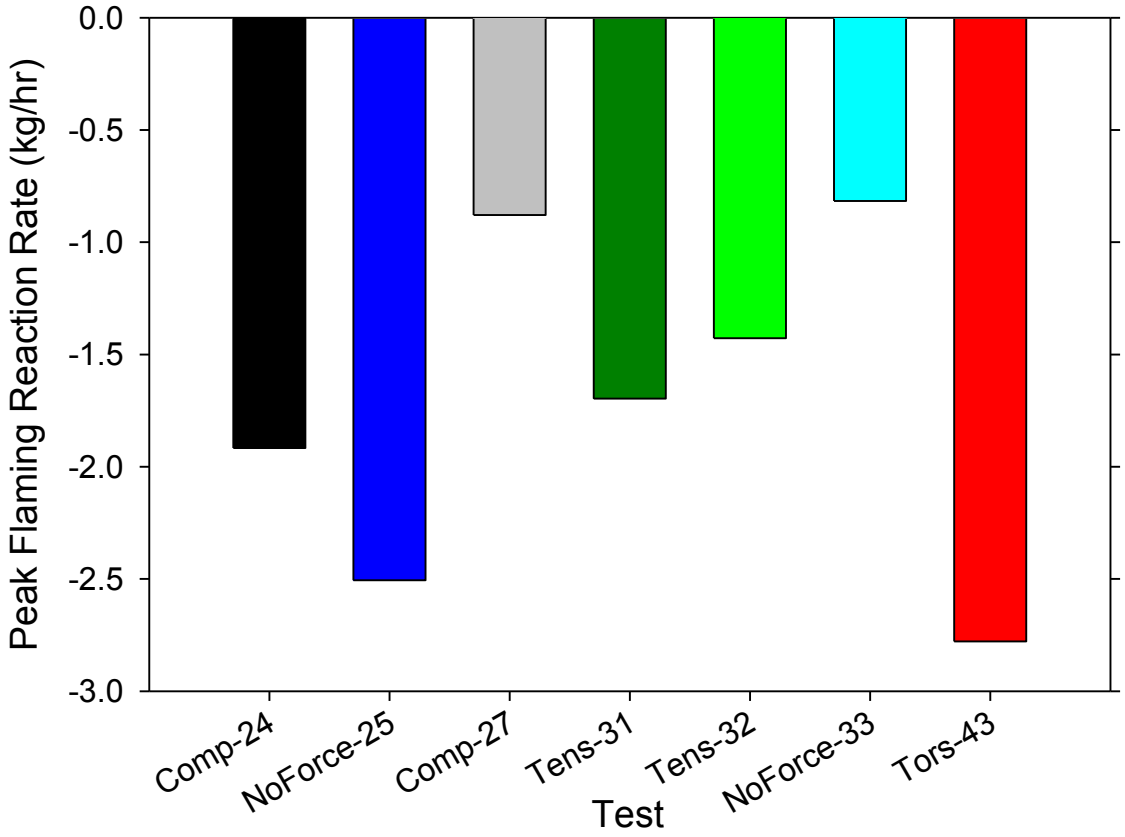


**Figure 34. Peak flaming reaction rate for the ABDR sandwich panels.**

The flaming reaction rates were extracted from the data by evaluating the steepest slope during flaming times on the mass loss data curves. These

results are shown in Figure 34. No obvious relationship is seen between the type of force and the peak flaming mass loss rate in these data.

The total time for each test was somewhat variable, with the values plotted in Figure 35. The termination time was somewhat subjective (probably repeatable to within a few minutes), as tests were generally terminated when two of the oven rods were clearly visible in the back-side cameras through the hole in the panel. Figure 35 is suggestive of a relationship between type of loading and test duration, but later discussions will cast doubt on this finding.

Noise in the data inhibits extraction of good mass loss rates during flaming. Since the non-flaming portion of the tests was fairly uniform and long-duration, the mass loss rate during this time can be extracted with higher accuracy.

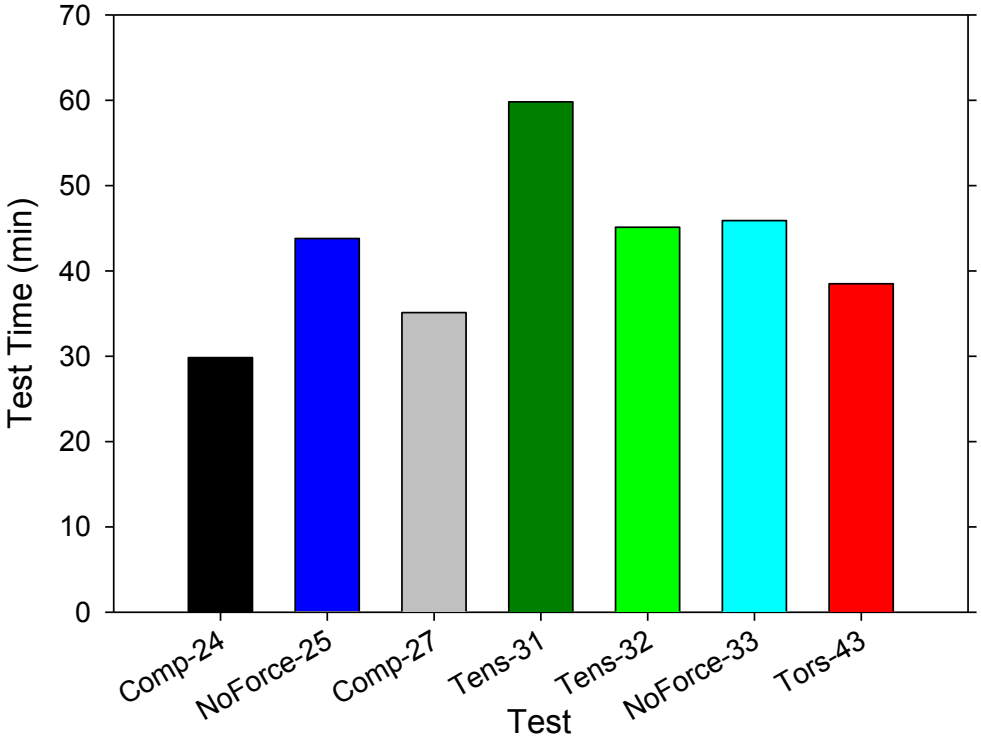


**Figure 35. Test time summary data for the ABDR sandwich panels.**

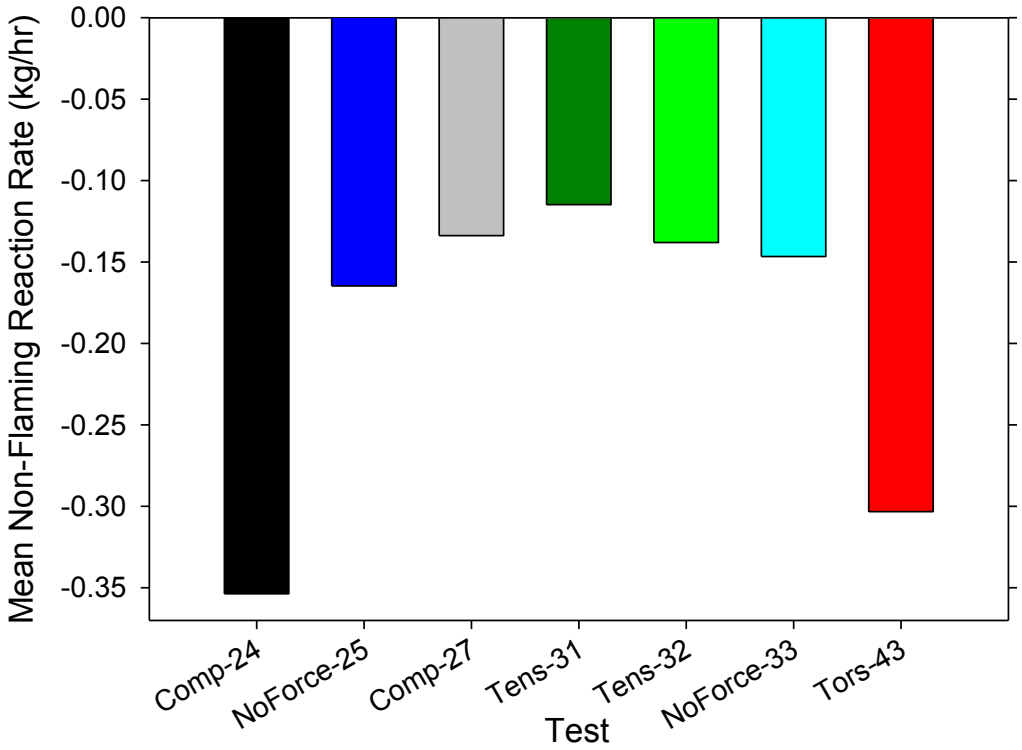


**Figure 36. Mean Non-Flaming mass loss rates for the ABDR sandwich panels.**

Figure 36 shows the mass loss rate rate extracted from approximately 10 minutes time through 5 minutes prior to the end of the test. These data show wide variability, and do not suggest any correlation with the type of force on the panel.

In these tests, there was a lack of uniformity (most pronounced from test to test) in the oven temperature, as measured by two thermocouples located in the oven, with the range of steady-state oven temperatures falling between 1000-1200°C. Thermocouple locations are found in Figure 10, and are symmetrically oriented at the top and bottom of the furnace. Figure 37 shows the thermocouple readings for each ABDR panel test. Steady-state temperatures were typically constant, and the two thermocouples agree reasonably closely with each other for each test. Two features of this plot are of interest. First, Test 25 lost power briefly just after 1800 seconds. This was because one of the electrical components controlling the power supply went to sleep. This feature was disabled in future tests. Power was promptly restored, as is evident in the data. Also, notice that the thermocouple readings decrease slightly before the steep decline at the end of the test when the power to the furnace is turned off. This is because as a hole is formed in the panel, the oven is less able to maintain its steady-state temperature as when the panel was whole.

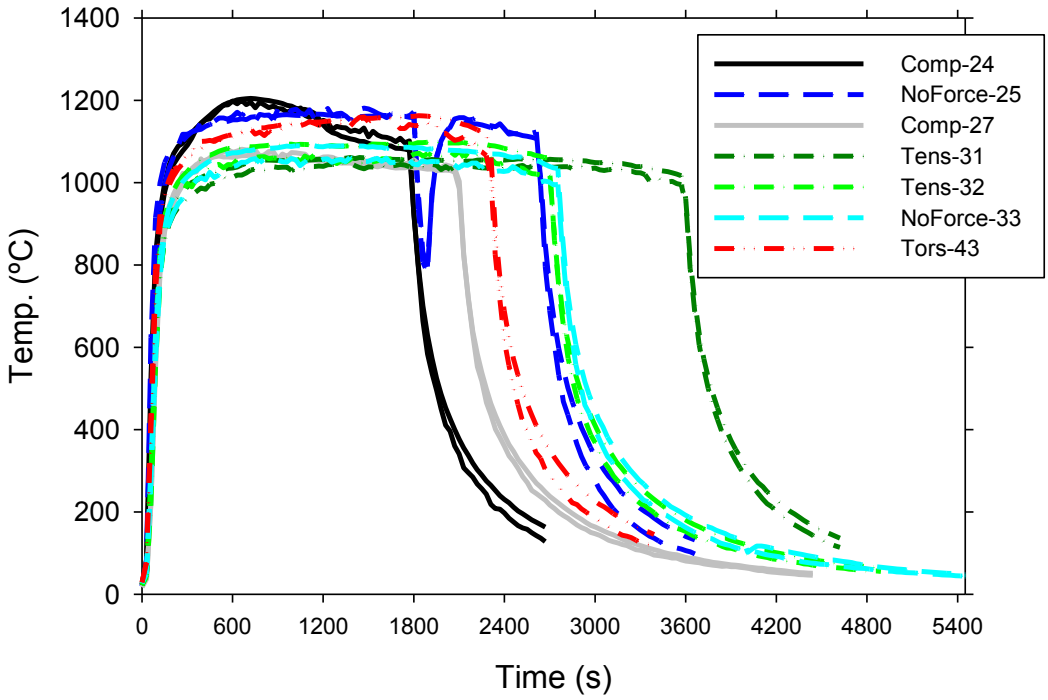


**Figure 37. Oven temperatures for the ABDR panel tests.**

### 3.1.2 Radiometer Data

Radiometer data from this test are illuminating. Figure 38 shows mid-point front side fluxes from the ABDR tests. The power loss is evident in Test 25. Three tests (24, 25, 27) exhibited much higher fluxes at this radiometer location. These are speculated to be due to distortions in the panel that enhance the view factor between the panel at the mid-point front side radiometer location and the oven. Figure 39 shows data from a radiometer location higher on the ABDR panel, suggesting greater consistency between the tests. Figure 40 shows back-side flux ¾ of the way up the panel. Fluxes are barely above ambient, suggesting the insulated nature of sandwich panels and the low temperature of the panel outside of the immediate fire area. Figure 41 shows data from the center of the back-side of the panel. Most results are in the 5-10 kW/m$^2$ range, with some exceeding this and being suggestive of a hole that burned through at higher elevation than the other tests (as compared with data in Figure 42). Figure 42 shows data where the hole broke through, with correspondingly high fluxes. Figure 43 shows data at an off-center location from the data in Figure 42. Fluxes peak at the end, and are high depending on the size and position of the hole relative to the radiometer target area.

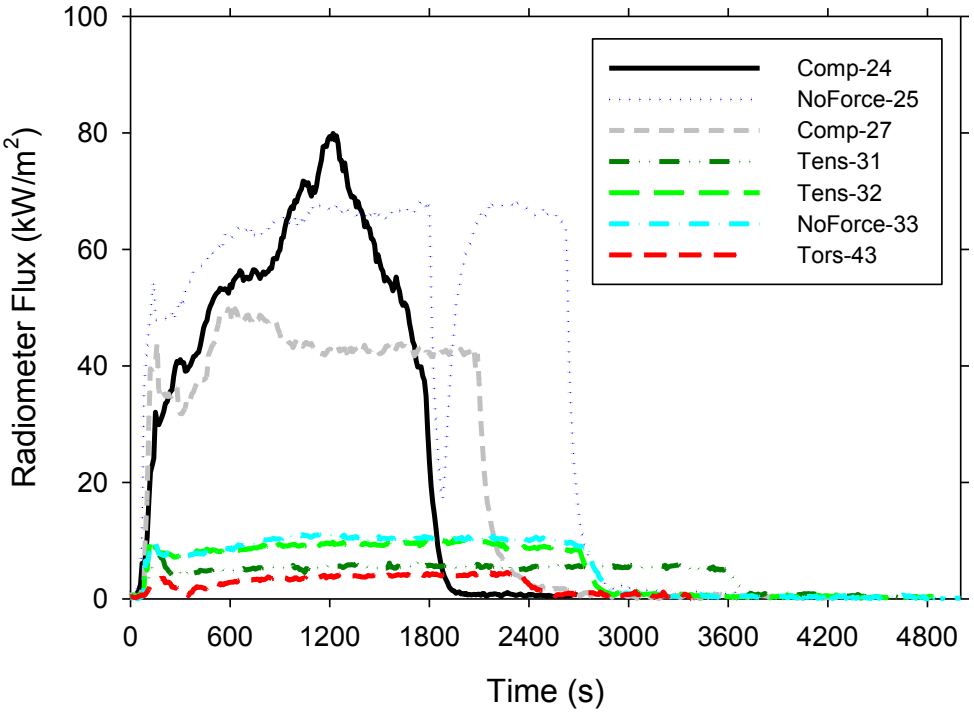


**Figure 38. ABDR radiometer readings from the front of the panel at ½ way up the panel from the bottom.**

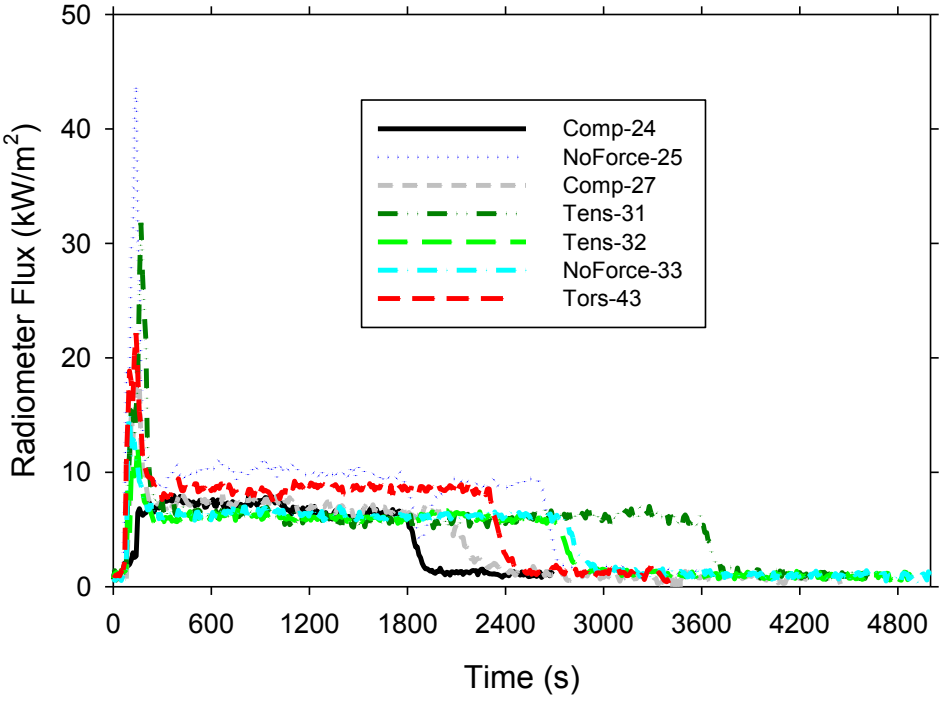


**Figure 39. ABDR radiometer readings from the front of the panel at ¾ of the way up the panel from the bottom.**

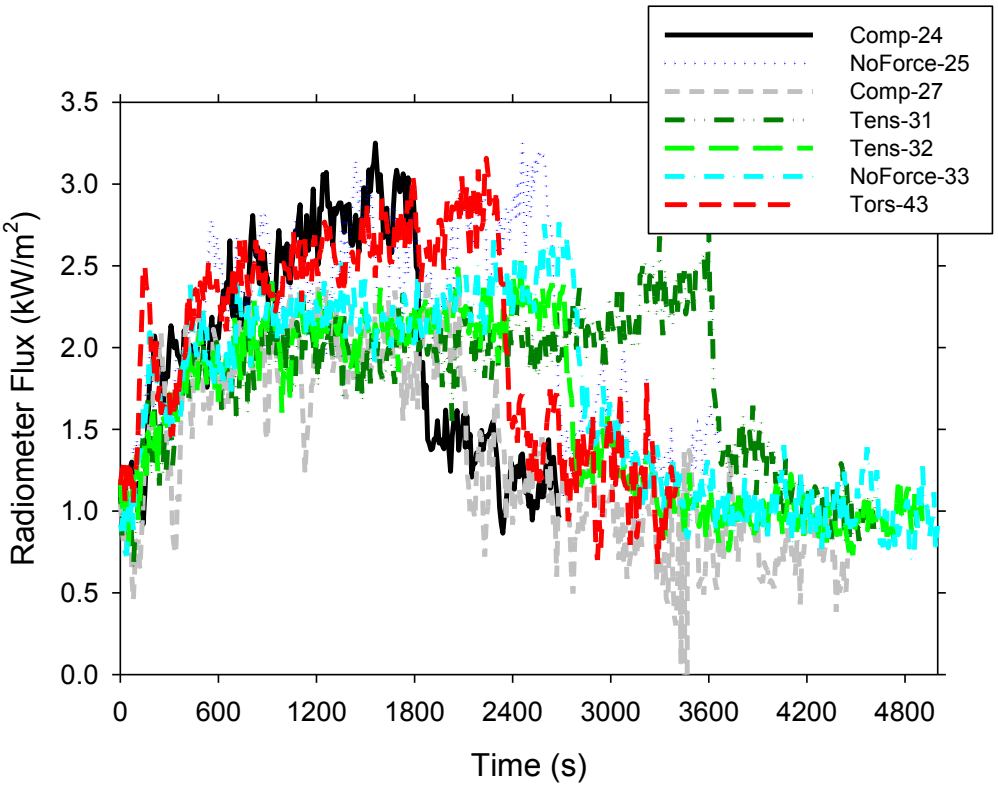


**Figure 40. ABDR radiometer readings from the back of the panel at ¾ of the way up the panel from the bottom.**

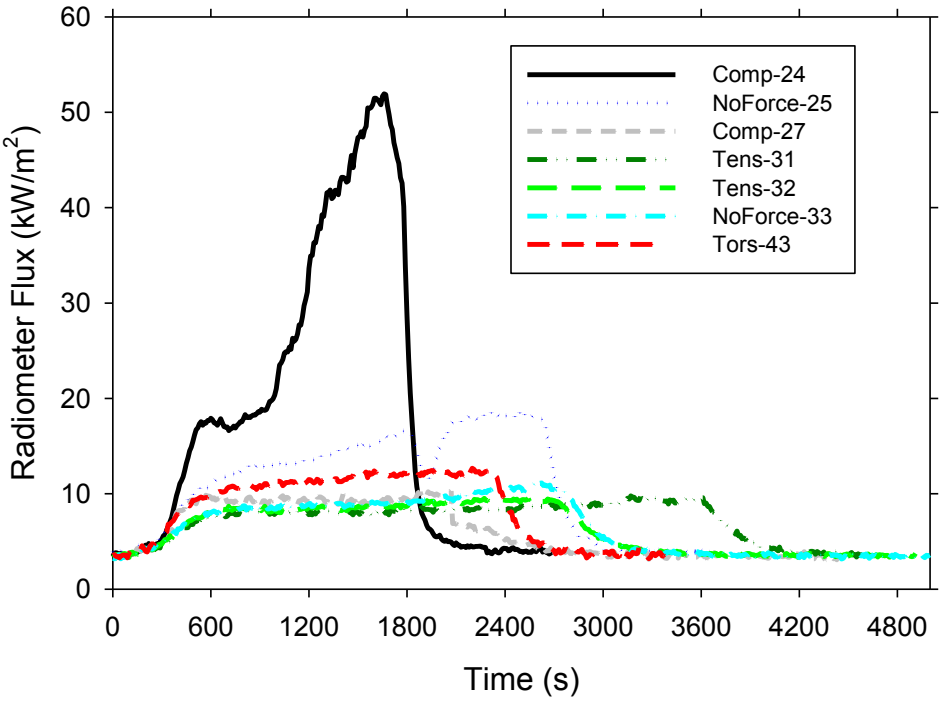


**Figure 41. ABDR radiometer readings from the back of the panel at ½ of the way up the panel from the bottom.**

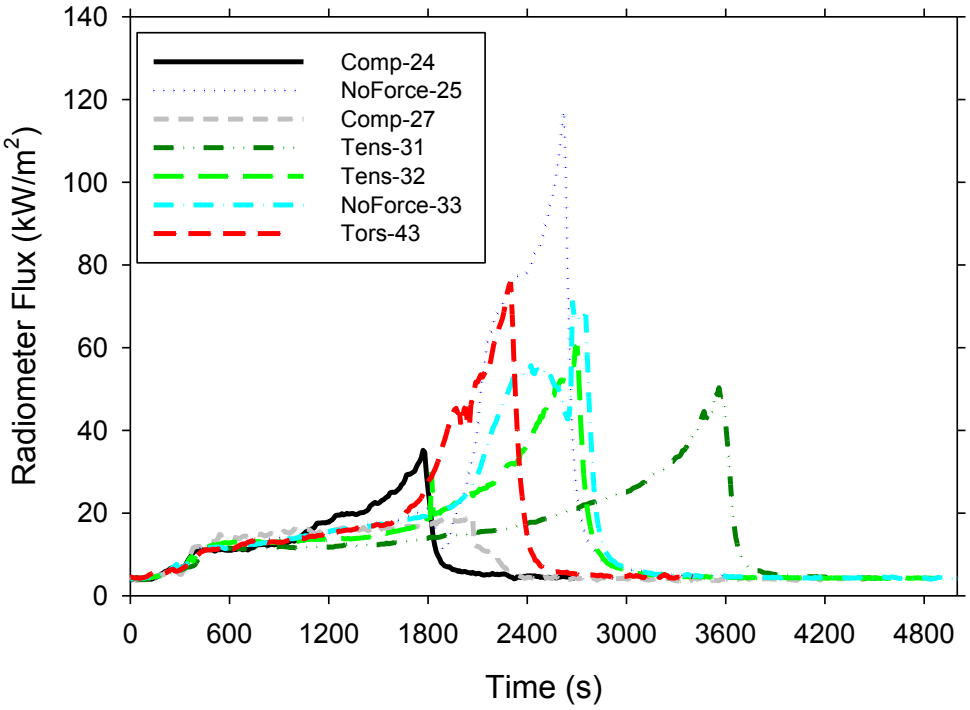


**Figure 42. ABDR radiometer readings from the back of the panel at ¼ of the way up the panel from the bottom.**

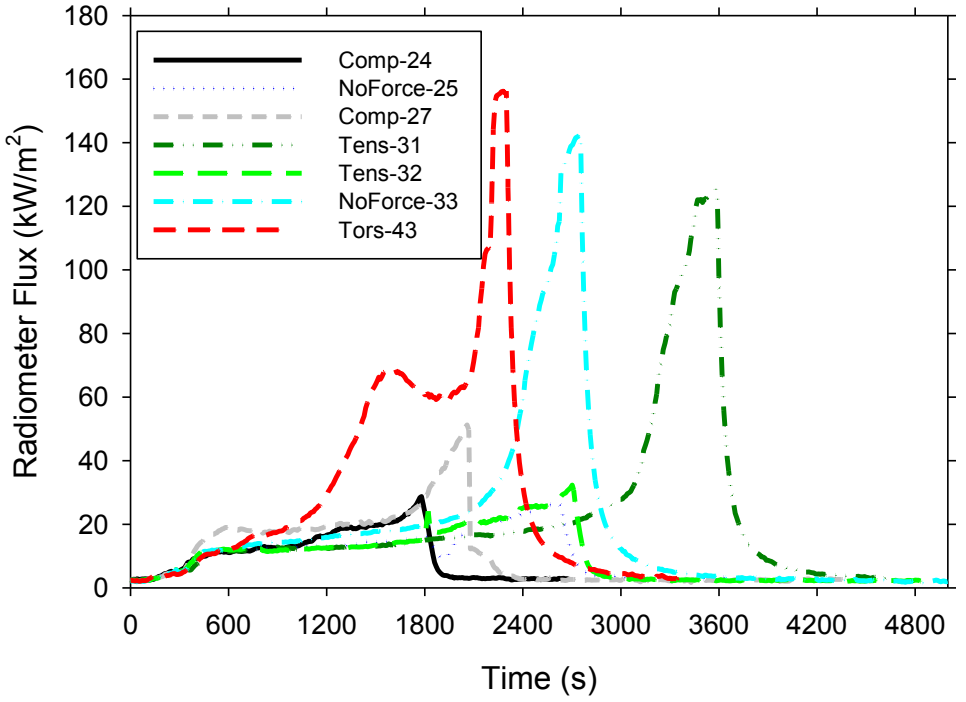


**Figure 43. ABDR radiometer readings from the back of the panel off-center at ¼ of the way up the panel from the bottom.**

### 3.1.3 IR data

Figure 44 shows a series of selected images from the IR camera exhibiting a range of results found during Test 24. These and all subsequent IR images show a reproduction of the temperature in degrees Celcius that is based on a material emissivity of 1.0 assumption. Please note that the scale is dynamic, and different for every image frame.

The first image at 2 minutes and 17 seconds shows the back side shortly after the appearance of visible flaming on the sides of the panel. The ABDR panels were prone to burn at the sides due to the exposed honeycomb at the edges. At this time, flaming was predominantly to one side, and significant jetting is seen. The panel is in the early phases of heat-up.

The next frame at 5 minutes shows regular flaming along the sides, and some distortion in the shape of the panel is evident. Back-side temperatures have increased to a few hundred degrees.

At 10 minutes, there is a significant fold that can be seen on the back side that was caused by the compressive force near the bottom of the panel. The back-side thermal contours are not smooth. Rather, random hot points appear to suggest some irregularities in the decomposition of the panel despite a presumably somewhat smooth oven heating profile.

By 20 minutes, some points of complete burn-through are evident in the peak temperatures extracted from the IR camera. An oddly shaped hole is formed, and is mostly vertical in shape. There appears to be significant temperature indicating near burn-through just below the fold, but not at the point of the fold.

At 25 minutes, a significant hole is observable in the panel, with the rods being evident through the hole in the panel. The frame at 27 minutes and 30 seconds was extracted just before the power to the oven was turned off, and reflects the final condition of the panel. The holes have grown slightly from those seen at 25 minutes.

2min 17 sec:

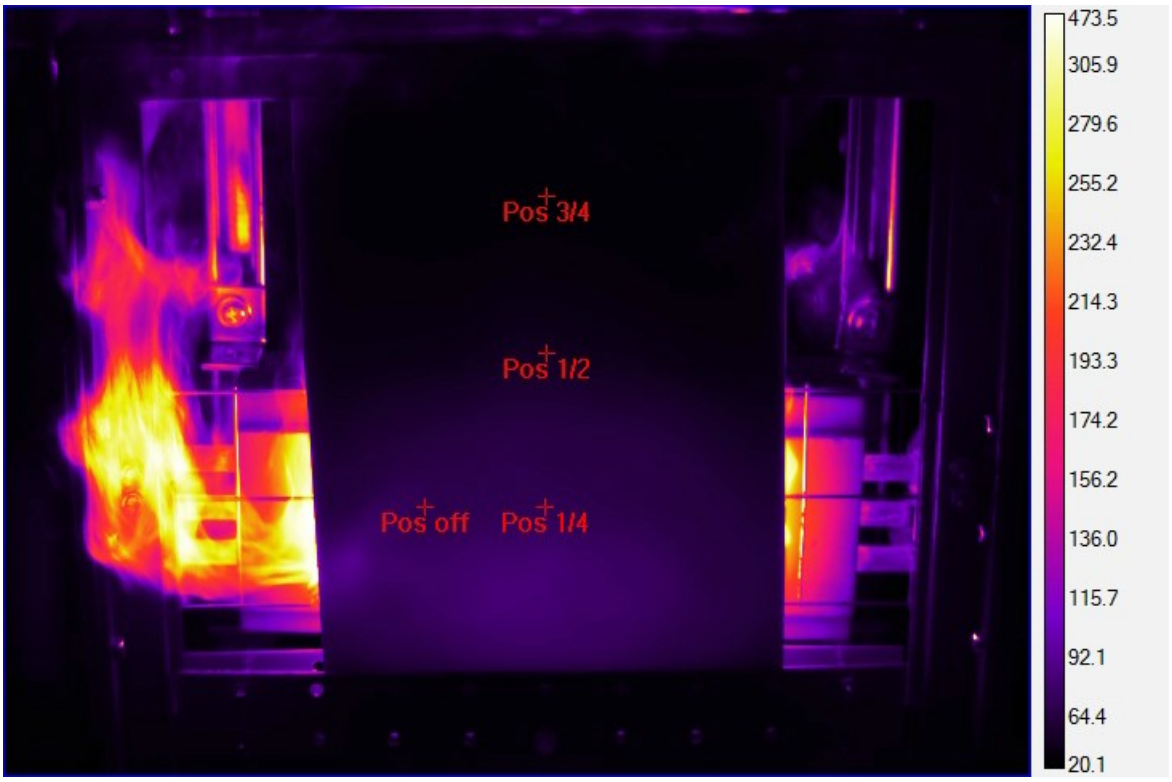


5 min:

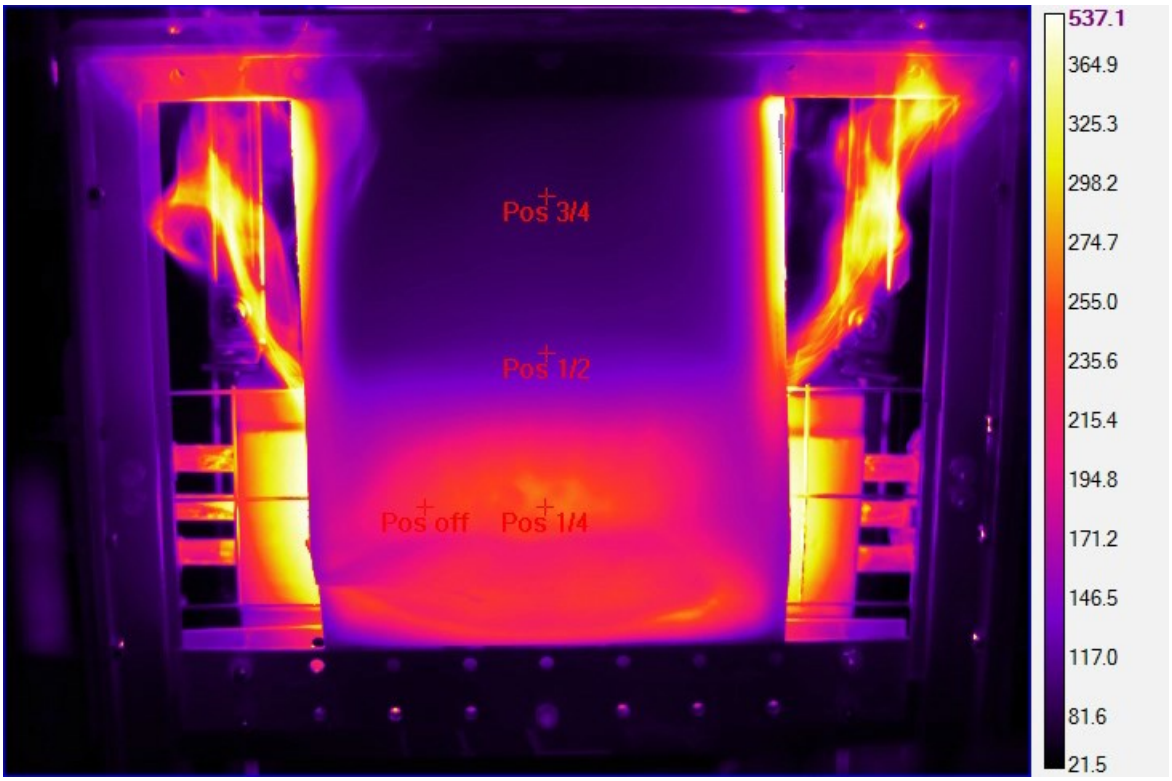

10 min:

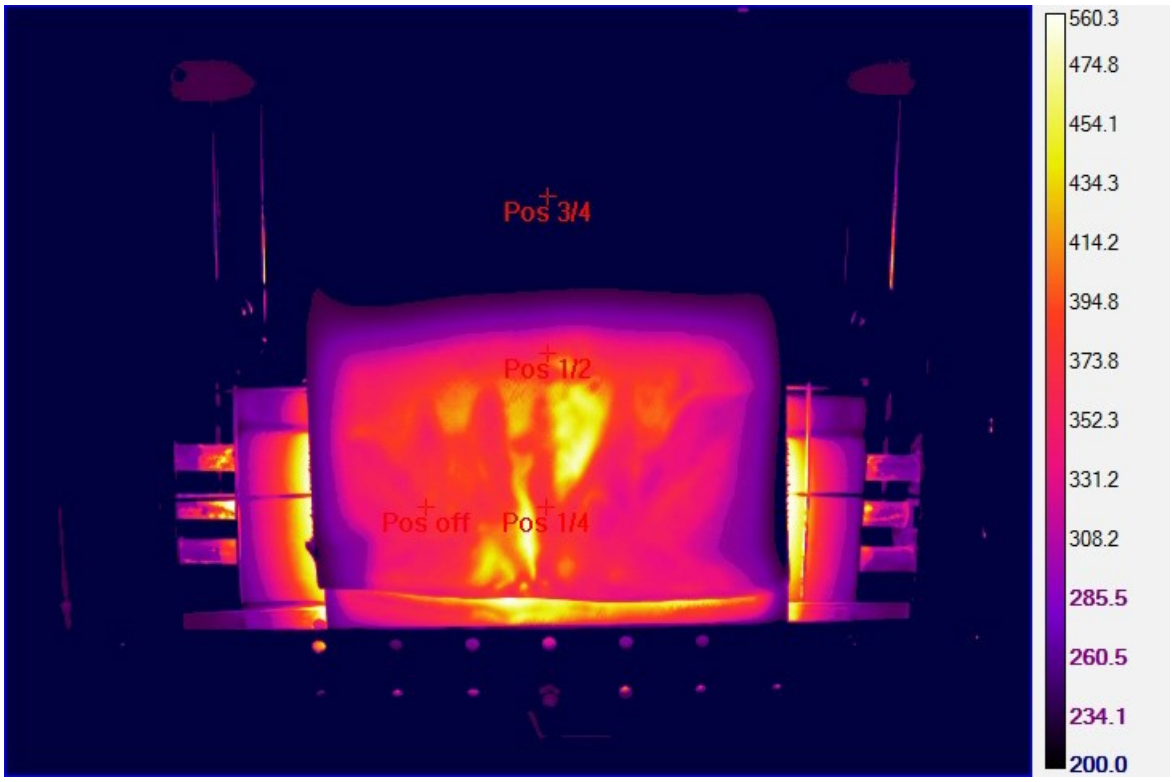
Pos 3/4
Pos 1/2
Pos off
Pos 1/4
560.3
474.8
454.1
434.3
414.2
394.8
373.8
352.3
331.2
308.2
285.5
260.5
234.1
200.0

20 min:

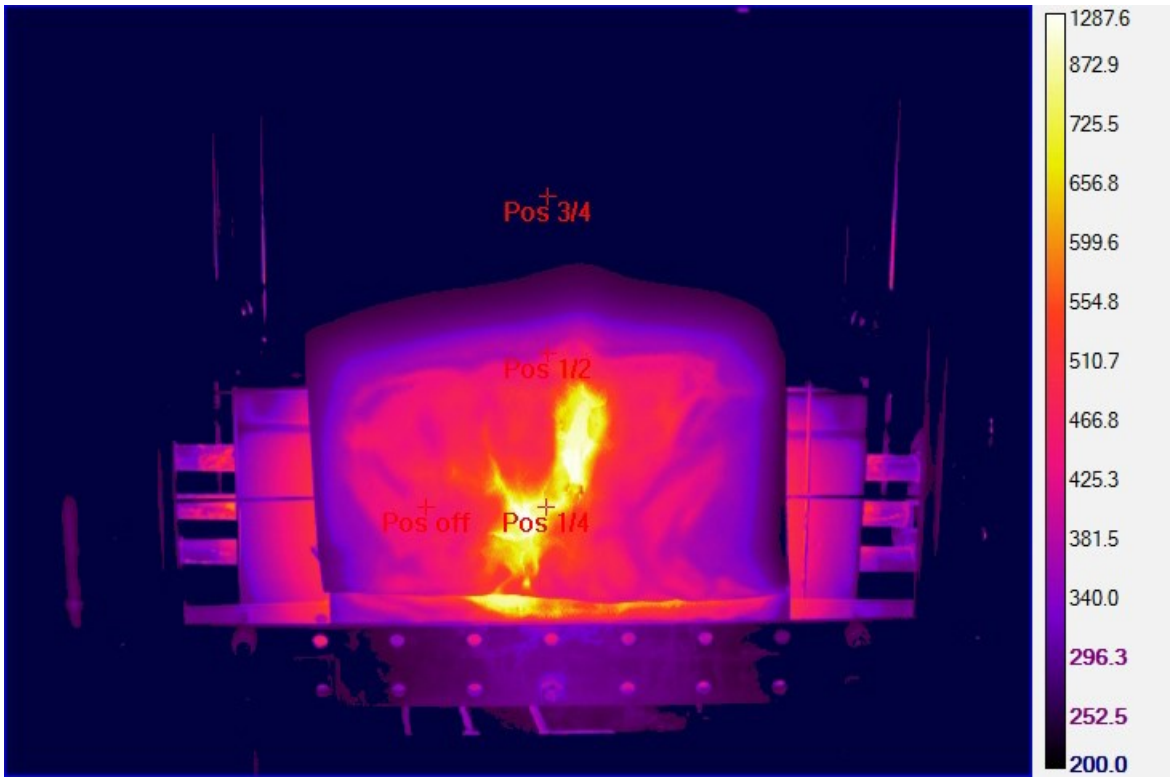
Pos 3/4
Pos 1/2
Pos off
Pos 1/4
1287.6
872.9
725.5
656.8
599.6
554.8
510.7
466.8
425.3
381.5
340.0
296.3
252.5
200.0

25 min:

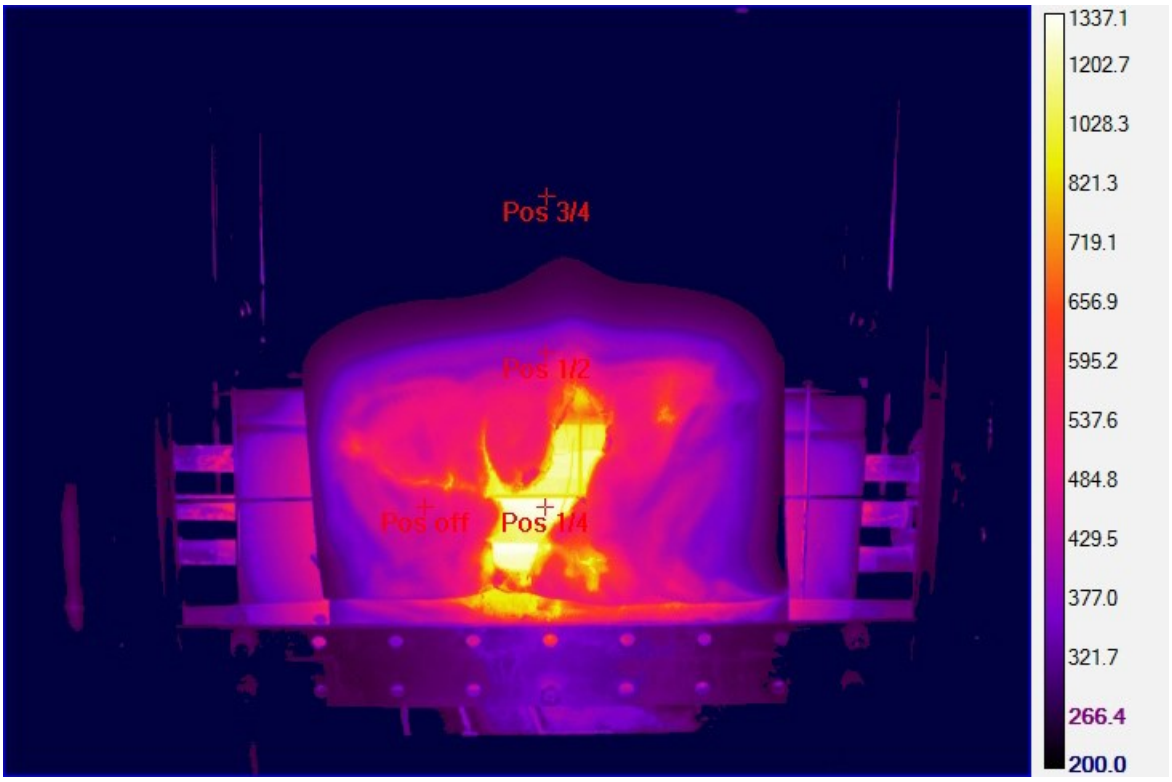


27 min 30 sec:

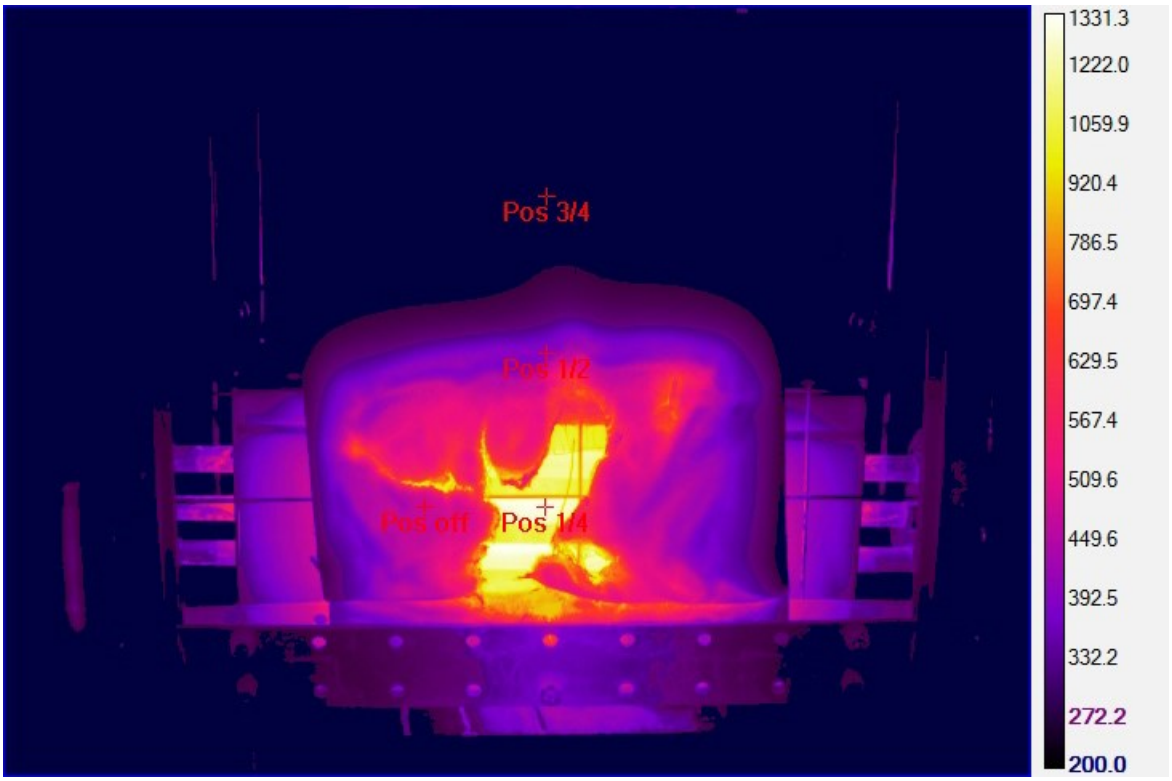


**Figure 44. IR camera images from Test 24, the ABDR sandwich panel is in compression.**

### 3.1.4 Load data

The ABDR panels exhibited interesting behavior with respect to the structural loading placed on the panels. Detailed results determined by examining the back-side camera results, and are found in Table 6. Here it can be seen that the compressive and torsional deformations occur early in the event, whereas tensional deformations occur later.

**Table 6. ABDR spring movement summary.**

| Test | Force Type | First Movement | Last Movement | Nature of Movement |
|---|---|---|---|---|
| 24 | Compression | 1 min 48 sec | 19 min 52 sec | Smooth changes at early times, diminishing at late times |
| 27 | Compression | 2 min 58 sec | 36 min 16 sec | Big steady movements for the first 4 minutes, small movements for the next 17 minutes, panel collapsed and fell out of top holder at about 34.5 minutes. |
| 31 | Tension | 36 min 9 sec | End of test | Minor movement (thermal expansion) before first significant movement, small regular movements until test end. |
| 32 | Tension | 24 min 32 sec | 42 min 21 sec | A tear opened up over the last half of the test, with periodic small movements over this time frame. |
| 43 | Torsion | 2 min 37 sec | 3 min 22 sec | Steady movements for about a minute, slowing afterwards to a creep. |

The tension tests were clearly differentiated from the compression and torsion cases, in that they were able to support the full load of the frame through a large portion of the test. The torsion and compression tests exhibited movement very early in the test. The torsion test did not exhibit much strength, but there was clearly residual compressive strength through a good portion of the compression tests.

Analysis of the spring cameras gives a more complete picture of the estimated load on the panels during the test. The motion of the springs was extracted for these plots from analysis of video editing software. The force equivalent mass was deduced from the spring constant. There is a degree of subjectivity to this analysis, and these results should be taken as accurate only to within 10% of the initial reading. Even though spatial fiducials were used to provide a reference length scale in the videos, some degree of

uncertainty remains from case to case due to combinations of movement in the cameras after the fiducial frames were taken and also due to the angular perspective. Maintaining a consistent measuring location was challenging. Quantified data are found in Figure 45. For the most part, the force was uniformly applied across the ABDR panel base, and the springs released force at about the same time. The torsion test used only one spring, which is why the initial force is about ¼ that of the other tests. The panel hit the back-plate on the frame of the composite holder, which is why further movement was not found for this test.

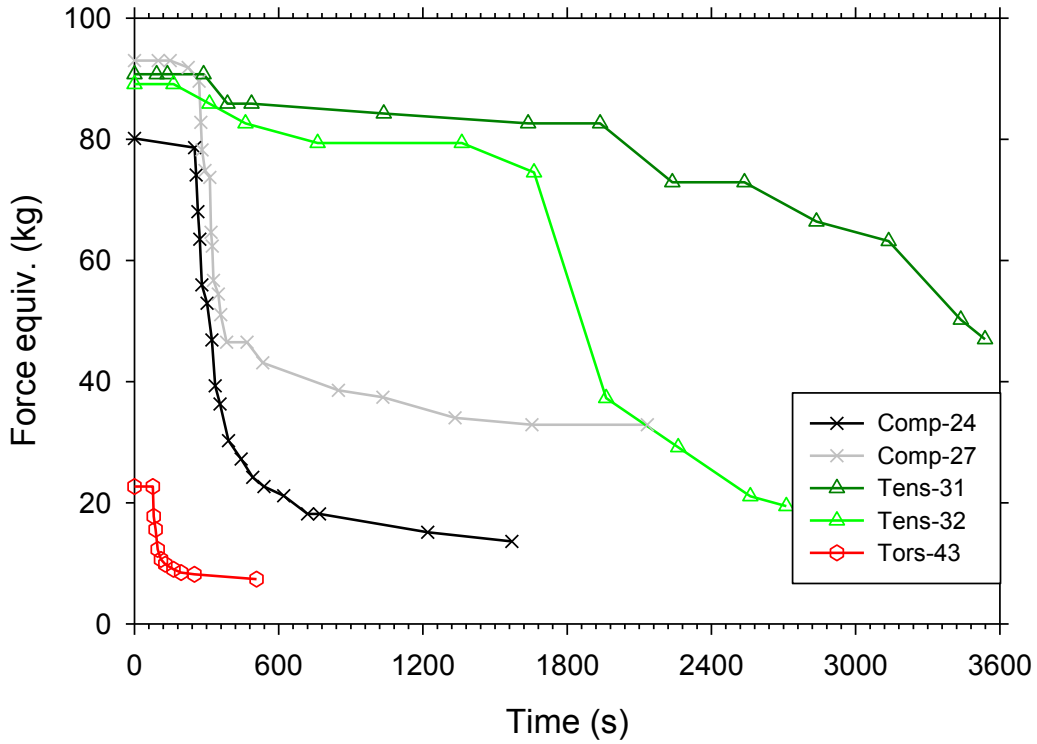


**Figure 45. Mass equivalent force on the ABDR panels as a function of time.**

Some discrepancies exist between the results of Table 6 and Figure 45. The start times were subjective and based on a wider angle view in the table. The figure reflects a more detailed view of the occurrence. More subtle motion is captured in the figure.

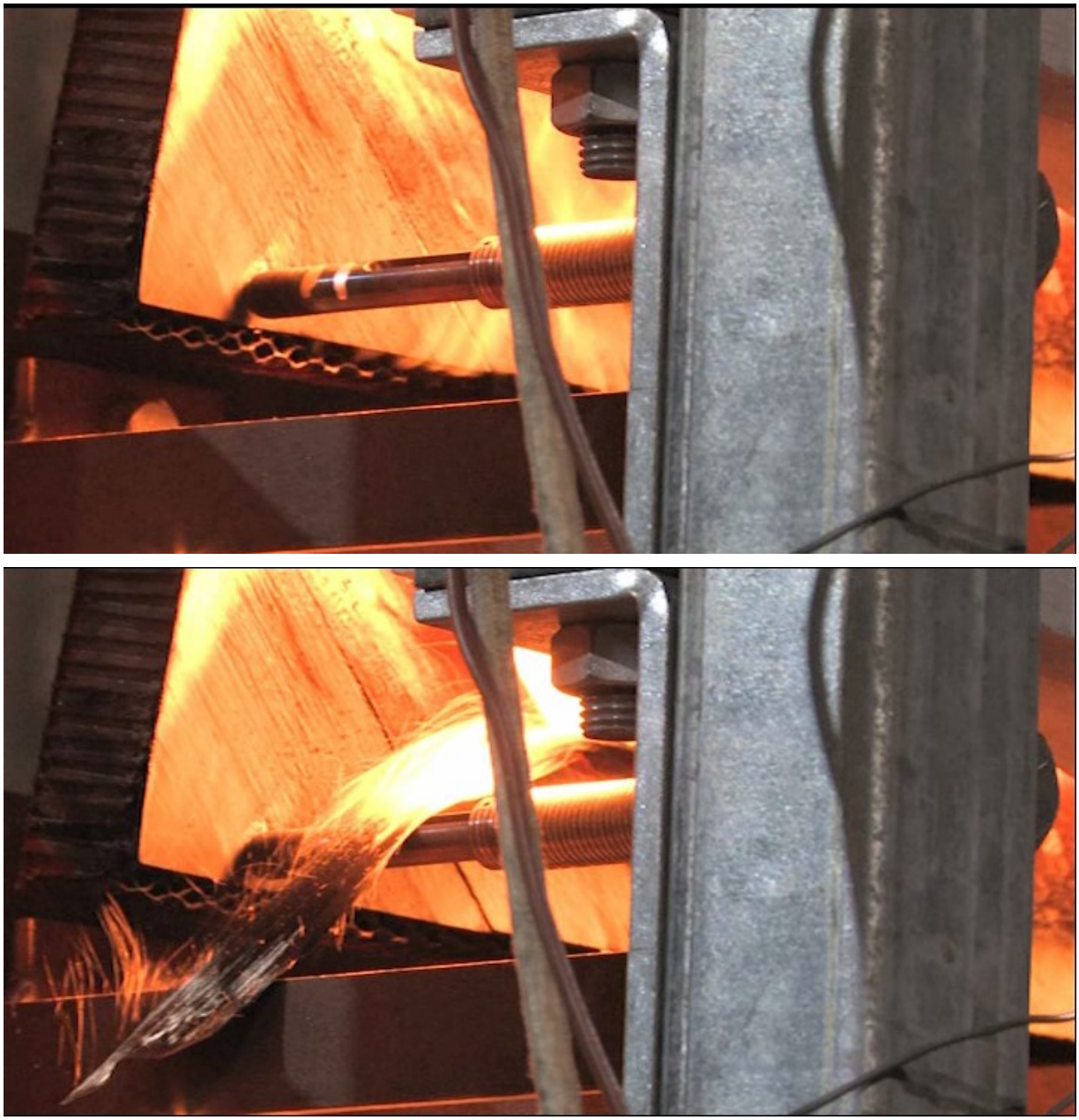

**Figure 46. Photographs of the Test 43 ABDR panel in torsion before and after the first significant movement of the fibers.**

An important note with respect to torsion Test 43 is that beside the impact of the panel on the back-plate, the data were obscured because a sheet of carbon fiber came loose and rested on the spring holder. This is illustrated in Figure 46. Subsequent motion could not be quantified. All the ABDR tests showed propensity for significant fiber movement on the front face. An important point about Test 27 is that the springs appear to have significant residual force at the end of the test. Yet in that test, the top part of the panel actually fell out of the holder at the end of the test. The residual strength cannot therefore be attributed to the panel. Minutes later, the springs relaxed slightly. The residual strength may be attributed to sticking or some

other residual force in the test apparatus itself. Drawing significant conclusions from these data in this regard should therefore be done cautiously. These data are probably better considered general guidelines as to the relative residual strength. The qualitative accuracy is probably reasonably good, however the quantitative accuracy could be improved.

**Reflectometer data**

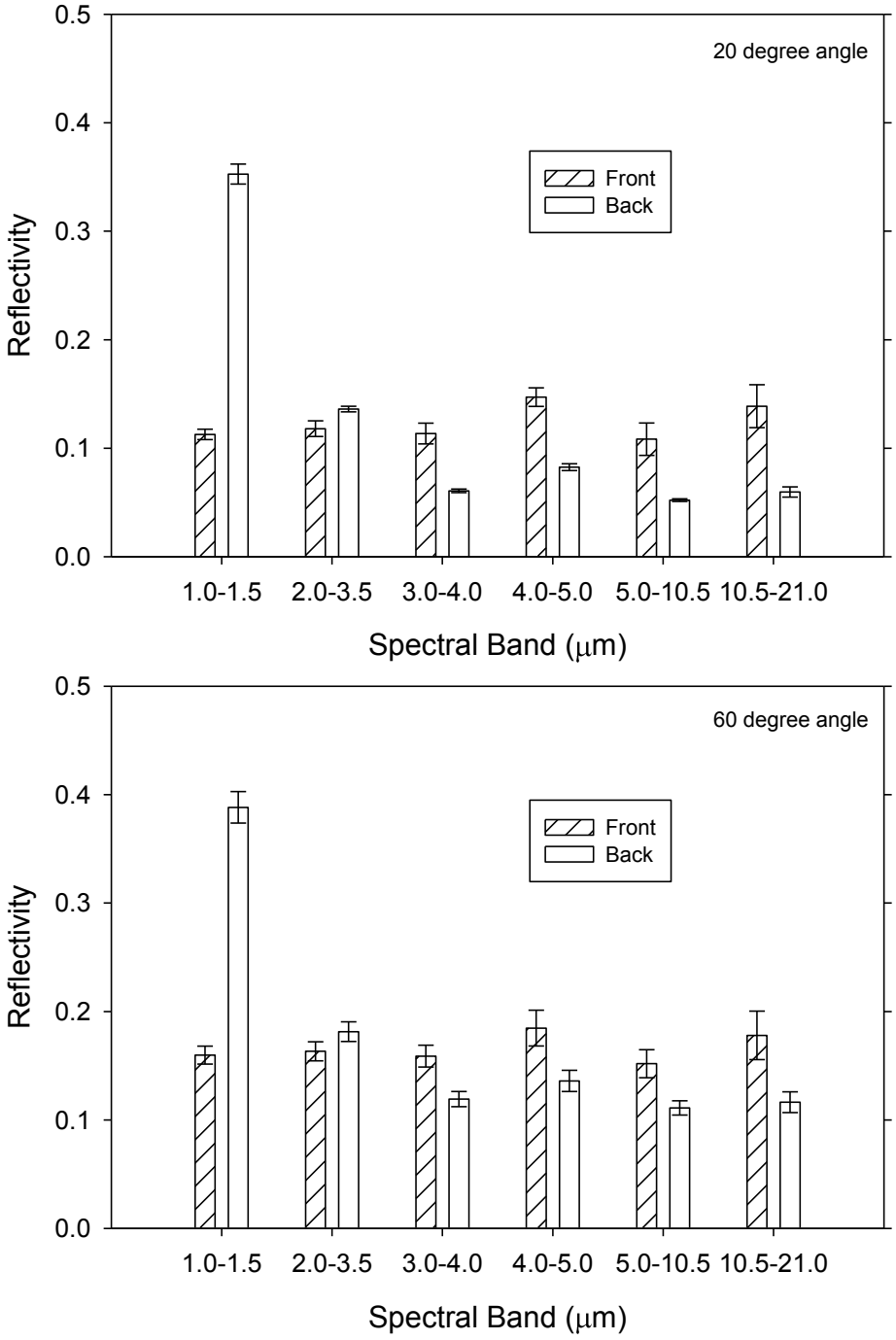


**Figure 47. Reflectivity of the ABDR panels at 20° (top) and 60° (bottom) from normal. Error bars are a single standard deviation.**

The reflectometer was used pre-test to look at spectral reflectivity of the composite surfaces, with results of these evaluations found in Figure 47. The back side was the Kevlar material, and has substantially different spectral reflectivity than the front side made from carbon fiber epoxy material. Almost every spectral band is quantitatively different between front and back side.

## *3.2 19x24 Thin Panels*

Originally not part of the test plan, this series was created mostly in response to the inability to achieve burn-through for the thicker (18x24) panels in a reasonable amount of time. The 19x24 thin panels generally burned through to completion in a little under an hour. This gave good data on the burn rates and on the structural integrity as decomposition progressed. Panels were on average. 1.35 kg with a standard deviation of .0084 kg.

This series of panel tests contained two compressive tests, a tension test, a torsion test, two tests with no force, and one test with no force with a panel that was pre-damaged. The pre-damaged panel was placed in a device designed to shear sheets of metal. A force was placed on the panel until it cracked. This was done twice, with a photograph illustrating the X-shaped breaks in the panel just prior to testing being shown in Figure 48. The center of the break was positioned such that it would be in direct exposure to the oven.

**Figure 48. A photograph of the broken panel before testing.**

The front-view videos were used to extract flaming times from the tests. These are shown in Table 7. The point at which smoking started was subjective, probably repeatable to within about a couple of seconds. End of flaming was more subjective, and probably has uncertainty on the order of tens of seconds for some of the cases. The point at which first flaming occurs was easy to discern from the videos. It was coincident with a bright flash as the smoke transitioned to flaming combustion. These are accurate to within 1 second, and only this large because the data acquisition recorded the fiducial signal to this degree of accuracy.

**Table 7. 19x24 thin panel flaming times.**

| Test | First Smoking | First Flaming | End Flaming |
|---|---|---|---|
| NoForce-37 | 1 min 26 sec | 1 min 43 sec | 8 min 1 sec |
| Comp-39 | 1 min 12 sec | 1 min 29 sec | 6 min 54 sec |
| NoForce-40 | 1 min 15 sec | 1 min 23 sec | 6 min 45 sec |
| Tens-41 | 1 min 11 sec | 1 min 20 sec | 6 min 46 sec |
| Tors-42 | 1 min 21 sec | 1 min 45 sec | 6 min 54 sec |
| Broken-44 | 1 min 7 sec | 1 min 52 sec | 5 min 58 sec |
| Comp-45 | 1 min 7 sec | 1 min 24 sec | 6 min 45 sec |

In general, between the first 1-1.5 minutes the first smoking started. Between 9 to 45 seconds later, flaming on the front face began. Active burning got stronger, diminished, and was finally done by between 6-8 minutes. Final flaming was usually small fluctuating flames around the perimeter of the peak zone of thermal intensity. A series of stills have been extracted during smoking, front face burning, and burning on the sides for each test. These are found in Figure 49 through Figure 55. At peak flaming, the front face of the panel was generally covered in flames. At later times (the 5 minute frames), the flaming was generally more restricted to localized parts of the panel face.

1 min 40 sec 2 min: 5 min:

**Figure 49. Front side images for 19x24 thin Test 37.**

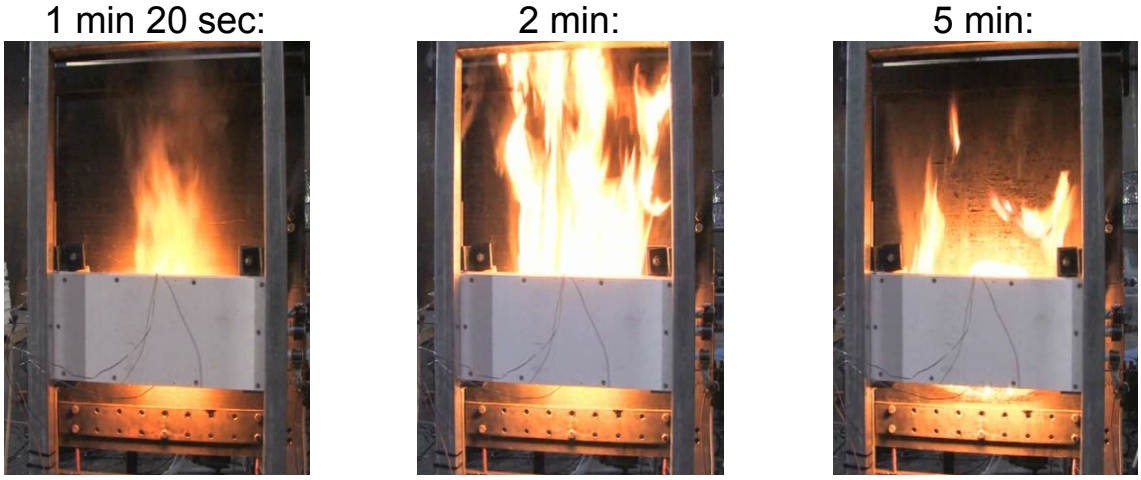


**Figure 50. Front side images for 19x24 thin compression Test 39.**

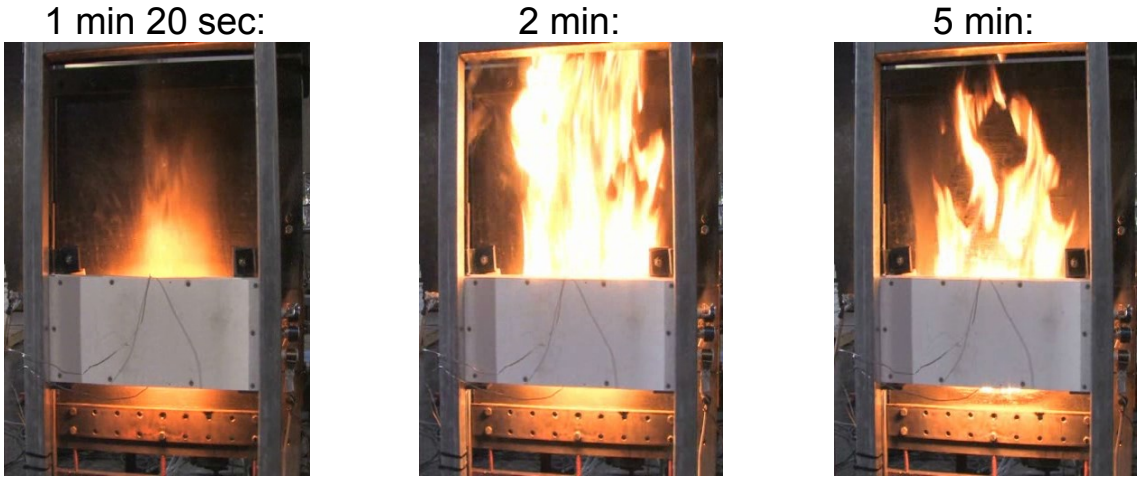


**Figure 51. Front side images for 19x24 thin Test 40.**

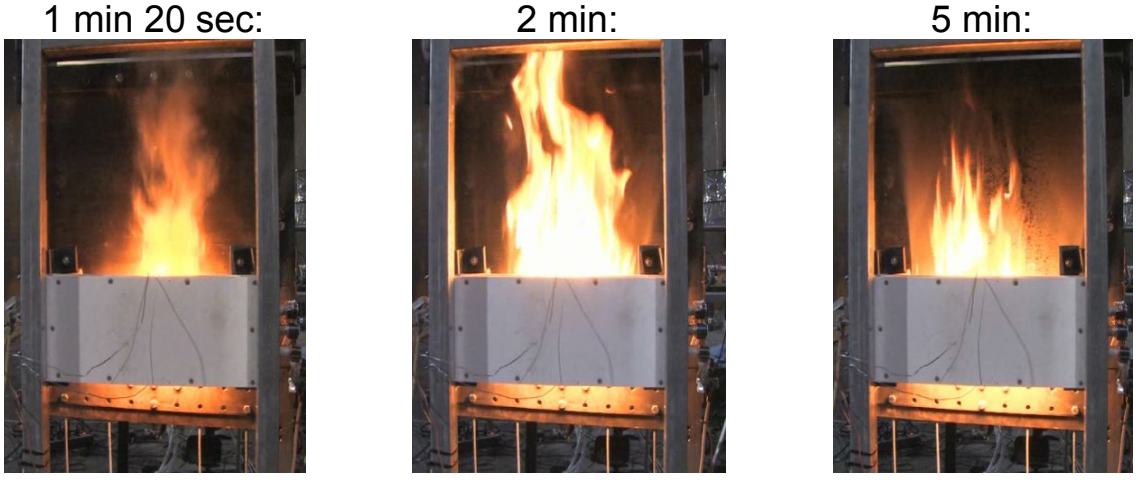


**Figure 52. Front side images for 19x24 thin tension Test 41.**

1 min 30 sec: 2 min: 5 min:

**Figure 53. Front side images for 19x24 thin torsion Test 42.**

1 min 20 sec: 2 min: 5 min:

**Figure 54. Front side images for 19x24 thin broken panel Test 44.**

1 min 20 sec: 2 min: 5 min:

**Figure 55. Front side images for 19x24 thin compression Test 45.**

### 3.2.1 Mass loss data

Panels on average lost 22.7% of their mass during the test (77.3% mass remaining). Percentage of the mass remaining is shown in Figure 56. These tests were fairly repeatable in terms of mass loss (within 3%), and there are no trends associated with the nature of the force on the panel.

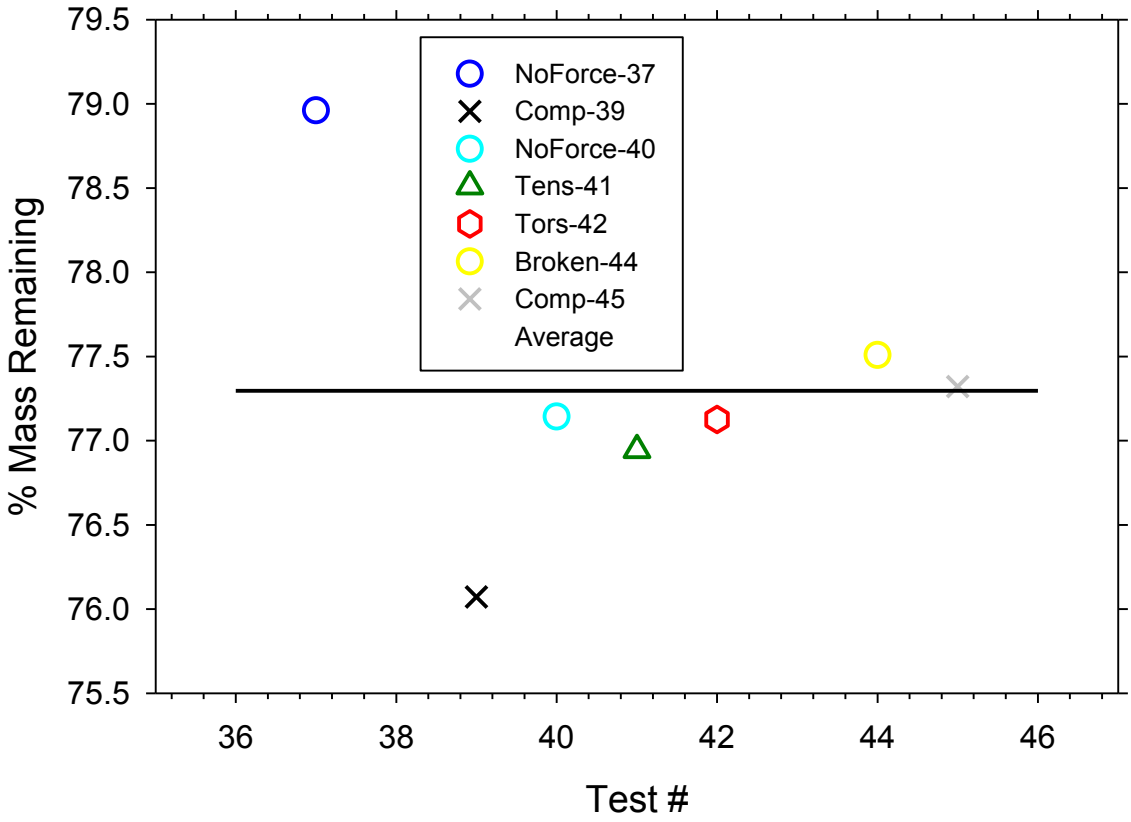


**Figure 56. Total mass loss summary for the 19x24 thin panels.**

Typical panel response involved a short period of flaming on the front face of the panel. Unlike the ABDR sandwich panels, these panels did not exhibit significant flaming on the edges. These panels had more mass, and consequently were less susceptible to noise. Typical raw mass traces are found in Figure 57. In this plot, raw data for test 39 were transposed down by about 0.1 kg to make them more visible in the plot.

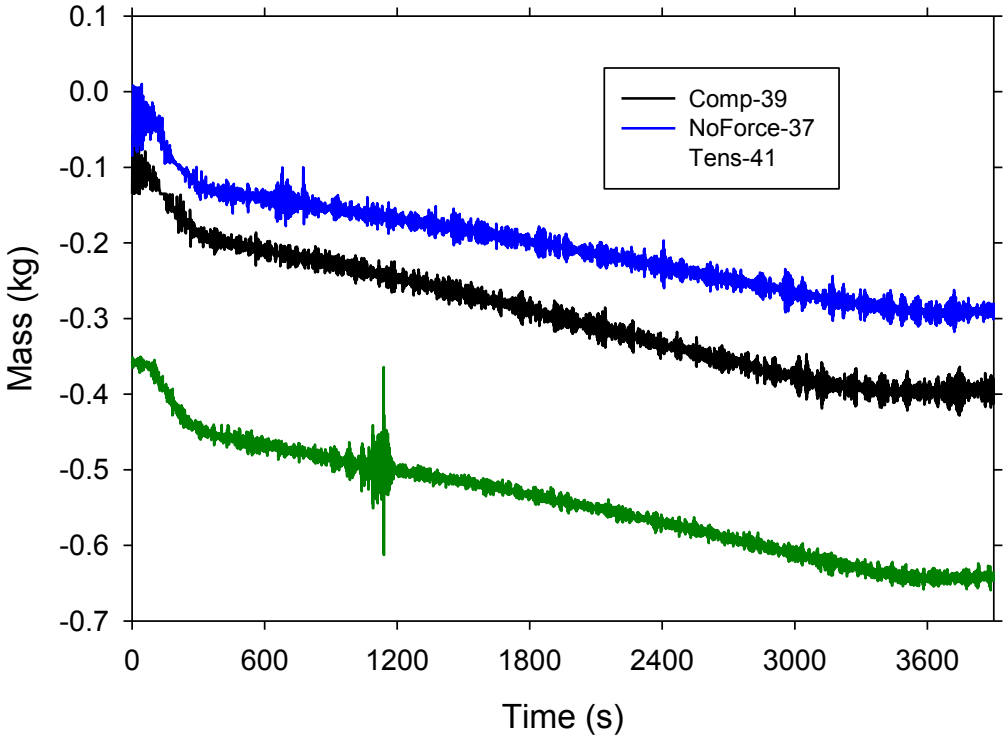


**Figure 57. Typical mass loss raw data for the 19x24 thin panels.**

Rate of mass change summary data for the 19x24 thin sandwich panels are found in Figure 58. These are plotted much like in the previous section, averaged at 5 minute intervals. Tests were fairly consistent with respect to mass loss. The most apparent outlier was the torsion test which tended to decompose slowly and thus lasted much longer than the others. The reason for this is believed to be due to the nature of the torsion test. The spring never fully compressed for the torsion scenario. As a consequence, the panel was from the start of the test distorted away from the oven. This is believed to have contributed to low mean oven temperatures and slower reaction rates, as the panel was further away from the heat source.

Like the ABDR sandwich panel tests, these 19x24 thin panel tests exhibited the highest decomposition rate during the first 5 minutes as flaming ensued. Flaming started between 1-1.5 minutes, and was fairly repeatable from panel to panel.

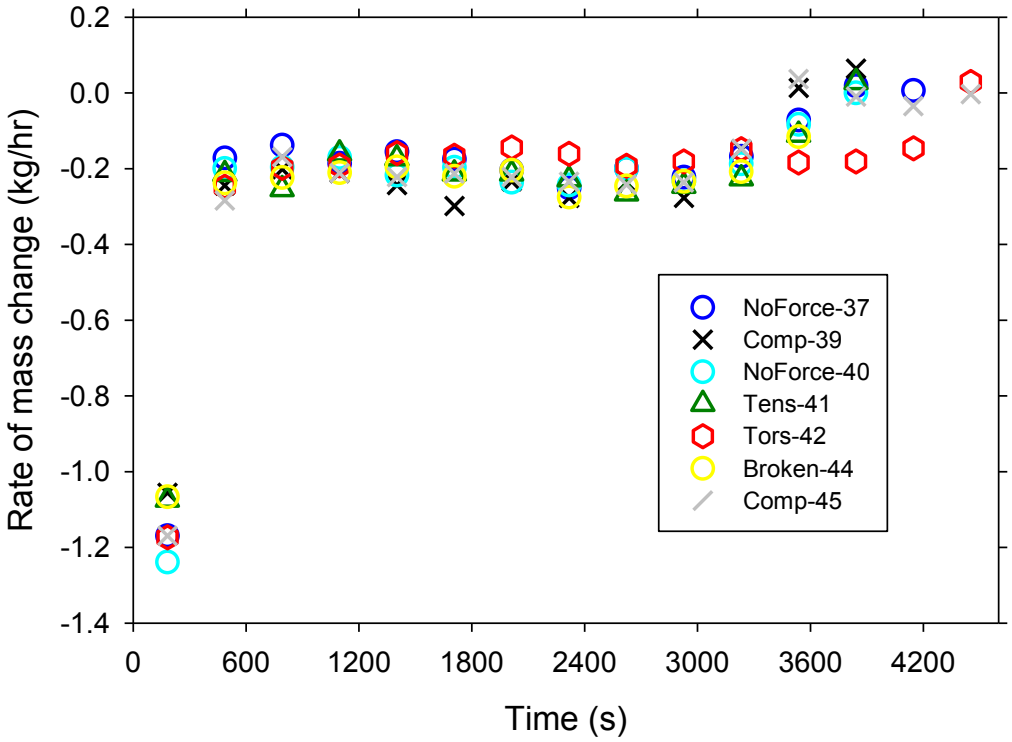


**Figure 58. Rate of mass change summary data for the 19x24 thin panels.**

Of the tests series conducted, this one (19x24 thin panels) had what are believed to be the most reproducable test times. This may in part be because the compression test resulted in less distortion than any of the other compression tests with different panels. Indeed the compression tests never showed any degree of relaxation of the springs due to the panel decomposition. Besides being thinner, these panels were slightly wider than the 18x24 panels by about 2.5 cm and than the ABDR panels by 17.7 cm. The reproducability is evident in the test time plot, Figure 59.

Figure 60 shows the peak flaming mass loss rate. There is not good indication of any relationship between the type of force on the panel and the rate of flaming decomposition.

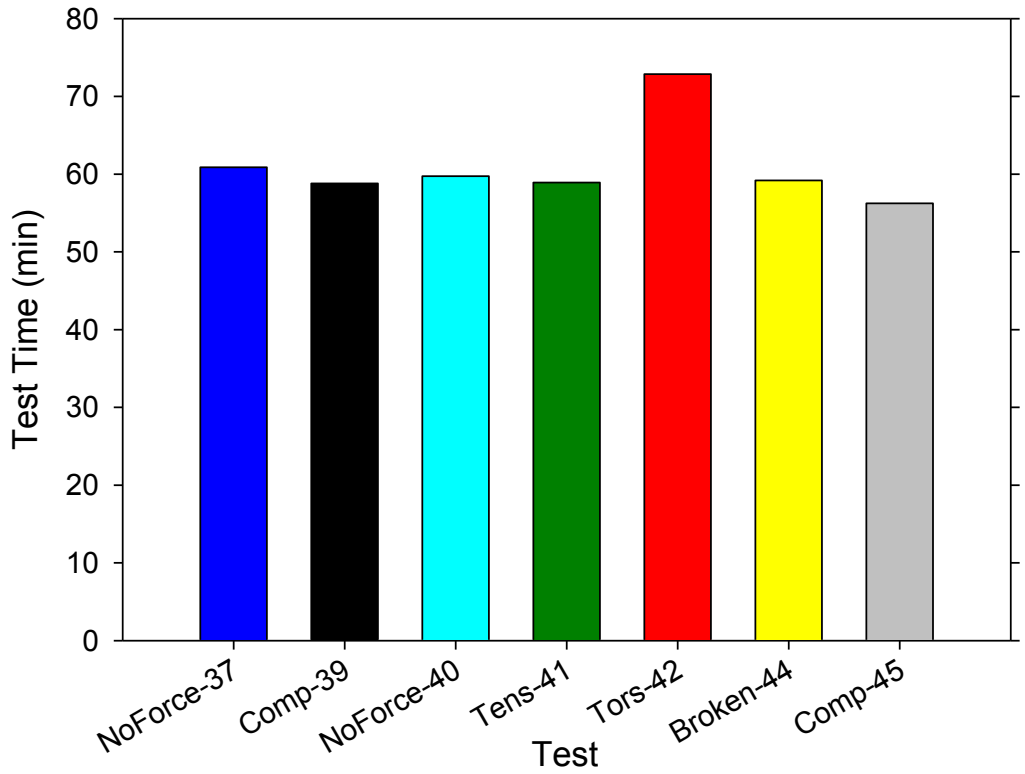


**Figure 59. Test time summary data for the 19x24 thin panels.**

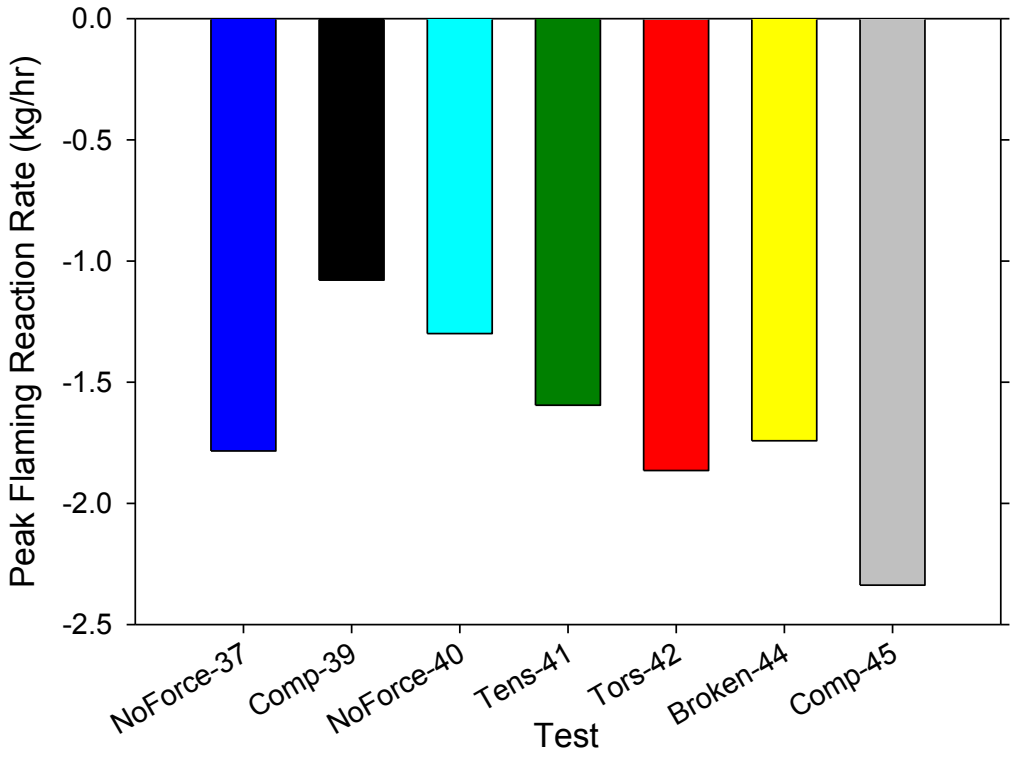


**Figure 60. Peak flaming mass loss rate data for the 19x24 thin panels.**

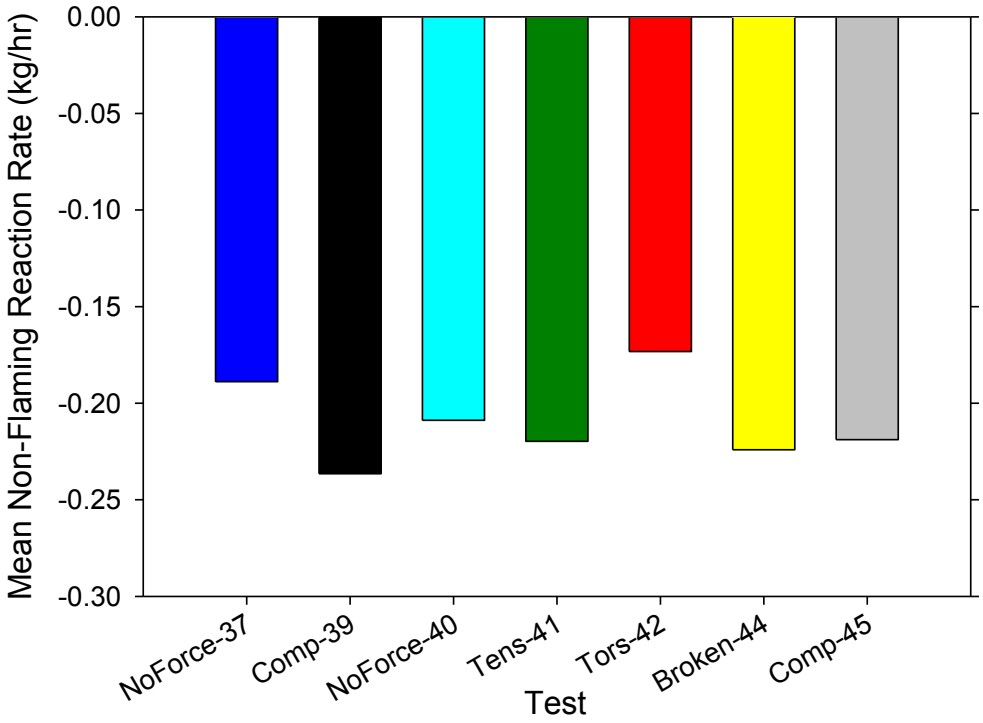


**Figure 61. Mean Non-Flaming mass loss rates for the 19x24 thin panels.**

Figure 61 shows the mean non-flaming mass loss rates for the 19x24 thick panels. No relationship between the type of force and the rate of reaction is evident.

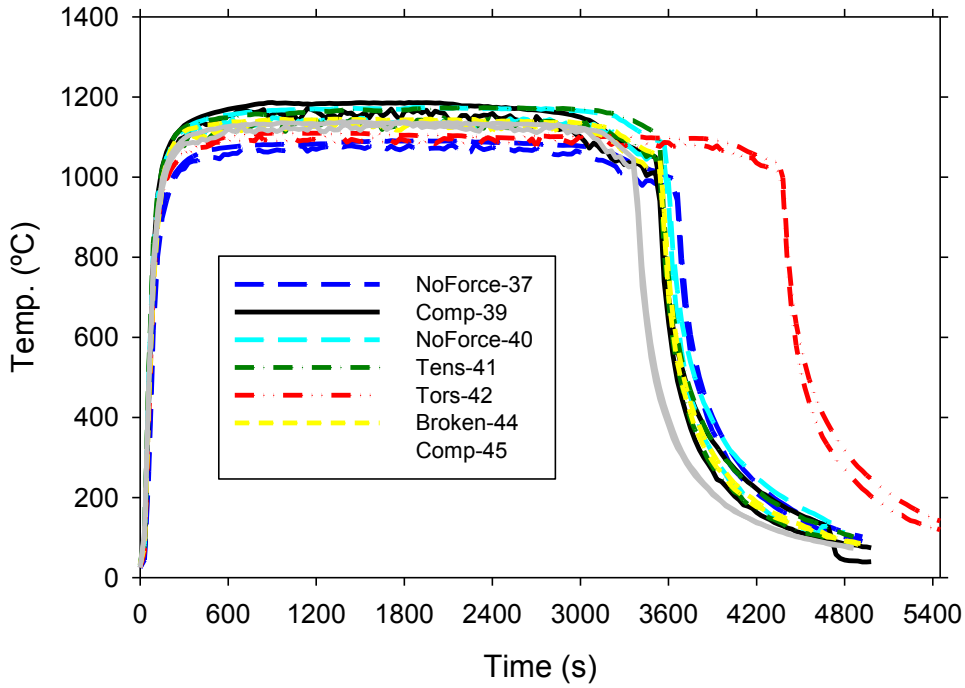


**Figure 62. Oven temperatures for the 19x24 thin panel tests.**

As with the previously described test series, the 19x24 thin panels exhibited some variability in oven thermocouple readings. Figure 62 shows these measurements. The results from Figure 61 and Figure 62 appear to be correlated, as the low and high oven temperature data appear to result in low and high non-flaming mass loss rates respectively.

### 3.2.1 Radiometer Data

Radiometer data are found in the next six plots. Figure 63 shows front side measurements at the mid-point of the panel. Similar to the previous dataset, the flaming is evident at early times and characterized by the highest fluxes. Post-flaming steady-state fluxes appear to vary widely, with a spread of about 15 $kW/m^2$. However, this spread does not appear to correlate to any type of imposed force on the panels. Figure 64 shows a similar flaming peak, and much less variability during post-flaming reactions. Figure 65 shows data from a back-side point 3/4 up the panel directly opposite to the data in Figure 64. Unlike the ABDR data, which showed no relationship, the 19x24 thin panel data suggest a close relationship between results at the two locations. Back-side fluxes are around one half to one third that of the front side, and vary high during flaming combustion followed by low during glowing combustion. Figure 66 also shows back-side trends that echoes those found on the front-side directly opposite the measuring point for Figure 63. Figure 67 and Figure 68 show back-side fluxes at a point a quarter of the way up from the bottom of the panel. These show gradual increases until near the end of the test where there is a rapid increase as a hole develops in the panel and the oven is exposed to the radiometer. The off-center data in Figure 68 are a little more variable, probably due to variability in the shape of the hole created by the oven.

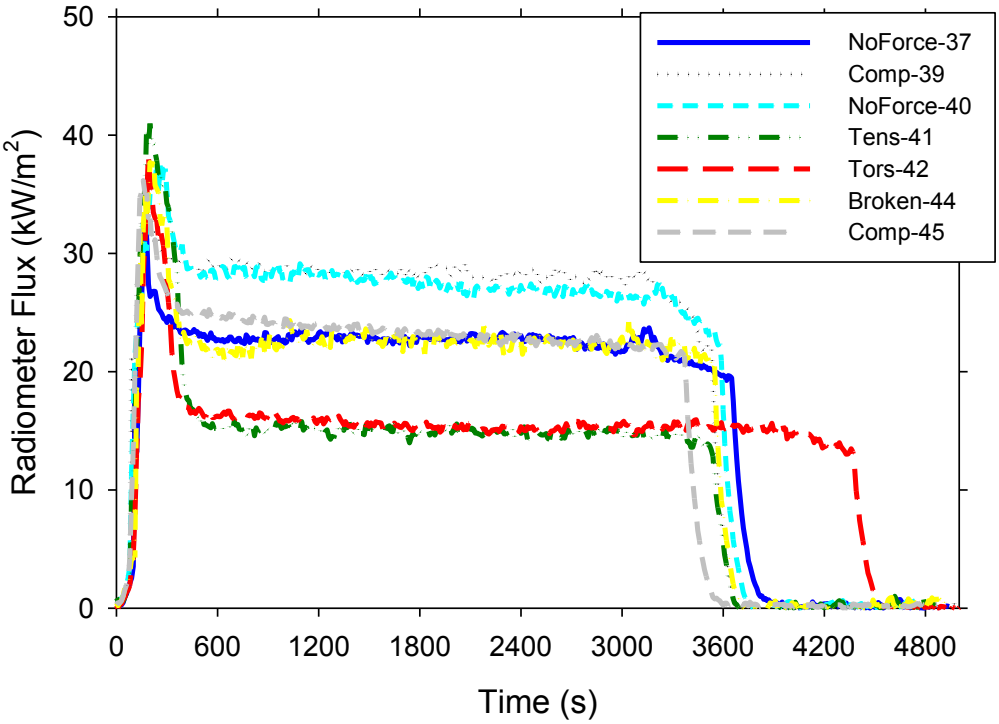


**Figure 63. 19x24 thin panel radiometer readings from the front of the panel at ½ way up the panel from the bottom.**

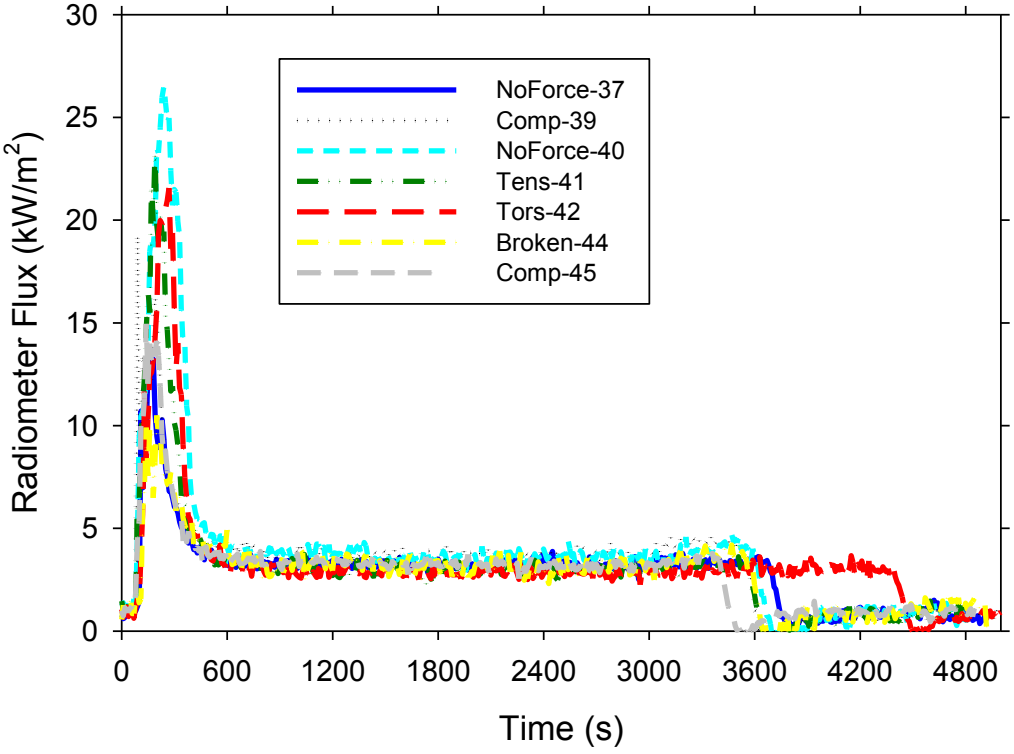


**Figure 64. 19x24 thin panel radiometer readings from the front of the panel at ¾ of theway up the panel from the bottom.**

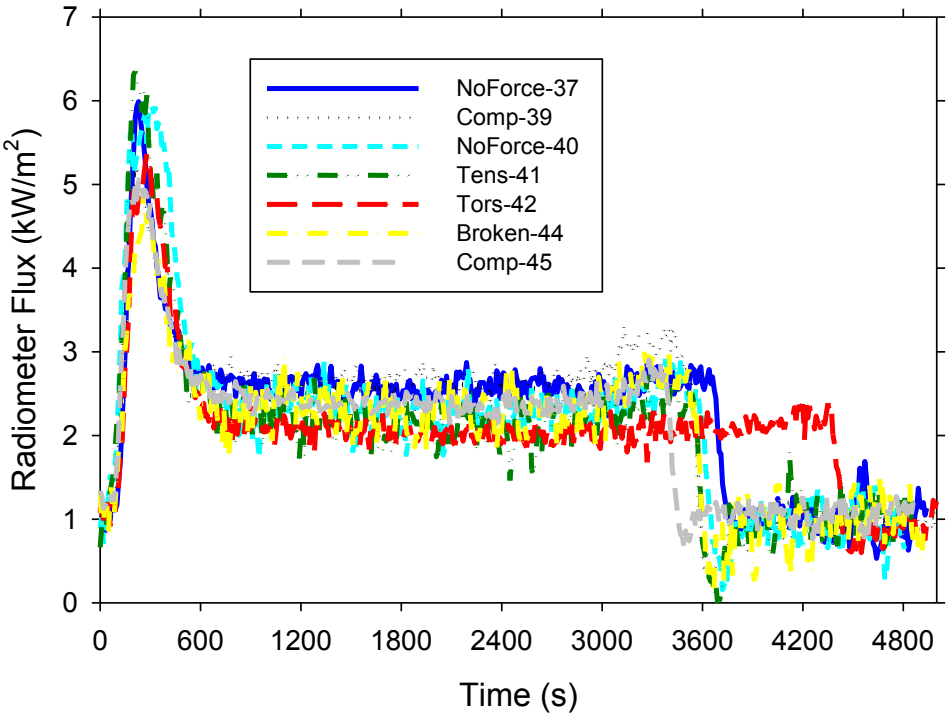


**Figure 65. 19x24 thin panel radiometer readings from the back of the panel at ¾ of the way up the panel from the bottom.**

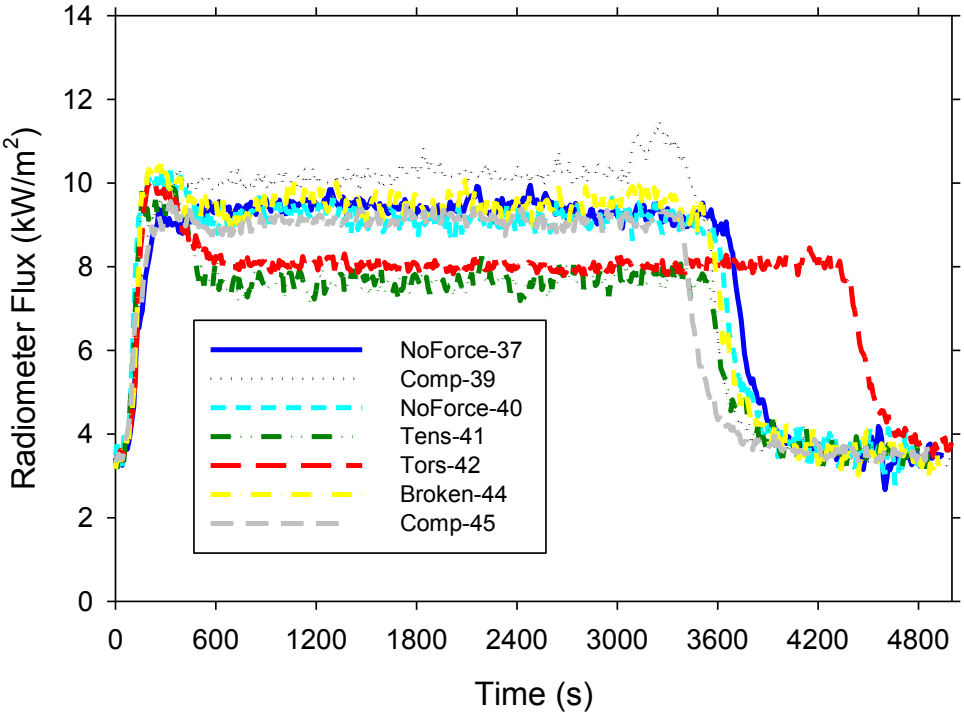


**Figure 66. 19x24 thin panel radiometer readings from the back of the panel at ½ way up the panel from the bottom.**

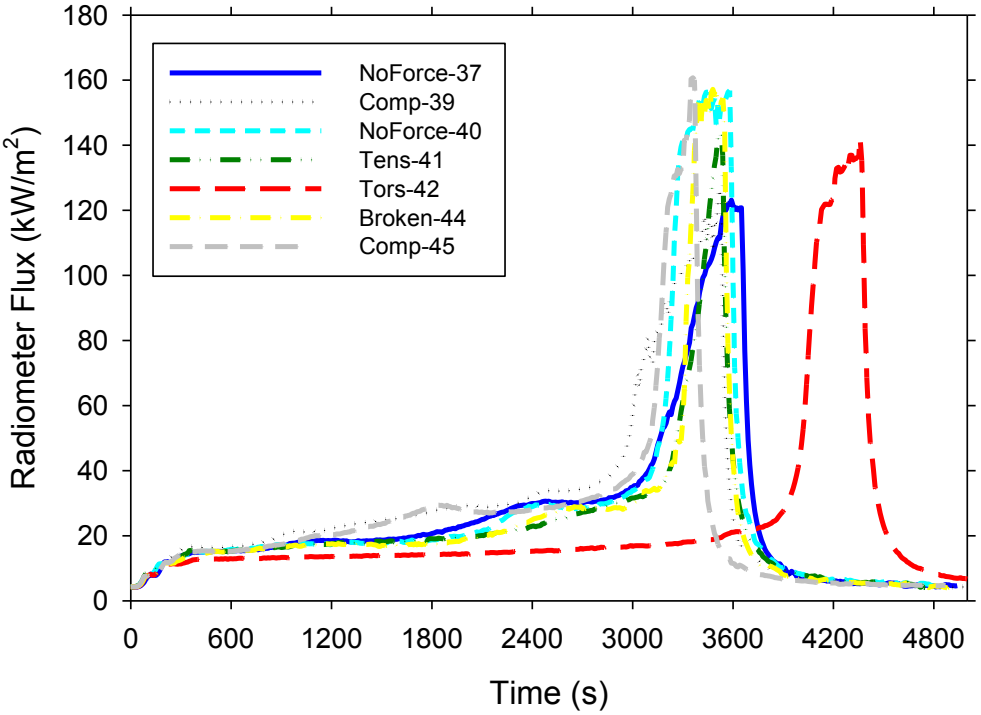


**Figure 67. 19x24 thin panel radiometer readings from the back of the panel at 0.25 from the bottom.**

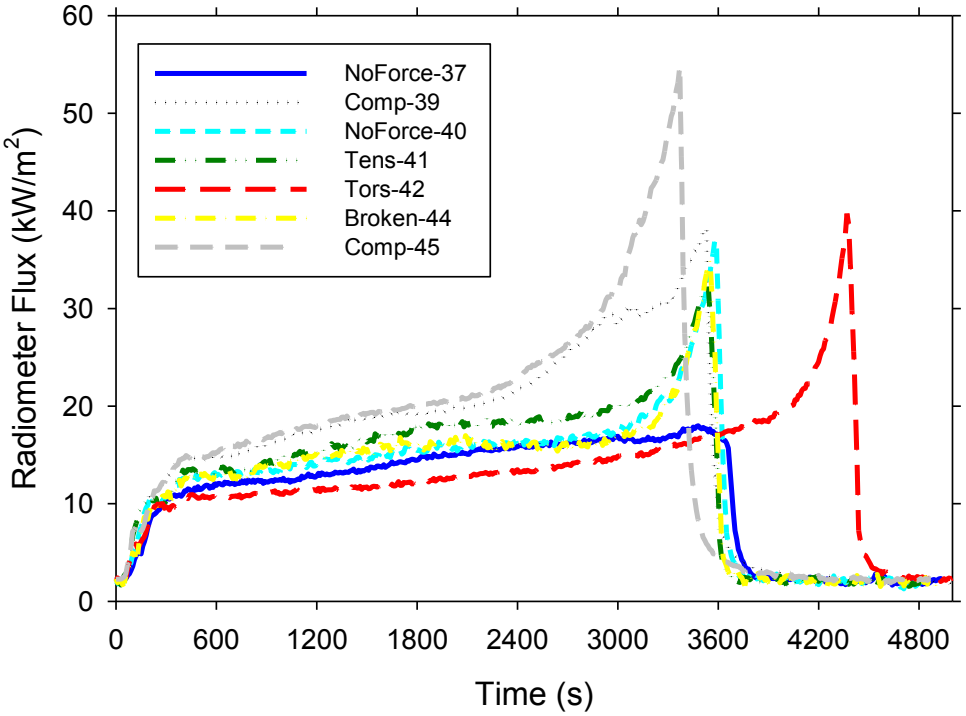


**Figure 68. 19x24 thin panel radiometer readings from the back of the panel offset at 0.25 from the bottom.**

### 3.2.2 IR Data

The radiometer data were confirmed with the IR camera data by extracting the temperature at the measurement locations. Because the IR camera had fixed ranges of data extraction and the data were often saturated, only an example series of camera images are reproduced here to show the typical measurements. Highlighted on each image are the focus points for the radiometers. Figure 69 shows frames extracted at various times during the progress of compression Test 45.

IR camera data mostly show the shape of the thermal environment imposed by the oven on the panel as it conducts through the panel. Early frames at 1 minute 7 seconds and 13 minutes 20 seconds show progression at early times. From 40 to 50 minutes at every 5 minutes, the late-term heat-up of the back side is seen in the scale of the images. By about 50 minutes, only a thin layer of fibers hid the oven rods from the camera view. By about 55 minutes, a significant hole had formed through which the oven rods were visible.

1 min 7 sec:

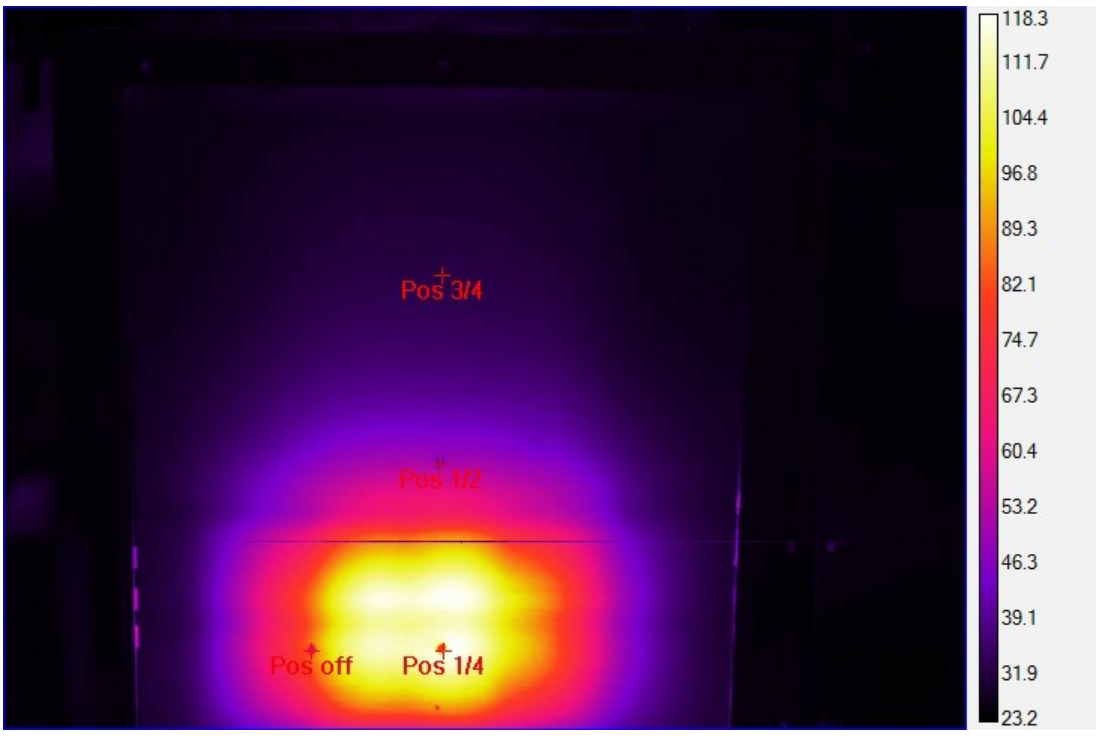

13 min 20 sec:

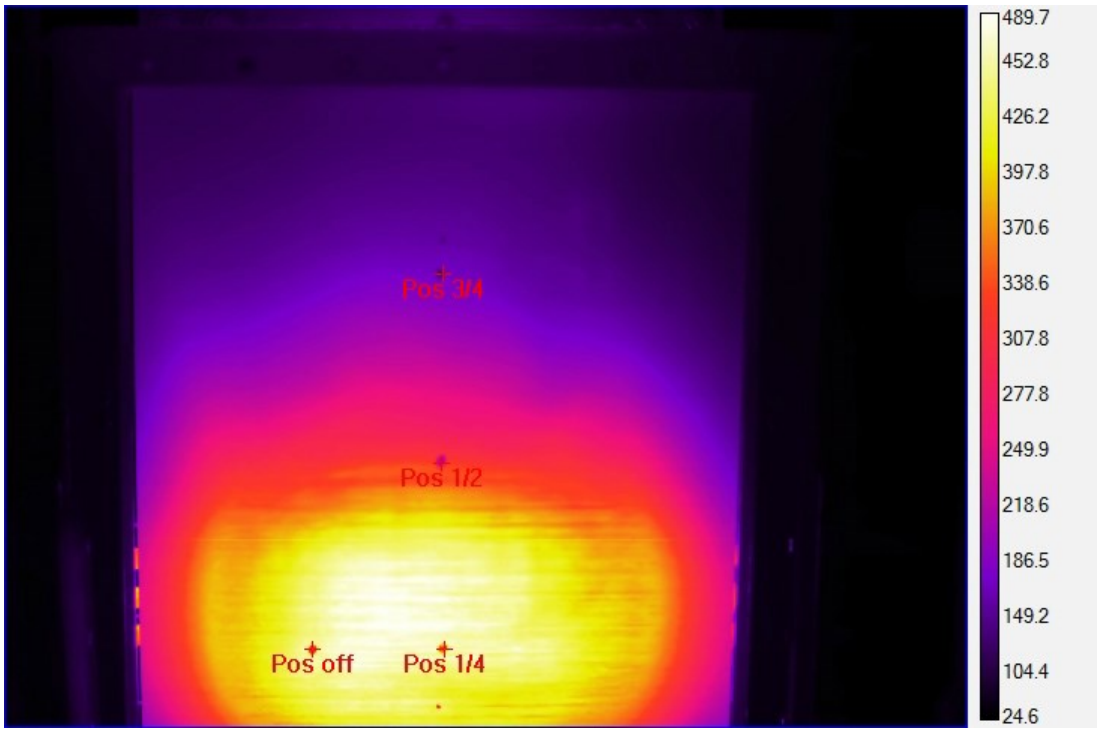


40 min:

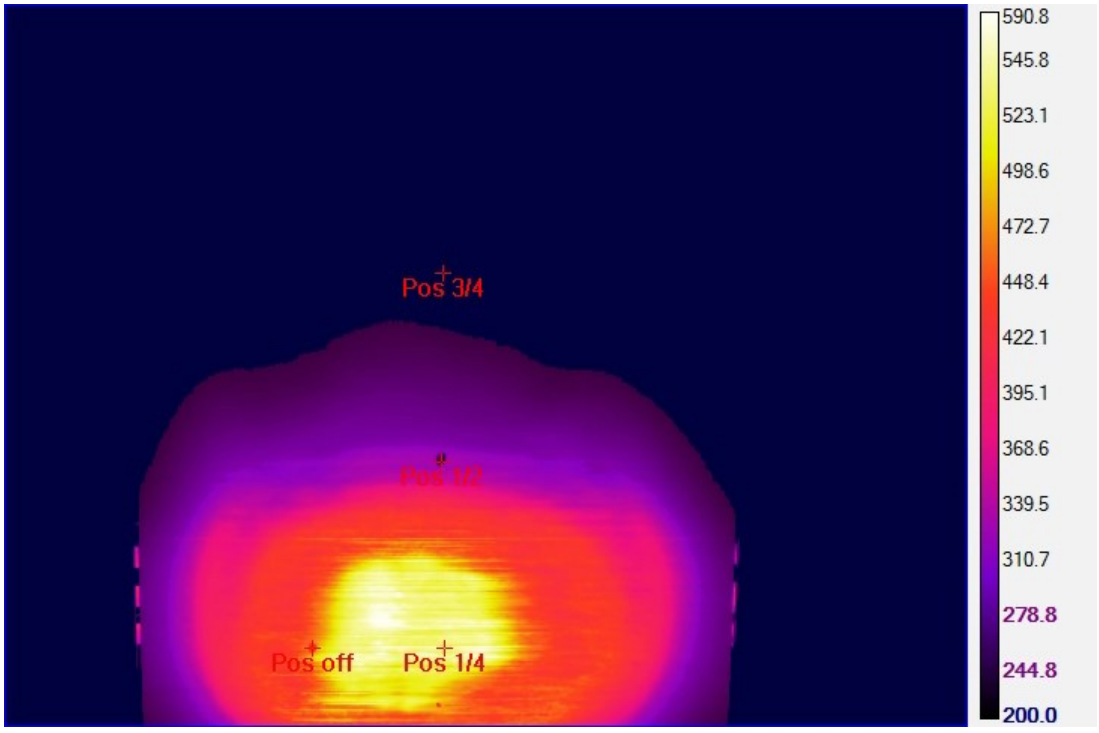

45 min 7 sec:

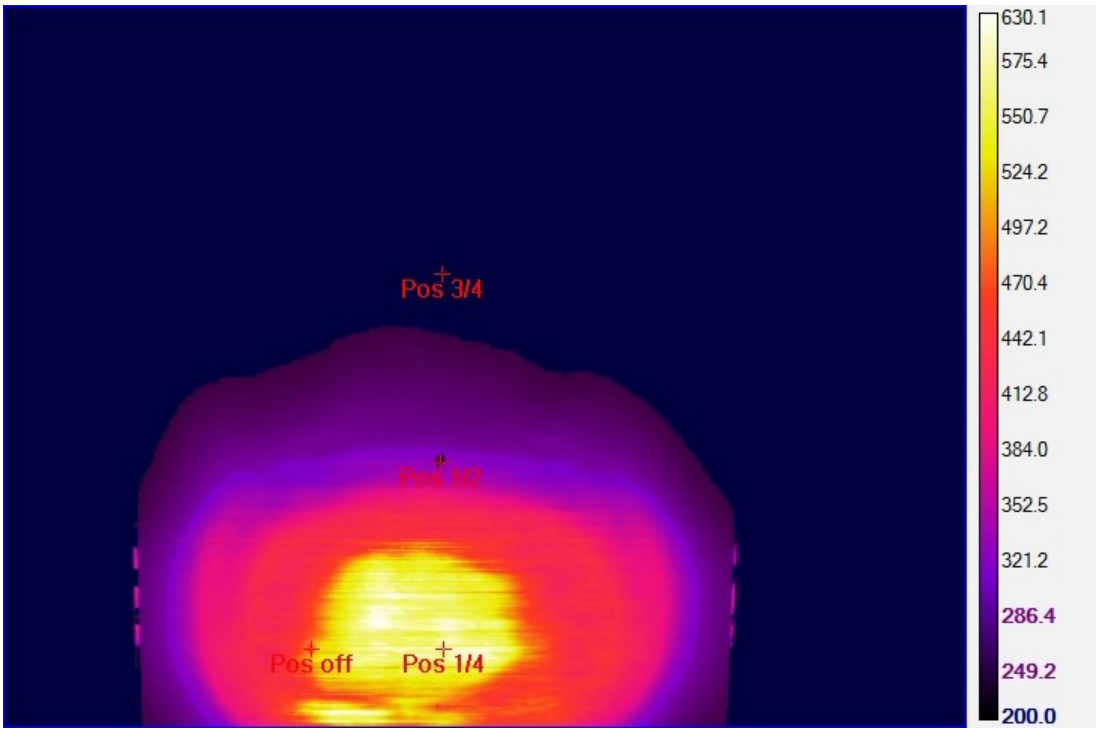


50 min:

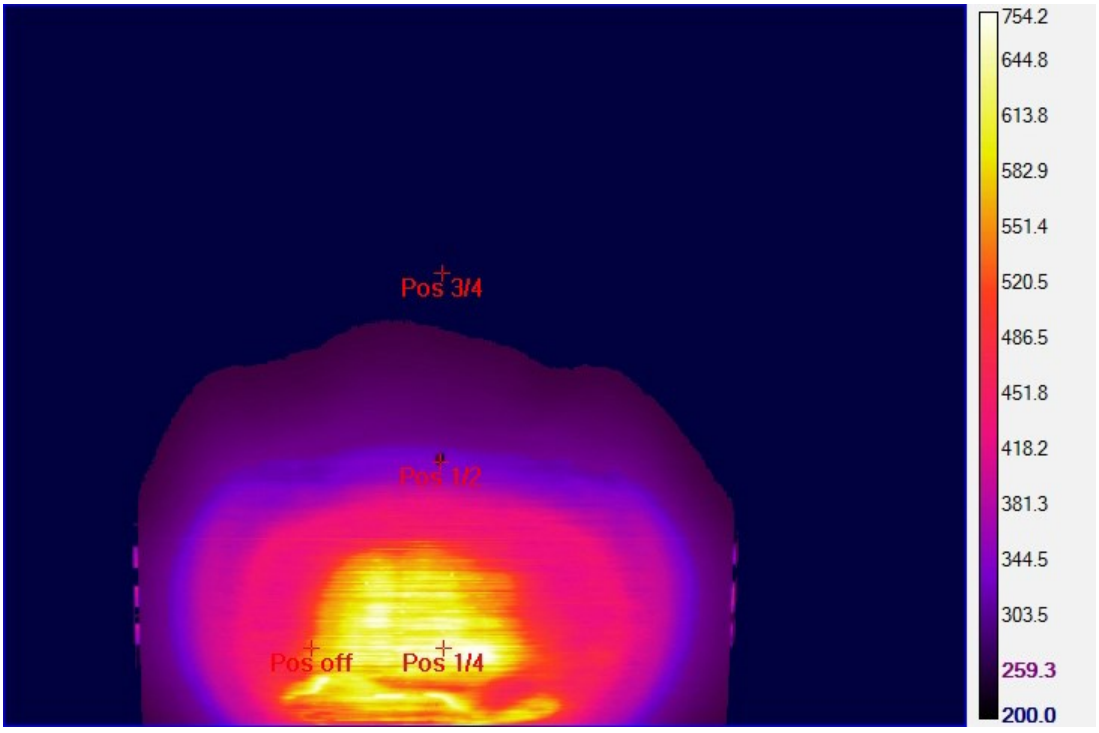

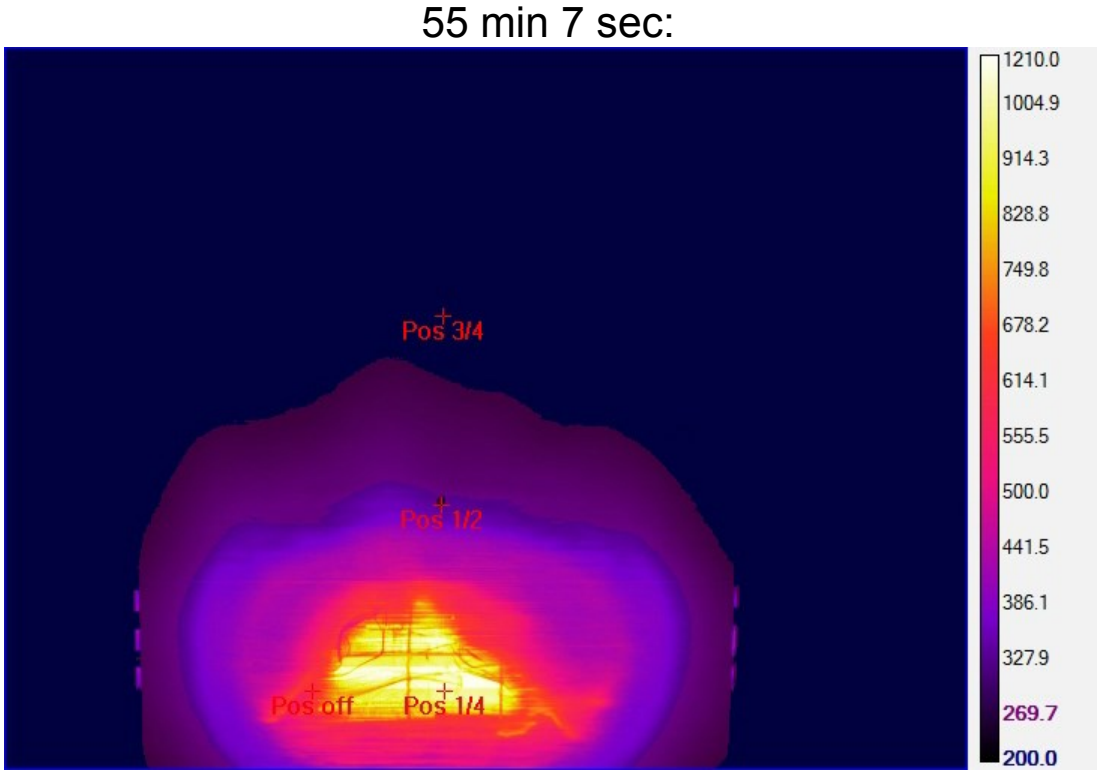


**Figure 69. IR camera images from Test 45, the 19x24 thin panel in compression (Temperatures in °C).**

### 3.2.3 Load data

The 19x24 thin panels were unique in that they did not tend to move significantly with the force imposed. Compression tests exhibited full loading at the end of each test, despite a hole having been formed in the panel. The tension test did not exhibit stretching or tearing like the ABDR tests, rather the material softened around the bolt holes and the panel sheared across the bolts. This was not the desired behavior, and possibly would not have happened except that the three bolts were placed as centered as possible on the panel. Had they been spaced wider, the panel might not have behaved the same way. The torsion test did not exhibit significant movement because this panel would not hold much torsional force. The spring would not compress more than a few millimeters, as the panel deformed with the smallest imposed force. Consequently, the deformation data in this section is not as interesting as was found in the other sections. Details on the structural response for the tests are found in Table 8.

**Table 8. 19x24 thin panel spring movement summary.**

| Test | Force Type | First Movement | Last Movement | Nature of Movement |
|---|---|---|---|---|
| 39 | Compression | - | - | None |
| 41 | Tension | 15 min 48 sec | 19 min 28 sec | Shearing off the bottom bolts at a slow pace over about 3.5 minutes. |
| 42 | Torsion | 3 min 3 sec | 12 min 28 sec | Steady movements for about six or seven minutes, slowing afterwards to a creep. |
| 45 | Compression | - | - | None |

It is in a way fortuitous that the compression tests did not deform, as this presumably gave better repeatability in the data. Without significant deformations, the effect of the deformations on the reaction rate due to material moving closer to the oven is minimized. However, this difference in behavior of these tests compared to the tests with the other two panels is surprising, and difficult to attribute. This point is discussed in more detail in a later section.

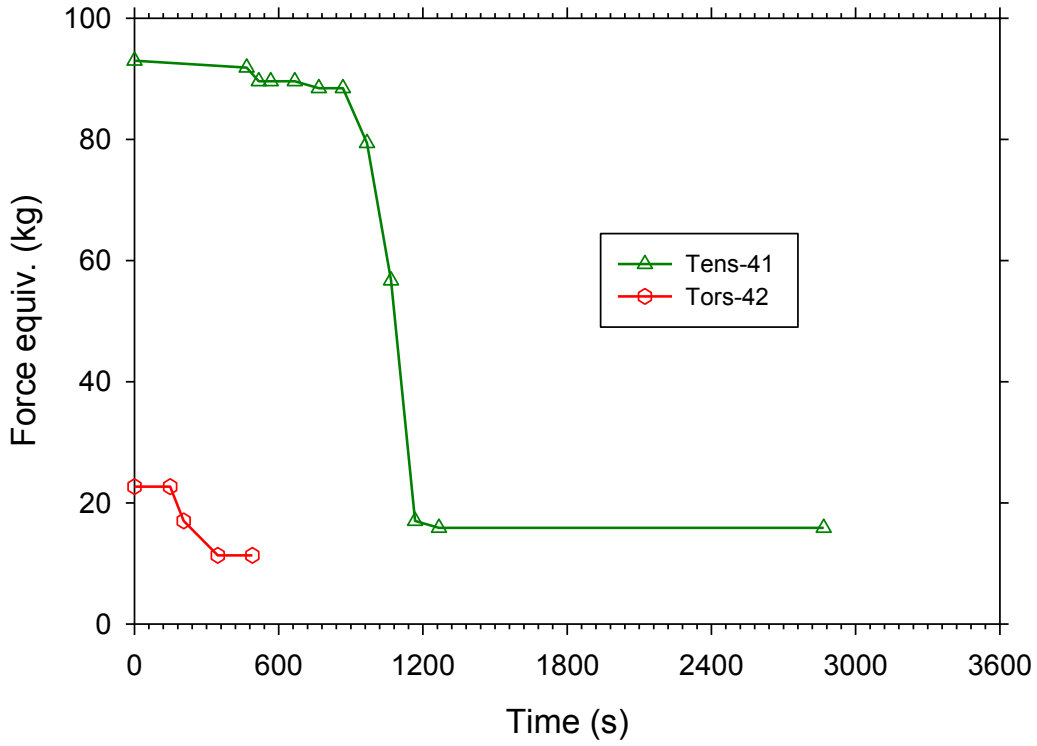


**Figure 70. Mass equivalent force on the 19x24 thin panels as a function of time.**

Figure 70 shows a more detailed view of the movement in the two tests where movement occurred. The tension panel was mostly rigid until about 15

minutes, after which rapid movements ensued as the panel pulled clear of the retaining bolts. The torsion test results look very similar to those of the ABDR panel. The panel was unable to support much force in torsion.

### 3.2.4 Reflectometer data

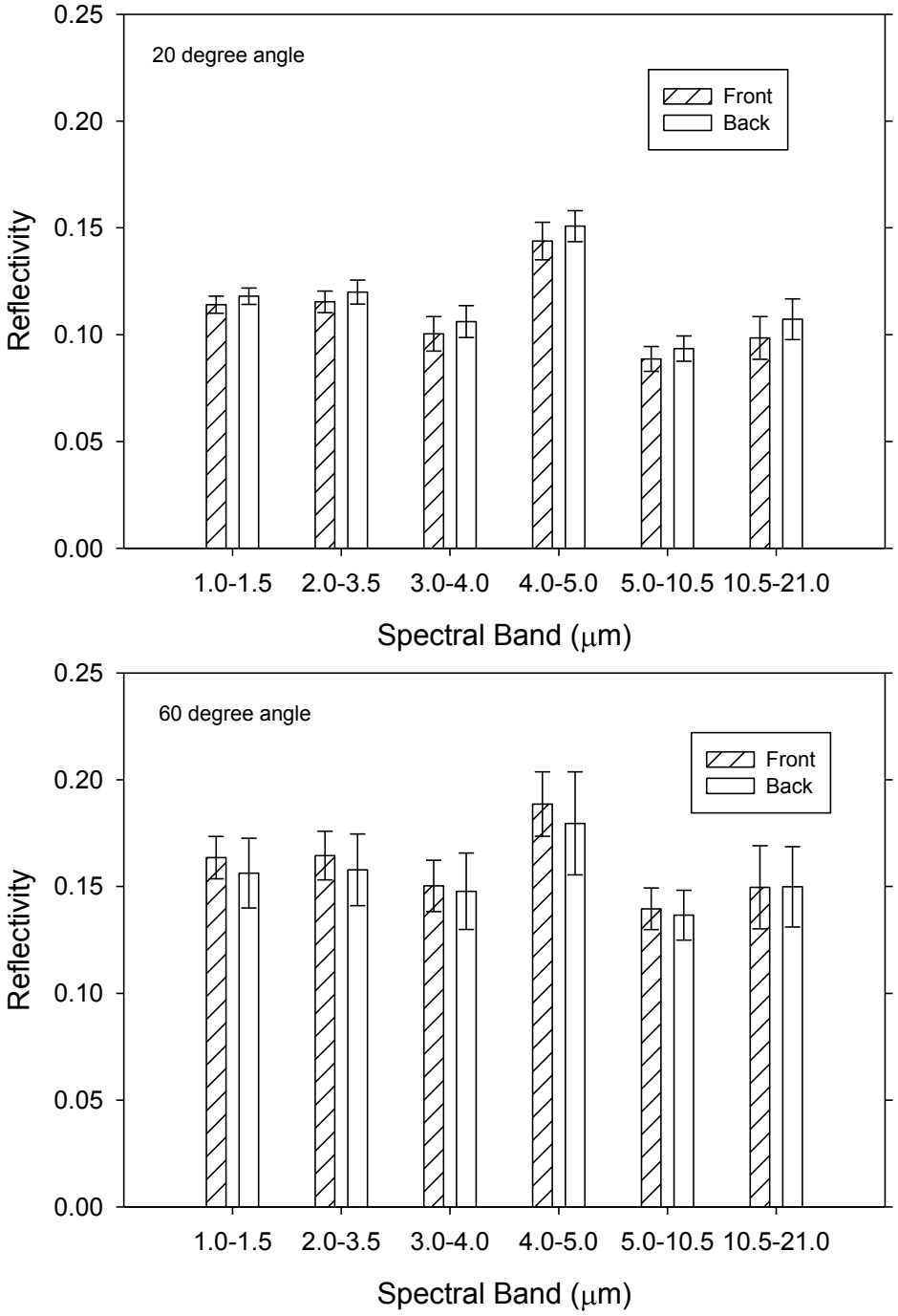


**Figure 71. Reflectivity of the 19x24 thin panels at 20° (top) and 60° (bottom) from normal. Error bars are a single standard deviation.**

Figure 71 shows reflectometer data from 19x24 thin panels. These panels were considered the same on the front and back sides, as there was not a discernable difference. These front and back side data therefore reflect the variability in measurements. Repeatability is demonstrated in that the front and back side IR reflectivities are within the single standard deviation error bars of each other for all spectral bands at both incidence angles.

## *3.3 18x24 Thick Panels*

The 18x24 thick panel tests were significantly different from the other two tests in that they involved reactions over a fixed amount of time. Tests were run for approximately four hours, after which time the tests were suspended. Examination of the panels after the first test showed little chance of being able to consume a hole completely through the panels in a reasonable amount of time. In fact, after four hours, a surprisingly small amount of decomposition was evident on the surface, as suggested by Figure 72. This finding was somewhat unexpected, as the same material had been tested in the previous test series (Brown et al., 2012) and found under thermally immersive conditions to consume approximately 26 kg of material in five hours. Like the previous tests, decomposed material left a white film or residue. Unlike the previous tests, there were tracer strips that appear to be a strand of bundled glass fibers which were traversing the layers. These also did not decompose during the tests. These residual materials presumably formed a protective layer that inhibited oxygen transport to the carbon beneath. This may account for the lower reaction rates in late-term testing.

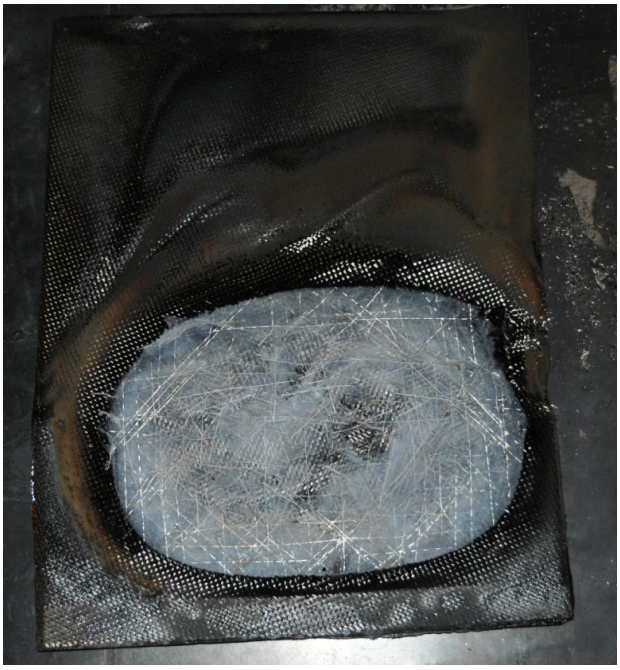

**Figure 72. A front-side post-test photograph of the panel from Test 26.**

The front-view videos were used to extract flaming times from the tests. These are shown in Table 9. Because of the blown fuse in Test 29, the extracted times are only approximate. End of flaming was very subjective, and probably has uncertainty on the order of tens of seconds to minutes for some of the cases. Flames and smoke can be difficult to distinguish in some videos, and often times flames can re-emerge after being out for a short time. The point at which first flaming occurs was typically easy to discern from the videos. Test 30 never exhibited profuse flaming, rather at around 9 minutes it exhibited spot flaming near the oven, and was an outlier compared to the rest of the tests.

**Table 9. 18x24 thick panel flaming times.**

| Test | First Smoking | First Flaming | End Flaming |
|---|---|---|---|
| Comp-26 | 0 min 57 sec | 3 min 50 sec | 19 min 46 sec |
| Tens-29 | 1 min 0 sec* | 5 min 19 sec | 15 min 26 sec |
| NoForce-30 | 1 min 11 sec | 8 min 46 sec | 14 min 27 sec |
| Comp-34 | 0 min 38 sec | 3 min 59 sec | 19 min 59 sec |
| Tens-35 | 1 min 2 sec | 6 min 7 sec | 18 min 44 sec |

*This value by assumption, subsequent values referenced from this time

In general, between the first 0.5-1.5 minutes the first smoking started. Flaming was not particularly repeatable for these tests, occurring over a wide range of times. Final flaming was usually small fluctuating flames at the edges of the panels. A series of stills have been extracted during smoking, front face burning, and burning on the sides for each test. These are found in Figure 73 through Figure 77. At peak flaming, the front face of the panel was generally covered in flames.

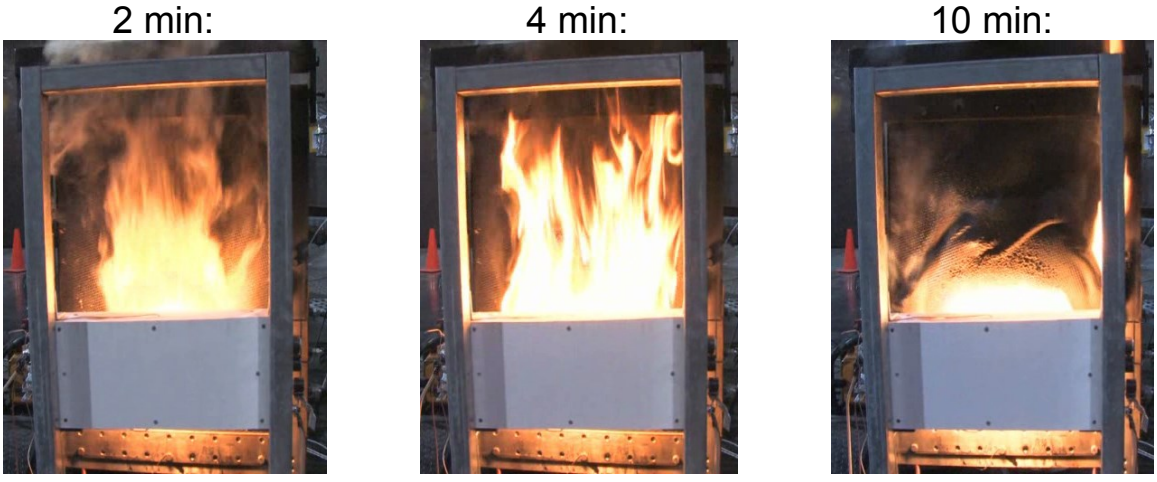


**Figure 73. Front side images for 18x24 thick compression Test 26.**

~2 min: ~6 min: ~10 min:

**Figure 74. Front side images for 18x24 thick tension Test 29.**

2 min: 9 min: 14 min:

**Figure 75. Front side images for 18x24 thick Test 30.**

2 min: 4 min: 10 min:

**Figure 76. Front side images for 18x24 thick compression Test 34.**

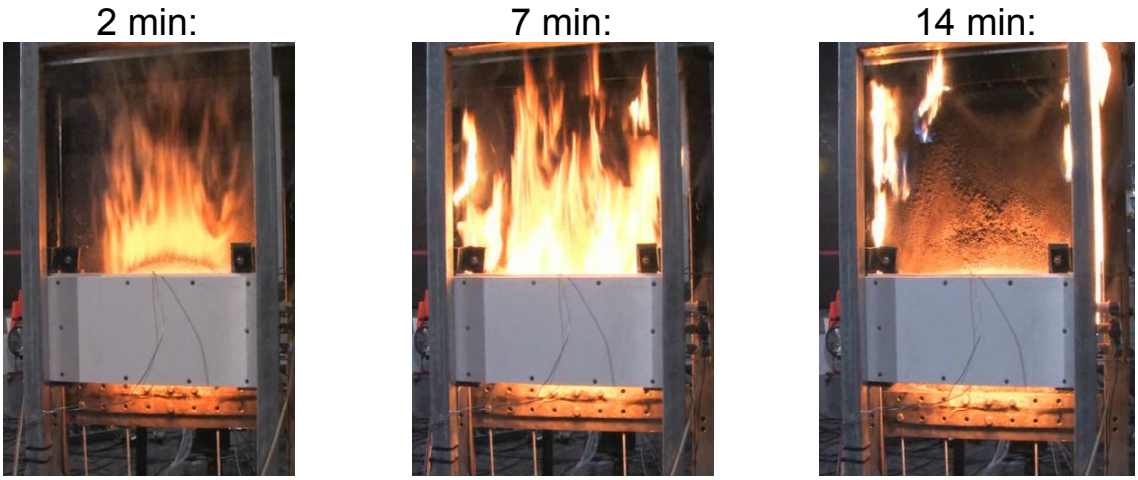


**Figure 77. Front side images for 18x24 thick tension Test 35.**

Test 30 exhibited unusual behavior, in that at 4 minutes 27 seconds the profusely smoking front face stopped of a sudden, and the smoke instead billowed from one of the sides. Presumably, before this event the gases were traversing the internal layers and emerging from the front face. The panel had pressurized and a side channel to release the pressure was completed at that point in time, resulting in a much easier release of the volatiles out the side path.

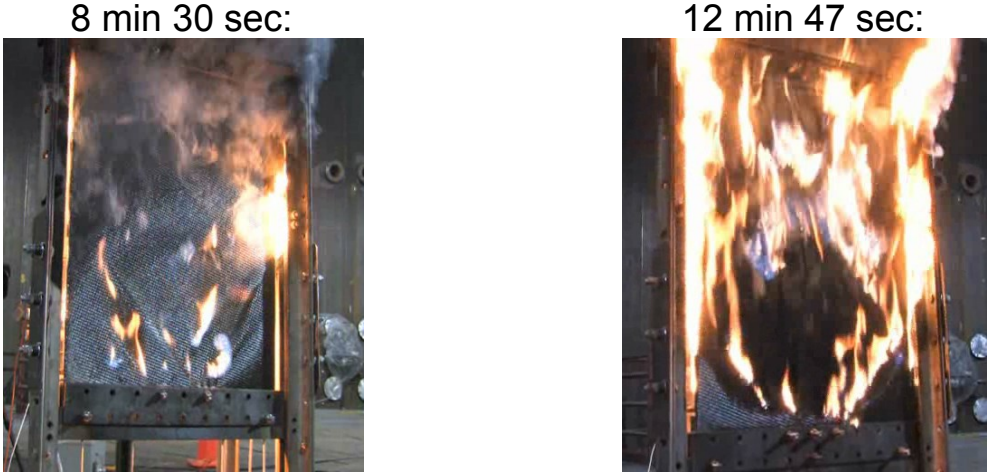


**Figure 78. Back side images for 18x24 thick tension Test 29 (Left: early flaming) and Test 35 (Right: late flaming).**

Two tests in this series additionally had back-side burning. Test 29 exhibited flaming that started around 8 minutes 30 seconds. Backside smoking started around 4 minutes 30 seconds. Test 35 exhibited backside smoking at 4 minutes 59 seconds, and started flaming at 7 minutes 49 seconds. Flaming had mostly ceased by 14 minutes 35 seconds time. In both cases, peak flaming vigorously engulfed the full back surface. The stills

in Figure 78 are representative of the typical behavior outside of the fully engulfing portion of the back-side flaming event. Initially, the flames were sparse and danced across the panel. Then the panel was engulfed, followed by thinning of the flaming to isolated regions.

### 3.3.1 Mass loss data

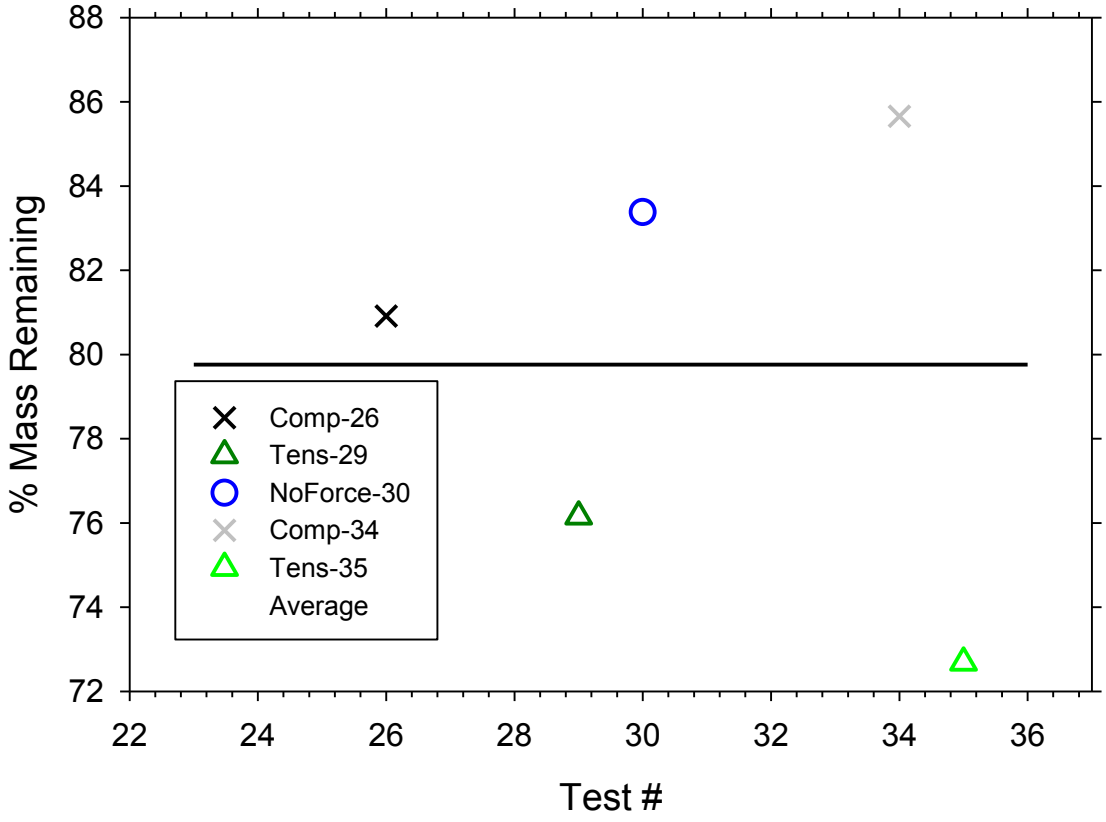


**Figure 79. Total mass loss summary for the 18x24 thick panels.**

In these tests, the tension tests lost the most mass as a percent of the initial panel weight. On average, tests had 20.2% weight loss. The two tension tests lost significantly more, whereas the rest of the tests lost less. Results are shown in Figure 79.

Typical results for the mass loss as a function of time are found in Figure 80. The tension test data (Tens-35) has a different response than the compression and no-force tests presented in Figure 80, both tension tests ignited on the back side of the panel, resulting in much higher flaming mass loss than when the back side did not ignite.

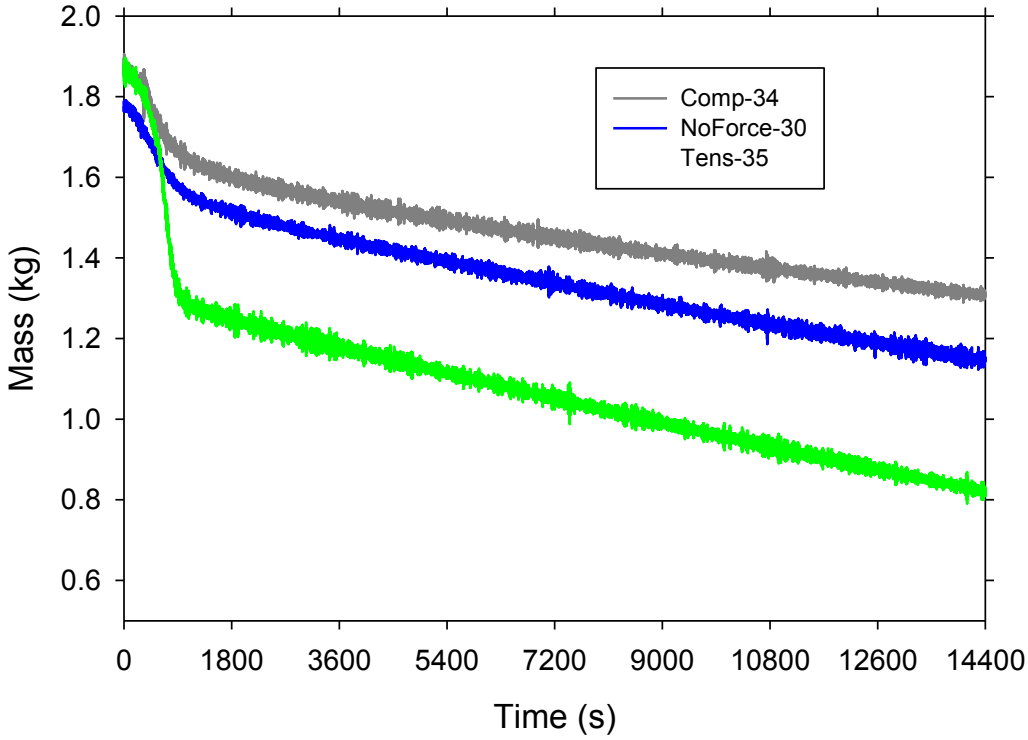


**Figure 80. Typical mass loss raw data for the 18x24 thick panels.**

Mass loss summary data are found in Figure 81. The tests were characterized by around 15 minutes of smoking and flaming devolatilization reactions. Burning typically ignited on the front side and transitioned to the sides, where it burned for a longer period of time. Mass loss was higher during this time-frame than later on in the tests when only glowing reactions were occurring. Once the volatilization was done, the glowing char and fiber decomposition ensued at a constant rate. Figure 83 shows the mean reaction rate during glowing combustion, with data averaged from the 20 minute mark until 10 minutes before the end of the test.

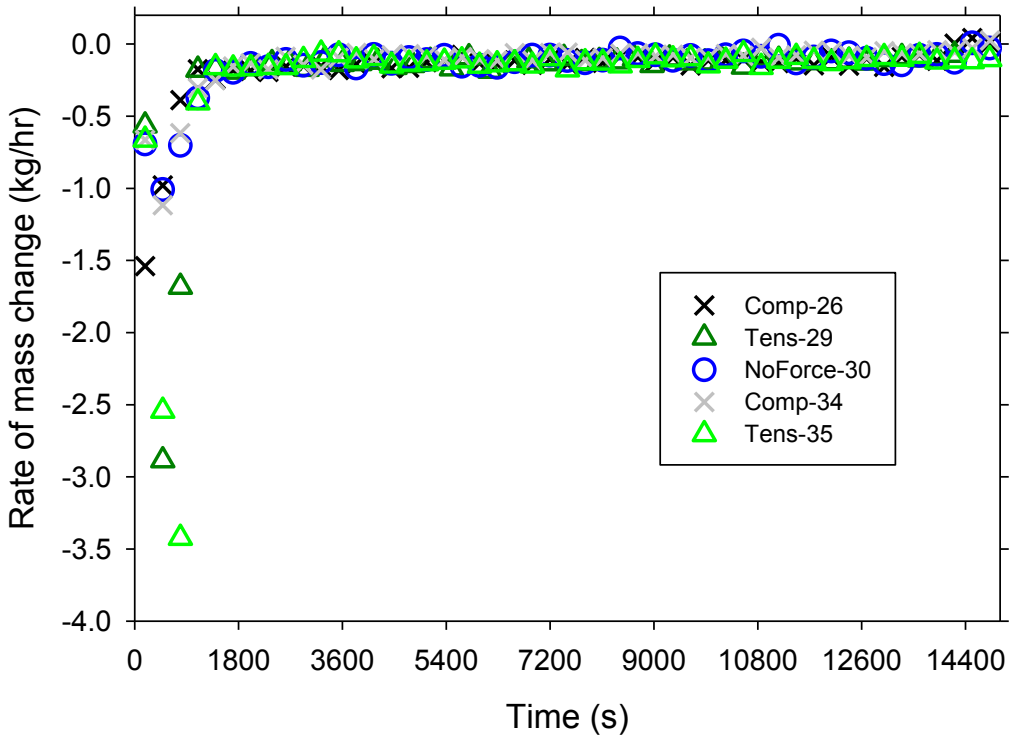


**Figure 81. Rate of mass change summary data for the 18x24 thick panels.**

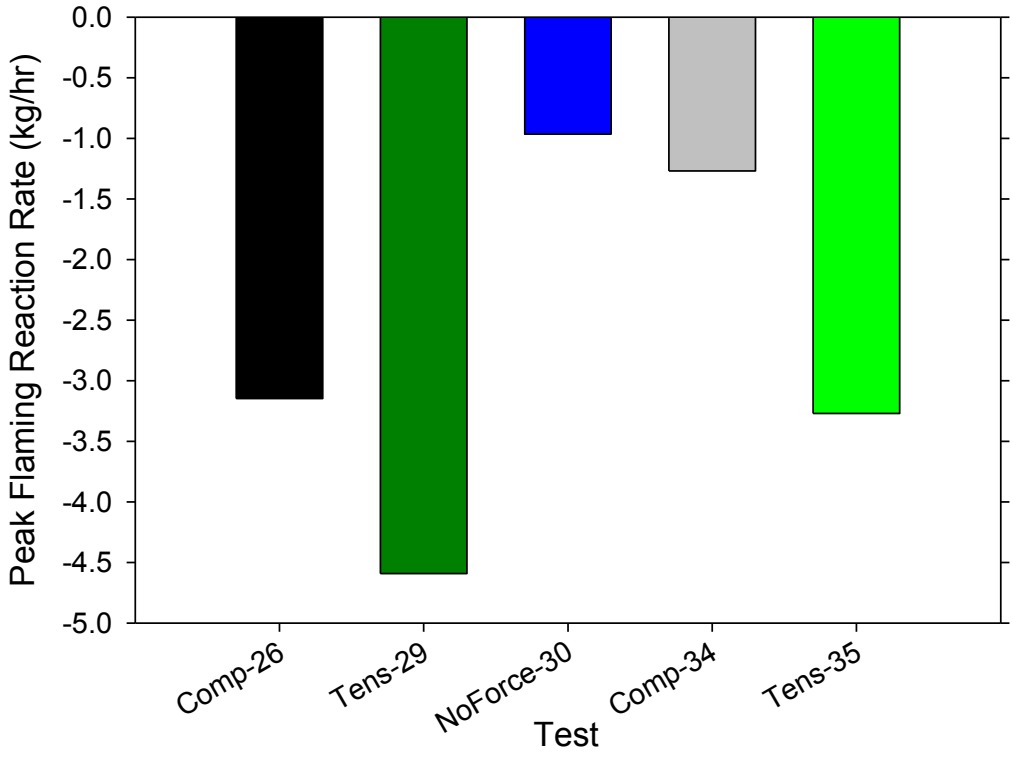


**Figure 82. Peak flaming reaction rates for the 18x24 thick panels.**

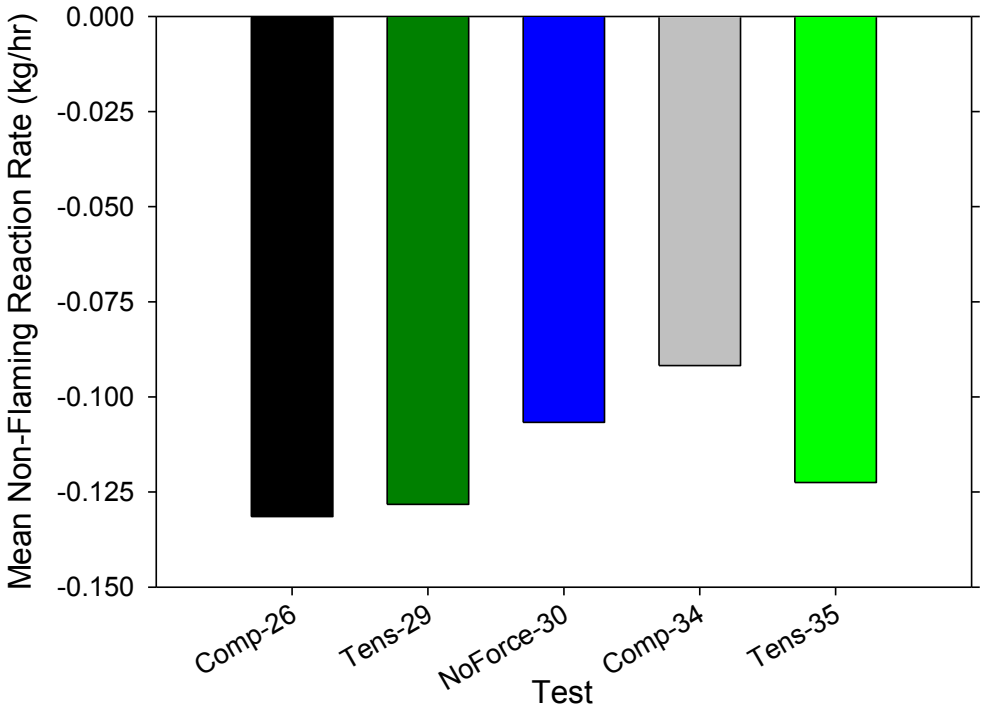


**Figure 83. Mean surface reaction rates for the 18x24 thick panels.**

As was the case for the previous two datasets, there was some variability in the furnace temperatures during these tests. Figure 84 shows the oven thermocouple data. A slight decreasing trend is evident in all the data in what should be steady-state conditions. This feature was more apparent here than in the other tests due to the test duration. This is difficult to attribute, but could have something to do with drift in the power supply, or it could be a response of changing environment conditions.

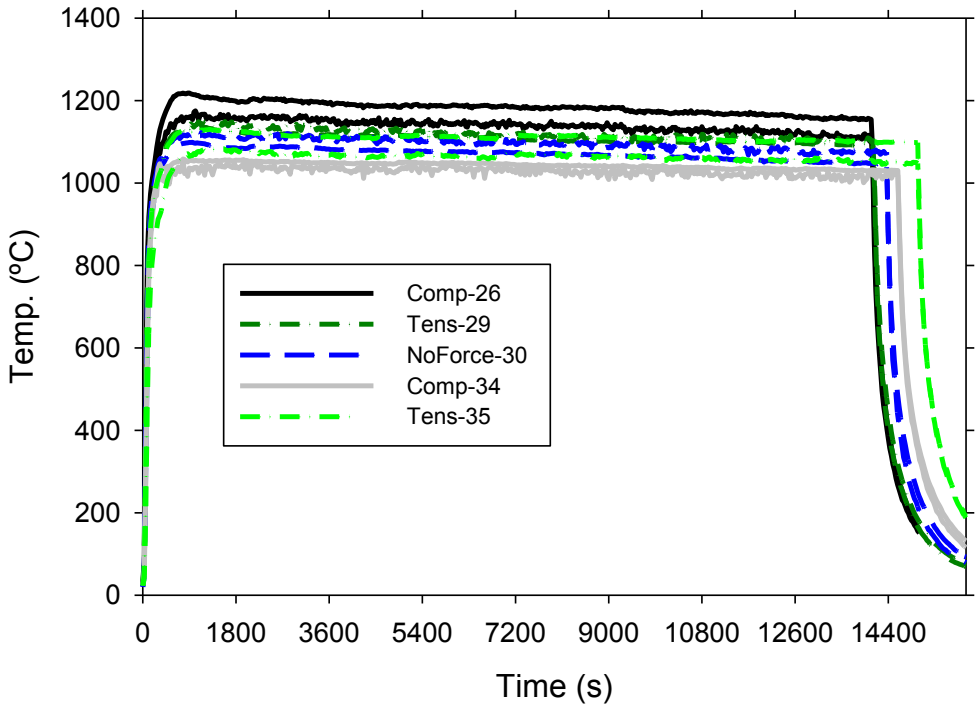


**Figure 84. Oven temperatures for the 18x24 thick panel tests.**

### 3.3.2 Radiometer Data

Radiometer data are plotted from Figure 85 through Figure 90. As in previous tests, the results from the front side at the middle of the panel are mixed, and vary significantly from test to test. Higher up on the front side (Figure 86), heat flux is low during glowing combustion, but peaks during the flaming. The data from high up on the back side in Figure 87 and Figure 88 show back-side flaming for the two tension tests. These were the only two tests in all the test series to exhibit back-side flaming. Heat fluxes were as high as 25 kW/m$^2$ during the flaming phase, but low during glowing combustion phase. Compression Test 26 results for the radiometer aimed at ¼ distance from the bottom of the panel (Figure 89) show unusual step changes at approximately one and two hours. These coincide roughly with when an operator entered the test room to change out video tapes. This event probably has something to do with that feature of the measurement, but why the radiometer read this way for just this test is unclear.

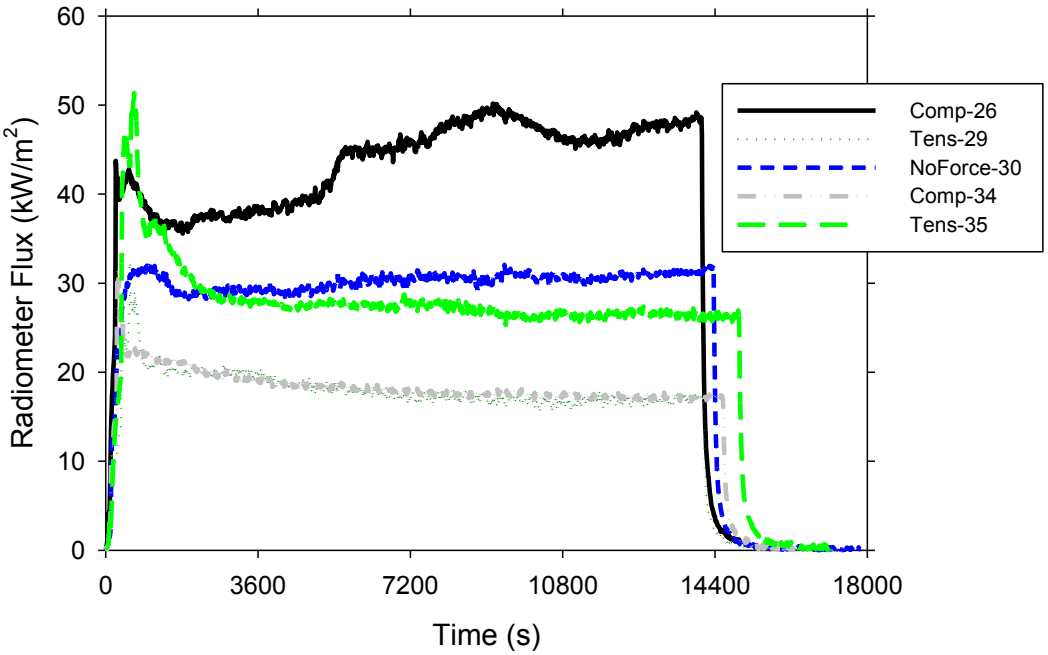


**Figure 85. 18x24 thick radiometer readings from the front of the panel at 0.5 from the bottom.**

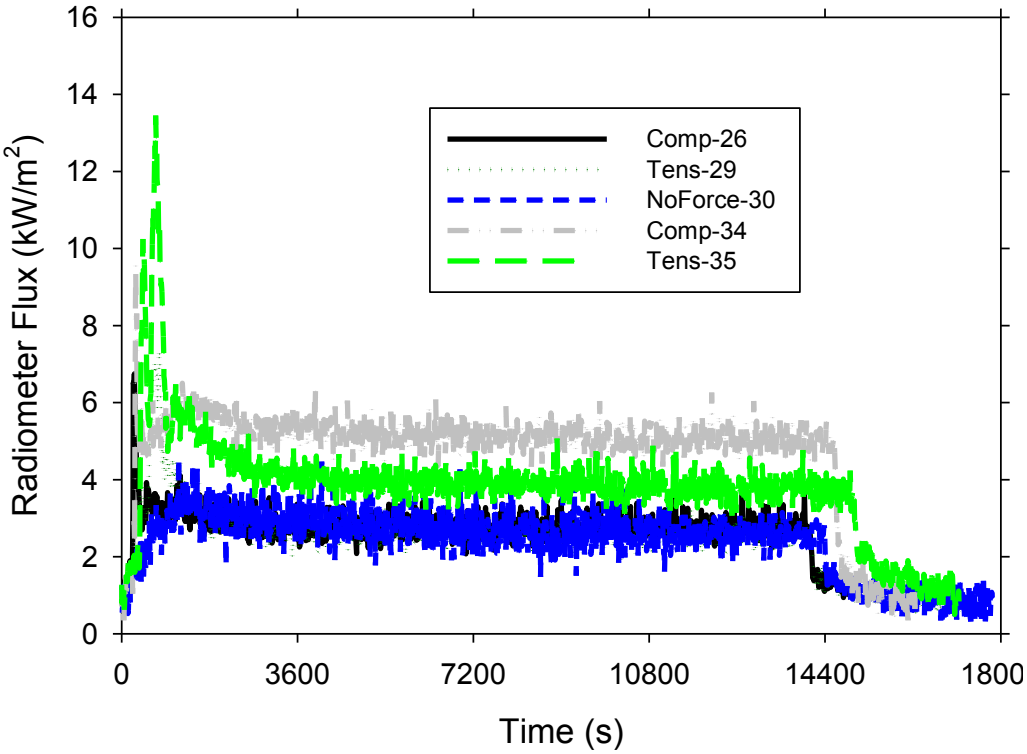


**Figure 86. 18x24 thick radiometer readings from the front of the panel at 0.75 from the bottom.**

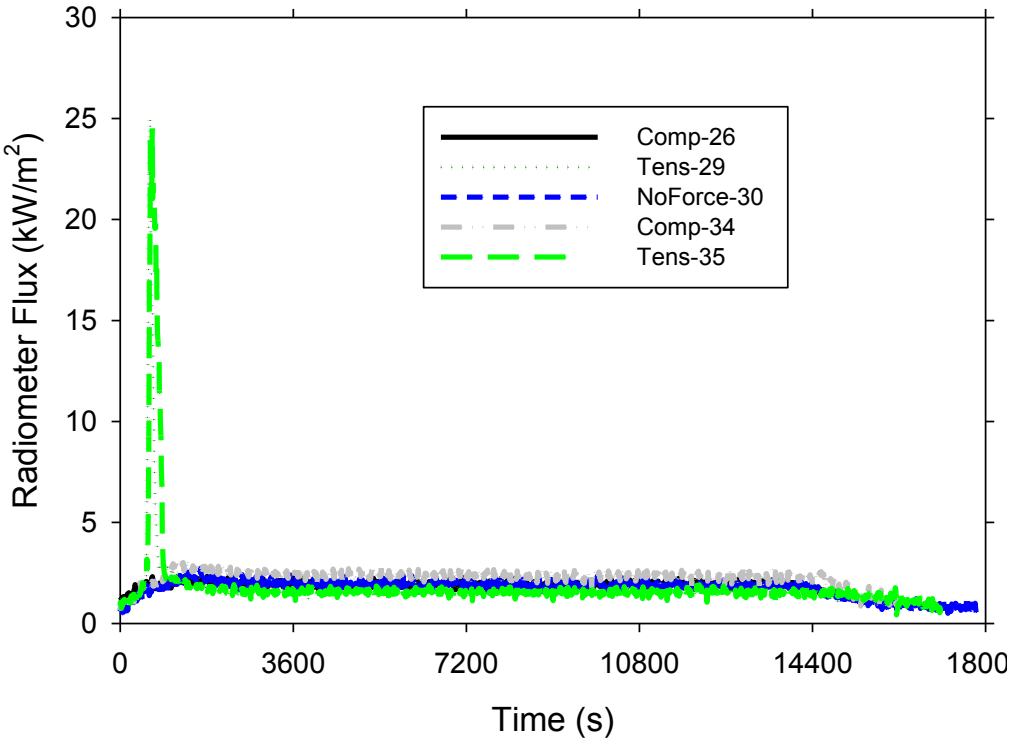


**Figure 87. 18x24 thick radiometer readings from the back of the panel at 0.75 from the bottom.**

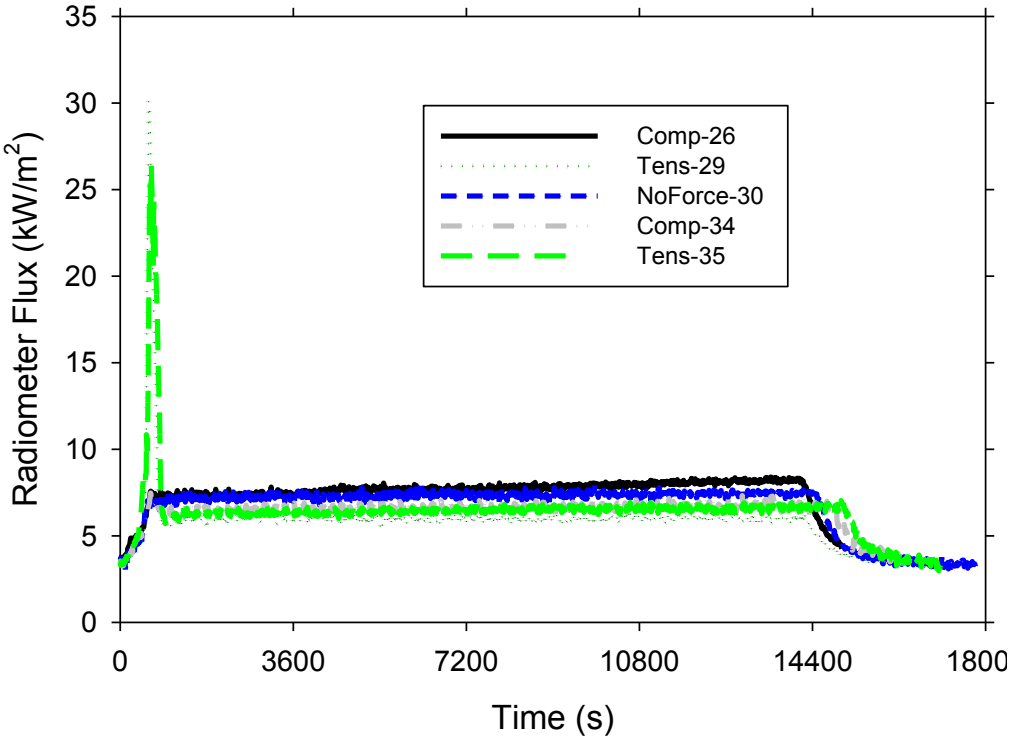


**Figure 88. 18x24 thick radiometer readings from the back of the panel at 0.5 from the bottom.**

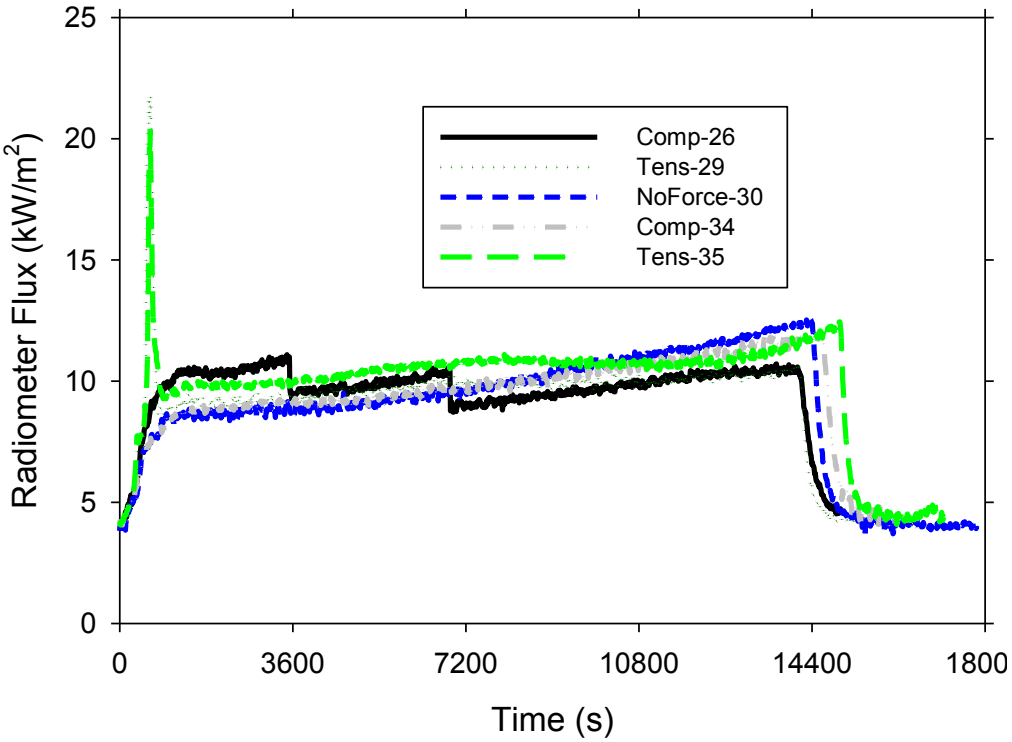


**Figure 89. 18x24 thick radiometer readings from the back of the panel at 0.25 from the bottom.**

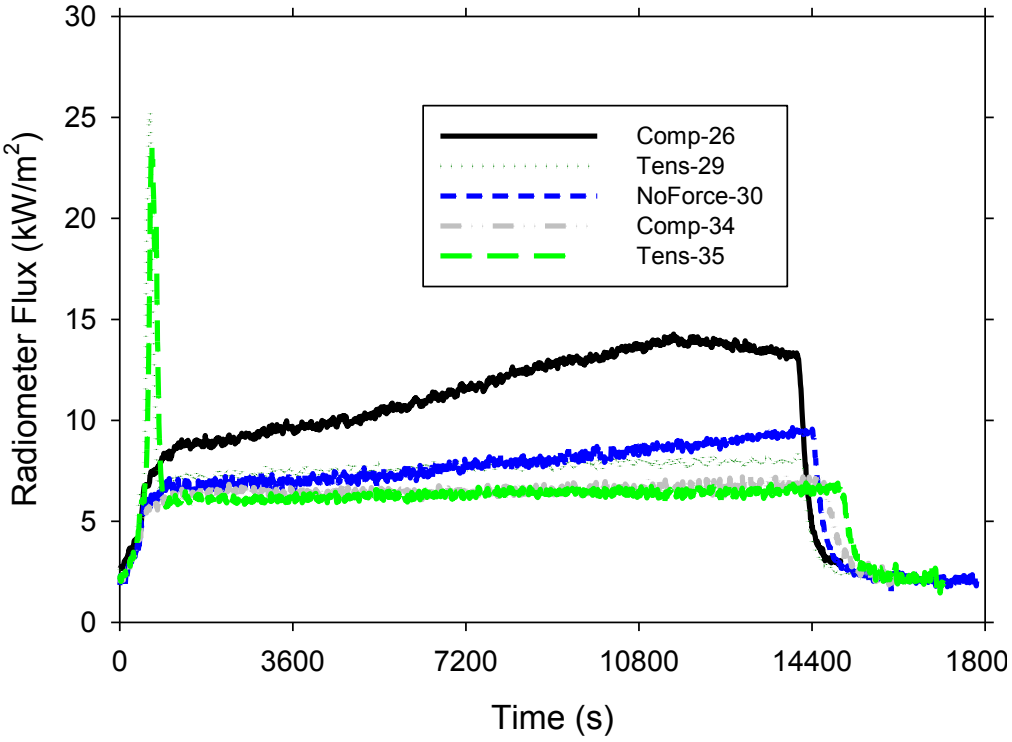


**Figure 90. 18x24 thick radiometer readings from the back of the panel offset at 0.25 from the bottom.**

### 3.3.3 IR data

Figure 91 shows a series of frames selected from the IR camera for Test 35, the 18x24 thick panel in tension. The frame at 6 minutes 15 seconds shows the panel just before back-side ignition of the panel. The subsequent frame at 12 minutes and 42 seconds shows the IR image during back-side flaming. This frame is nearing the end of the active flaming on the back side. A frame at 22 minutes and 55 seconds shows the post-flaming view of the back-side. Several variations exist in the contours compared with the 6 minute frame, and in the post-test examination appear to be stretch marks where the tensile force caused stretching in the fiber matrix. The last frame at 60 minutes shows how little the environment changes with time once the flaming is done when comparing it back to the 23 minute frame.

6 min 15 sec:

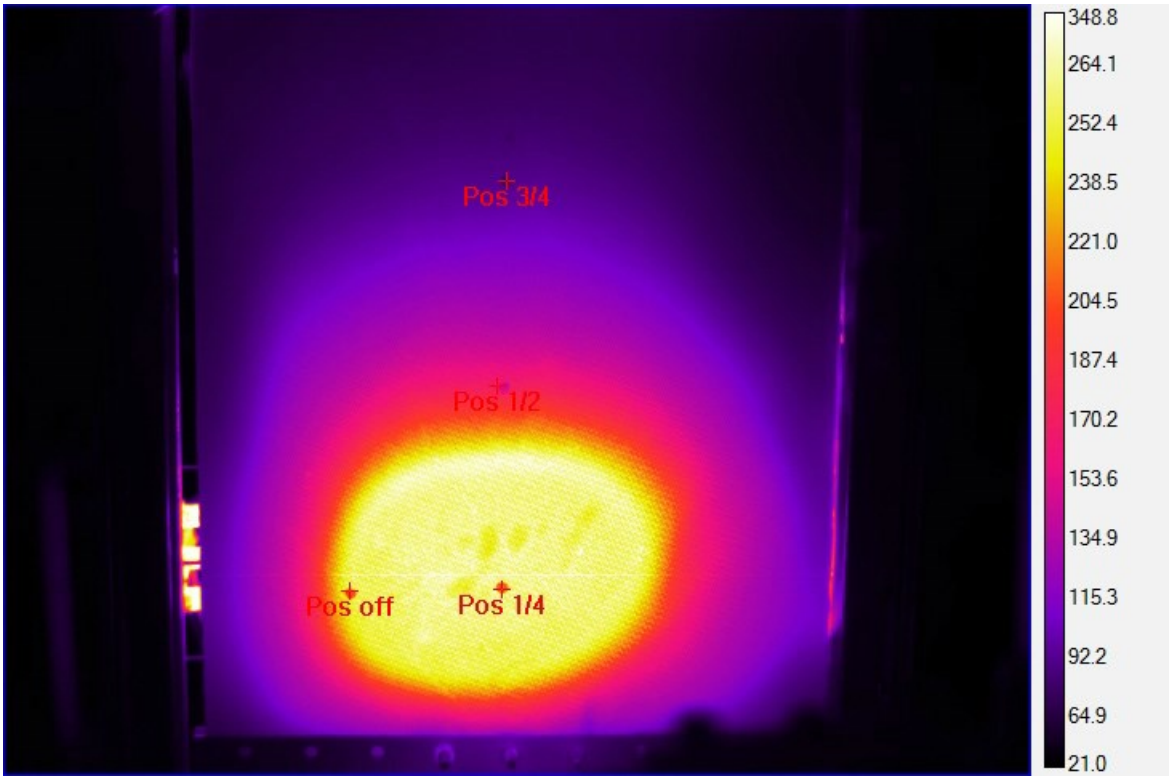

12 min 42 sec:

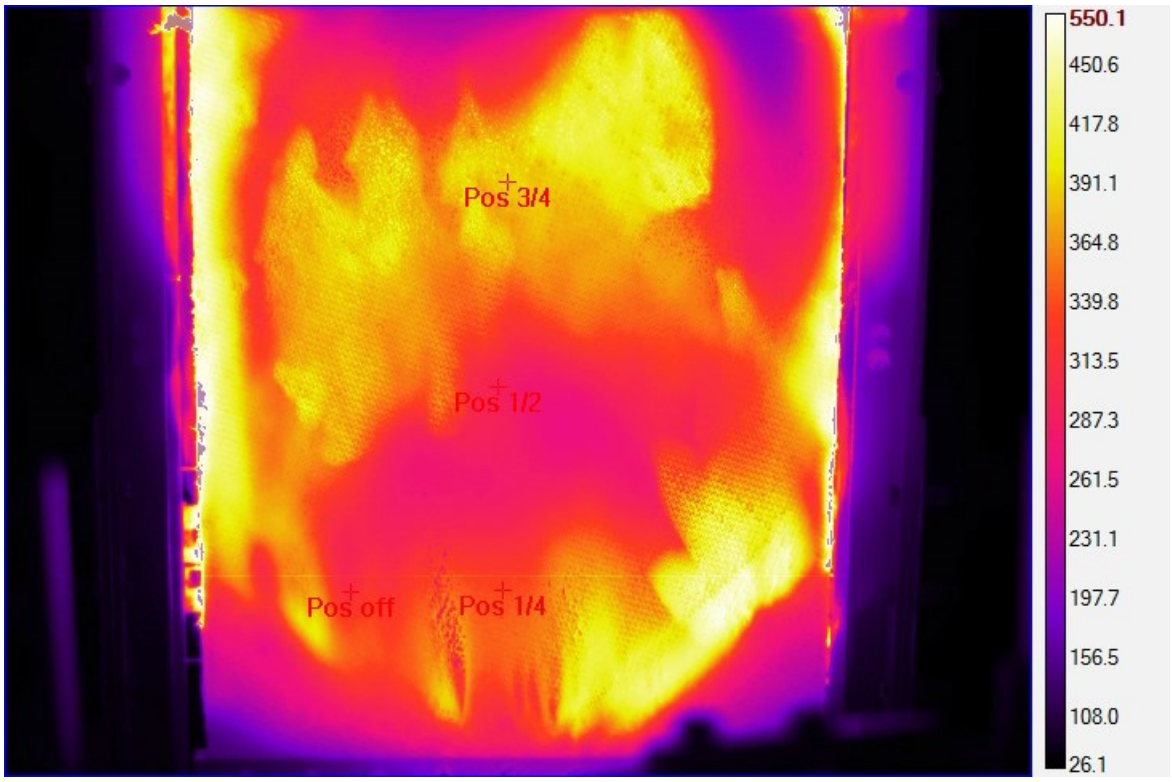


22 min 55 sec:

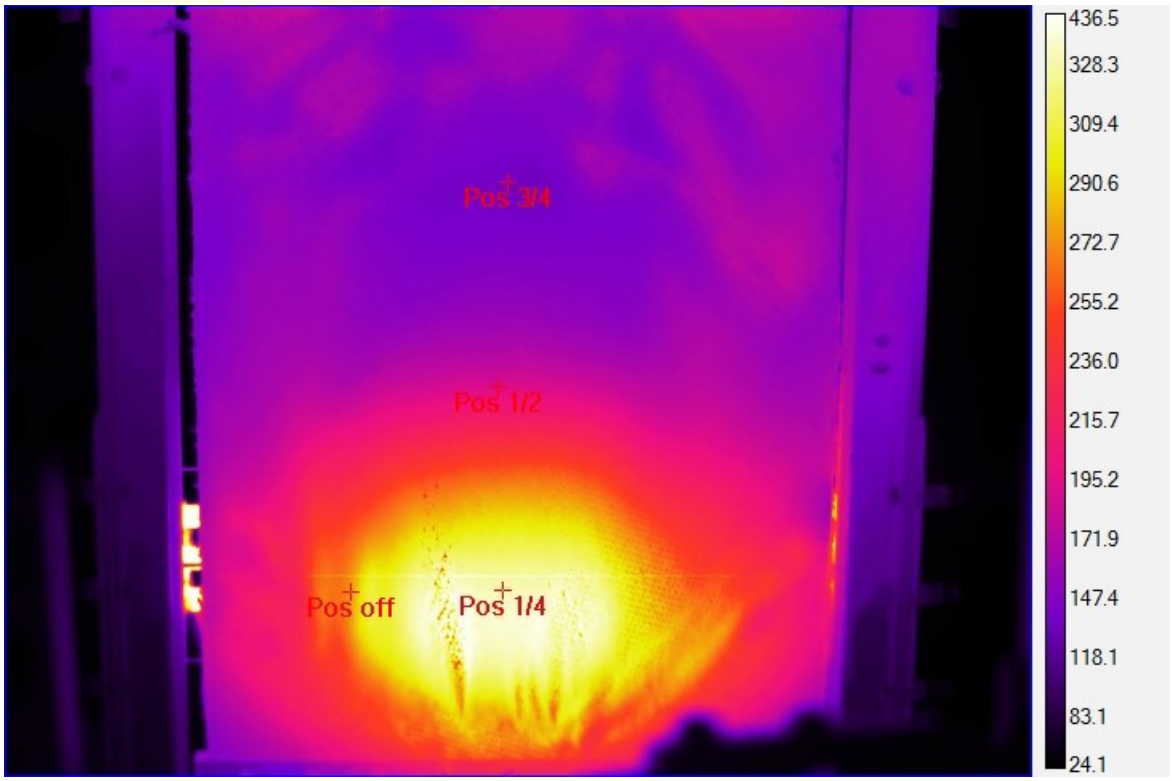

60 min:

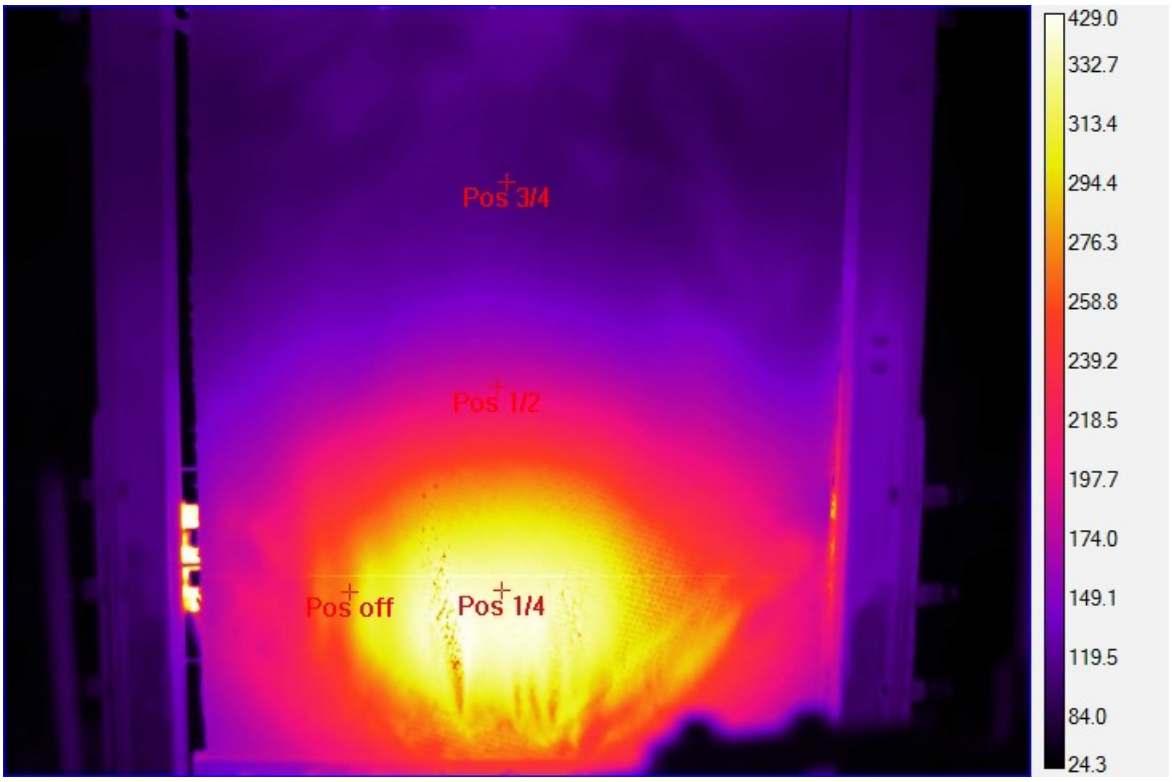


**Figure 91. IR camera images from Test 35, the 18x24 thick panel in tension.**

### 3.3.4 Load data

Movement of the springs can be correlated to force on the panel through the test. Table 10 shows a general description of the movement of the panel in response to the spring force. As with previous sections, these data were extracted from the back-side camera. On test 29, the exact movement times are not well understood, as a blown fuse as the oven was initially turned on resulted in a synchronization error between the cameras and the data.

It is important to note that after about 30 minutes, there was a significant reduction in the force on all of the panels. This is contrary to the findings for the 19x24 thin panels, which were able to maintain force throughout the test in compression.

**Table 10. 18x24 thick panel spring movement summary.**

| Test | Force Type | First Movement | Last Movement | Nature of Movement |
|---|---|---|---|---|
| 26 | Compression | 4 min 9 sec | 15 min 49 sec | Periodic spurts of movement over the indicated time. |
| 29 | Tension | Early | around 30 min | Some panel stretching early before back-side flaming at ~16.5 min. Some shearing of bottom bolt during back-side flaming. After back-side flaming, shearing of top bolts. |
| 34 | Compression | 5 min 4 sec | 6 min 33 sec | Rapid movement over a short time. The panel bent in the middle, distorting away from the oven. |
| 35 | Tension | 3 min 22 sec | 15 min 10 sec | Lower panel stretching occurs first, followed by big movements around 12 minutes as the panel shears from the top bolts. Final movements are mostly done by about 15 minutes. |

Details of the imposed force on the panel can be found in Figure 92, as extracted from the spring camera. Even though these panels had much more mass, they appear to have deformed much earlier in the tests compared to the other two panels. And their deformations finished earlier. Curiously, the compression test appear to retain more residual strength at the end of the test compared with the tension tests, as the final force on the panels is still moderately high for those tests.

These panels exhibited more uneven distribution of the force than the previous tests. Test 29 and 26 in particular manifested this behavior (test 34 to a lesser degree). Because the force was uneven, the data are broken out by individual springs to illustrate this feature. These results are shown in Figure 93. In this figure legend, the R and L indicate right hand and left hand side looking at the back side of the panel. In Test 26, the left hand side moved earlier, and in test 29 the right hand side moved earlier.

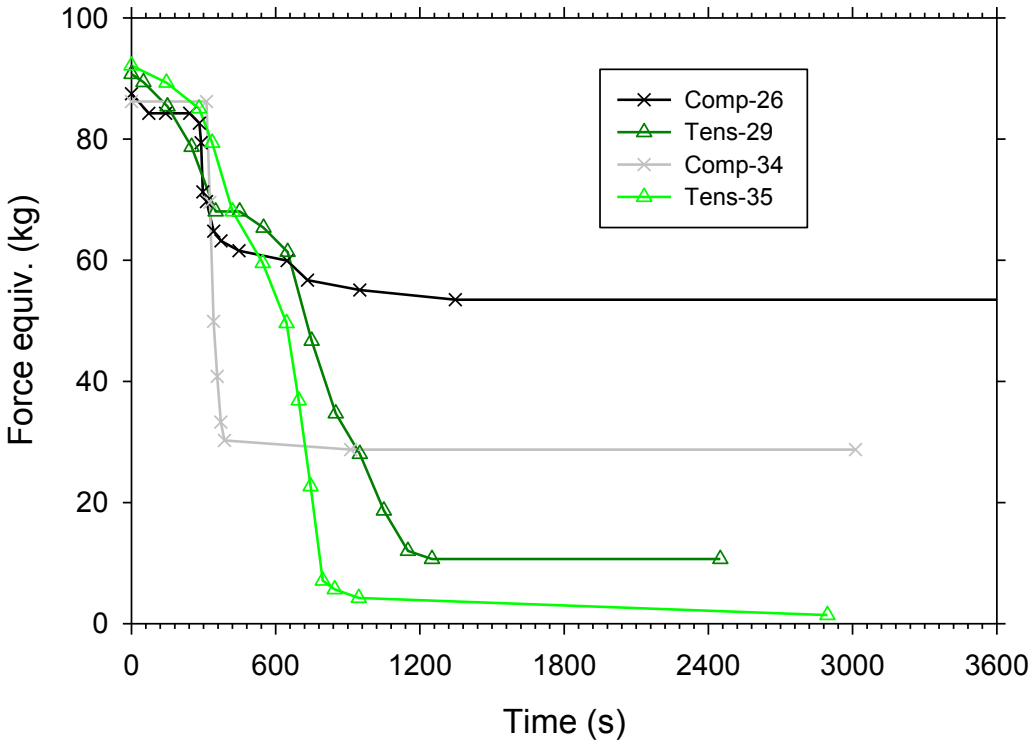


**Figure 92. Mass equivalent force on the 18x24 thick panels as a function of time.**

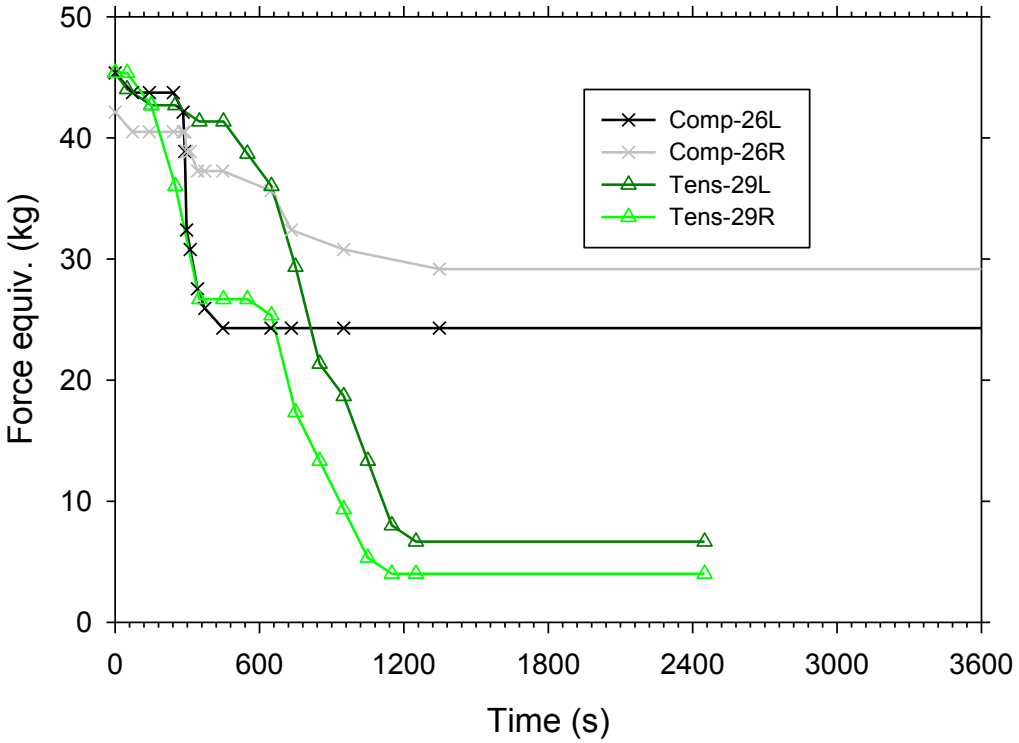


**Figure 93. Force mass equivalent broken out by side of panel for two tests to show details of the uneven force distribution.**

### 3.3.5 Reflectometer data

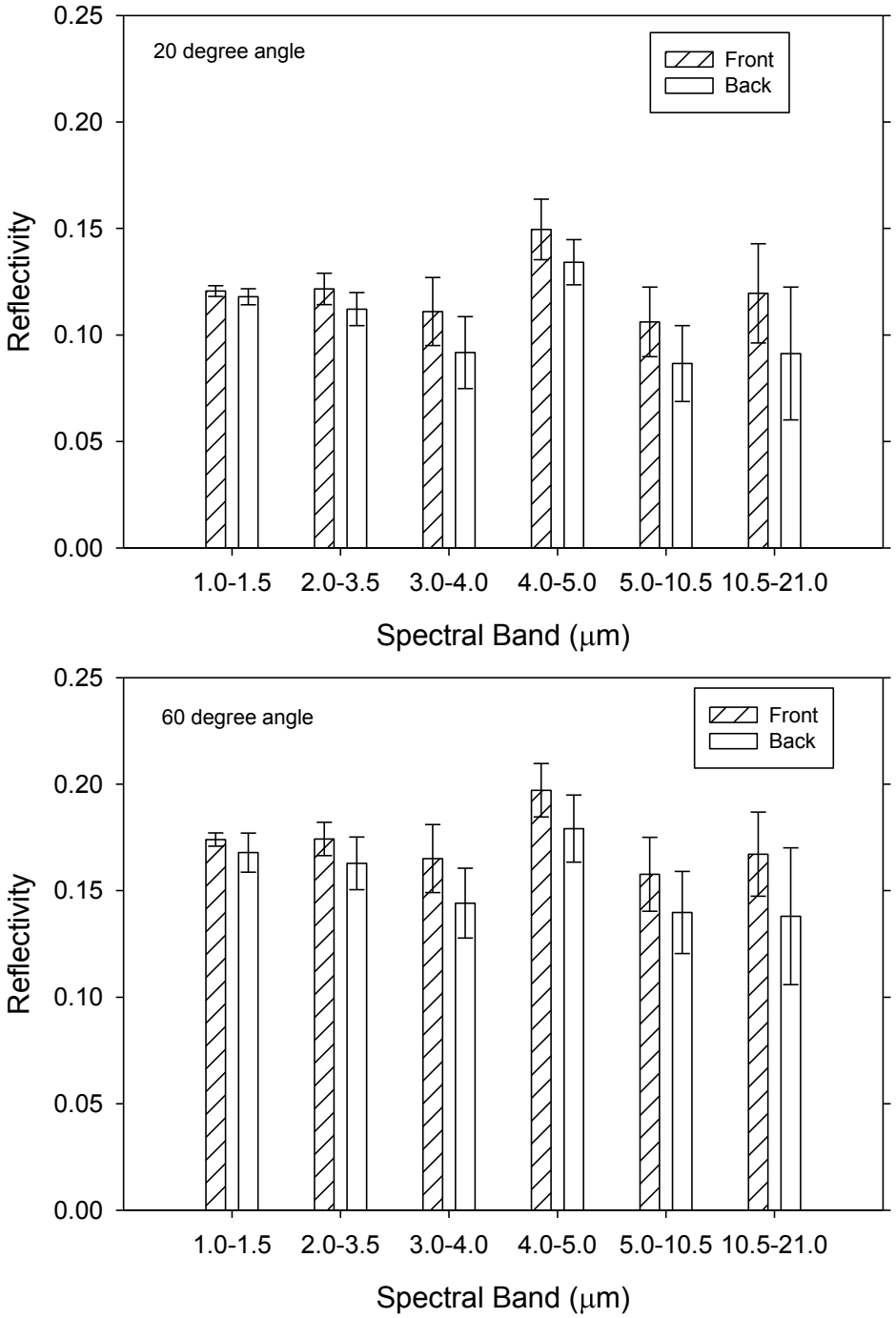


**Figure 94. Reflectivity of the 18x24 thick panels at 20° (top) and 60° (bottom) from normal. Error bars are a single standard deviation.**

Figure 94 shows reflectivity measurements for the 18x24 thick panels. The front side was different from the back side, as the back side was smoother. The reflectometer data suggest differences, but only subtle differences. The single standard deviation error bars don't encompass the similar data on the

opposite side of the panel. However, front and back side data would fall within a second standard deviation for all bands.

## *3.4 General Results and Discussion*

This section is intended to discuss general findings when considering the test series as a whole. It provides opportunity to summarize the findings and compare results to assess the impact of the parameters varied during the tests on the test results.

### 3.4.1 Mass Decomposition Rates

Examining the test results based on the type of force imposed, it is not clear that there is any effect of the type of force on the decomposition of the fibers. The oven temperature seems to have an effect, so an attempt was made to remove that variable as a contributing factor to the outcome of these tests. Plotted in Figure 95 are the mean glowing reaction rates versus the mean oven temperature over the same range (the numerical average of both oven thermocouple temperature readings). Plotted this way, there is a very clear linear trend between the reaction rate and the oven temperature when the data is examined by panel type. As a reminder, compression results are black or a shade of gray, tension tests are shades of green, torsion is red, and 'NoForce' indicating panels without any imposed forces are colored blue The type of panel is indicted by symbol ×=ABDR, ○=18x24 thick, and ▼=19x24 thin. There is a single outlier, which is ABDR compression test 25, which had oven power loss part way through the test.

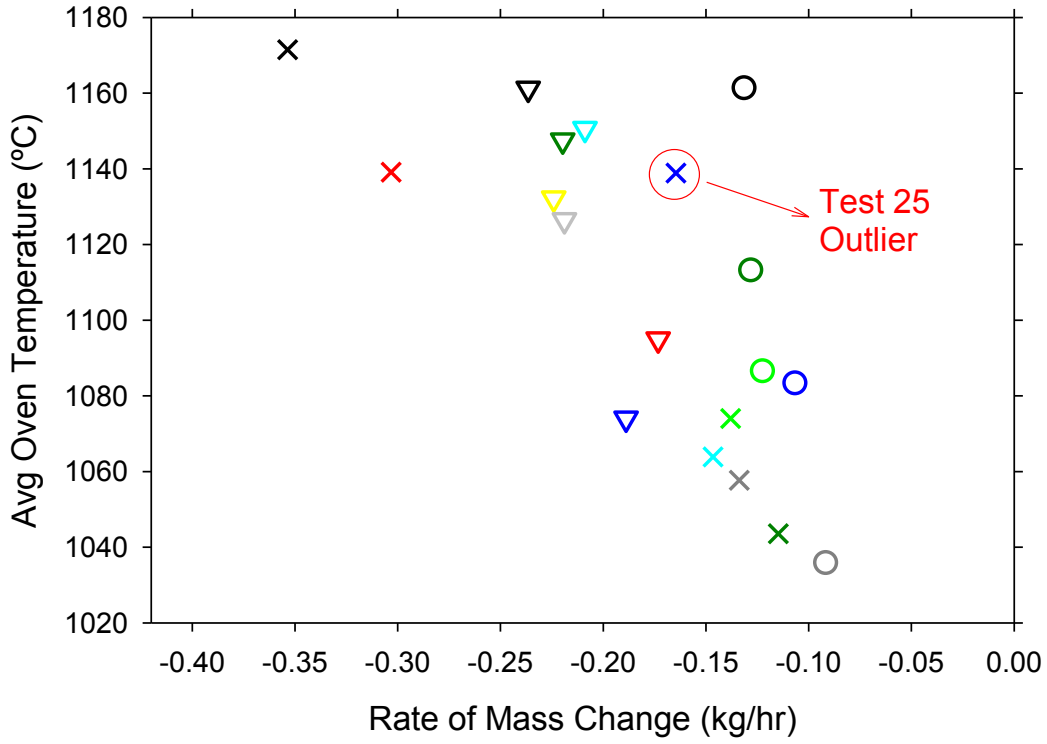


**Figure 95. Rate of mass change summary for glowing combustion. Colors indicate type of loading (standard scheme), while symbols suggest the material used in the test (×=ABDR, ○=18x24 thick, ▼=19x24 thin).**

The outlier is a significant piece of data because the reason for it being an outlier is well understood. The brief power failure caused a period of lower temperatures, during which time the reaction rate slowed significantly. Temperatures and reaction rates were averaged over this outage in the above data. This suggests that the apparent linear relationships shown in this section for oven temperature and decomposition rate does not maintain linearity at lower temperatures.

Regression analysis has been performed on these data to suggest the linearity of the trends. After omitting the single outlier from the previous dataset, the ABDR panels were linear with a coefficient of determination ($R^2$) of 0.98. The 18x24 thick panels are also fairly linear with a coefficient of determination of 0.80. Less correlated are the 19x24 thin panel results, ($R^2$=0.688). Table 11 summarizes the correlation results for these data. A linear fit is presented in the form of $y=mx+b$, where $y$ is the mass rate of change, $x$ is the oven temperature, $m$ the slope, and $b$ the intercept. Figure 96 shows the data re-plotted after omitting the outlier, and including linear trend lines that suggest correlation by panel type.

**Table 11. Summary of linear fit data for glowing rate of mass change to oven temperature.**

| Panel | $R^2$ | Slope (m) *[kg/hr°C]* | Intercept (b) *[kg/hr]* |
|---|---|---|---|
| ABDR | 0.98 | -1.98E-3 | 1.96 |
| 18x24 thick | 0.80 | -3.24E-4 | 0.239 |
| 19x24 thin | 0.688 | -5.74E-4 | 0.437 |

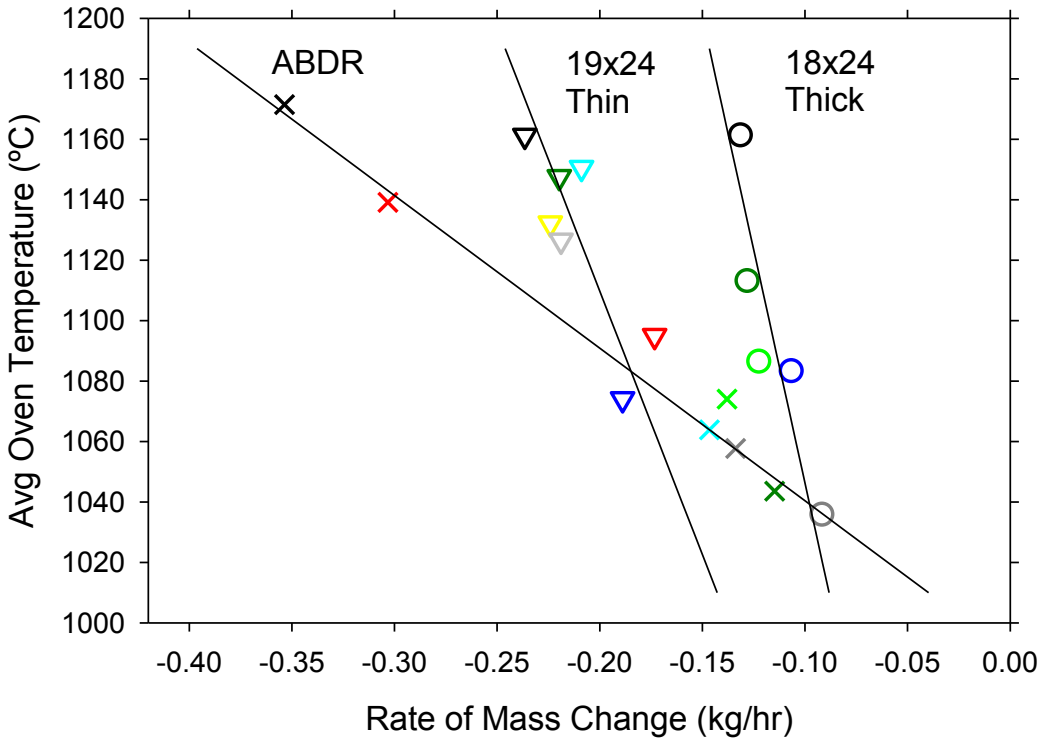


**Figure 96. Re-plotted glowing mass change rate versus oven temperature omitting the outlier and with linear regression trend lines.**

After the analysis including the oven temperature as a parameter, it appears conclusive that the nature of the structural loading does not have an appreciable effect on the rate at which the fibers and char decompose for panels of this type at the length scales and structural loadings studied. Based on the distortions that the structural loading imposed on the panels, it was expected that the reaction rate would augment or decrease if the distortions were mostly towards or away from the oven respectively. In preliminary testing before the cage was present to inhibit large distortions, this was a very clear and obvious effect when significant distortions were seen. The test series presented, however, had panels with distortions perpendicular to the plate face as large as 5 cm. The cage partially inhibited these from increasing beyond this point. Distortions in the other direction

that were not inhibited by the cage were not observed with the composite materials in this effort, but were in an earlier wood panel test that exhibited distortions much greater than 10 cm in that direction.

The 19x24 thin panels exhibited no significant distortions other than swelling. These panels did not buckle under compression, which one would expect would contribute to the variability in the mass loss rate data. Yet, those panels have the lowest coefficient of determination ($R^2$). Notice that the oven temperature did not vary as significantly for the tests on the 19x24 thin panels as it did for the other panels. This could be a contributing factor, as correlations are better determined when data are taken over a wider range of values.

While glowing combustion results show that the reaction results are almost exclusively a function of furnace temperature and panel type, the flaming combustion results suggest a different relationship. The rate of reaction is assessed by evaluating peak flaming rates of mass change. When plotted versus oven temperature as in Figure 97, there is not a significant linear response in reaction rate vs. oven temperature. It has already been well documented that the two tension tests for the 18x24 panels were the only ones to exhibit back-side flaming. It is therefore no surprise to find those two as the ones that exhibited the fastest decomposition during flaming. Ignoring those two data points, the 18x24 thick panels and the ABDR panels appear to have some linear relation between oven temperature and peak flaming mass loss rate, but not nearly as pronounced as was found for the glowing combustion data. No relationship between the type of force and the burn rate is observable. The 19x24 thin panels suggest no relationship between oven temperature and peak flaming rate, nor do they suggest a relationship between the type of forces on the panel and the decomposition rate. Examining the scale range for Figure 95 and Figure 97, the peak rate of mass change for flaming is generally about an order of magnitude greater than the comparable glowing combustion rate.

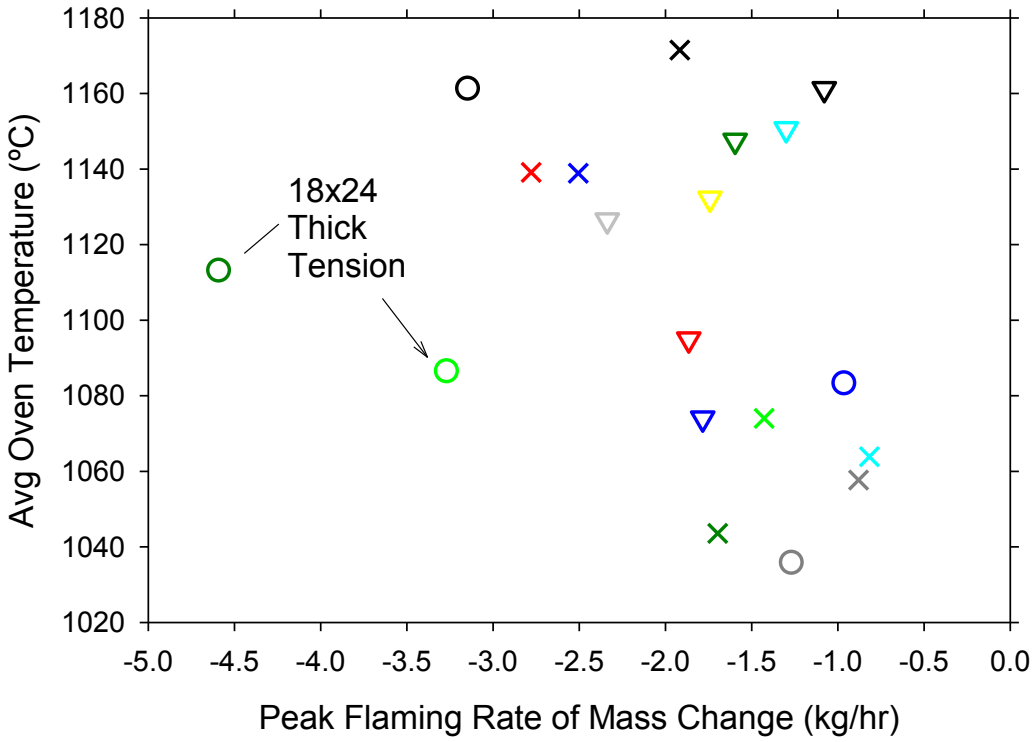


**Figure 97. Rate of mass change summary for peak flaming combustion. Colors indicate type of loading (standard scheme), while symbols suggest the material used in the test (×=ABDR, ○=18x24 thick, ▼=19x24 thin).**

This finding, that mass loss has some dependency on the type of force imposed during flaming combustion, is consistent with the findings of Elmughrabi et al. (2008), albeit these findings do not trend similarly (they found trending was somewhat linear according to the applied stress). The other panels types (besides the 18x24 thick panels) do not exhibit dependence on imposed force. It is important to note four significant differences between these tests and the work of Elmughrabi et al. First, the panels in this test series are much larger. Second, carbon fiber versus glass fiber was used in these tests. Third, this test series involved flaming reactions, whereas none was reported in Elmughrabi et al. (2008). Fourth, the imposed stresses are much lower in these tests (10-100 MPa compared to < 1 MPa in this work). Samples in the previous work were near the failure point. Normal operational stresses are considerably lower, which is why by design this test series exhibits this particular difference. Elmughrabi et al. speculate that microcracking in the epoxy contributes to the finding that there is a structural force dependence on the failure strength of the material in a fire. This might also be consistent with the observation from this test series that the 18x24 thick panels in tension exhibited greater rates of reaction. More data are needed to substantiate this theory, as these tests did not collect data on microcracking.

### 3.4.2 Duration of Flaming

Throughout the results sections, data were presented on the duration of flaming for each panel. Since each panel was exposed to essentially the same environment, the burn time data should show functionality to the most significant contributing factors. Panel type and initial panel mass are good prospective parameters that might be the dominant contributing factor. In Figure 98, the duration of flaming is plotted versus the initial panel mass. As with previous plots, color and symbol type are used to indicate the type of forcing imposed on the panel and the panel type. The clearest relationship appears to be the most intuitive relationship, which is that the initial panel mass correlates well with the duration of flaming. Flaming duration was fairly consistent for each panel type, with the exception of the 18x24 thick panels. These exhibited a wider range of flaming duration times. For these panels, the no force results from Test 30 were somewhat of an outlier. The line in Figure 98 is a best fit line. All 19x24 thin data points fall below the fit line, suggesting that these panels exhibited moderately longer flaming durations compared to the expectation given the trends of the other two panels. This is may be suggestive of a panel specific variation such as an increased volatile fraction, or a rate limiting factor imposed by the lack of deformation found for these panels. More work would be required to better attribute the correct variable that contributes to this finding.

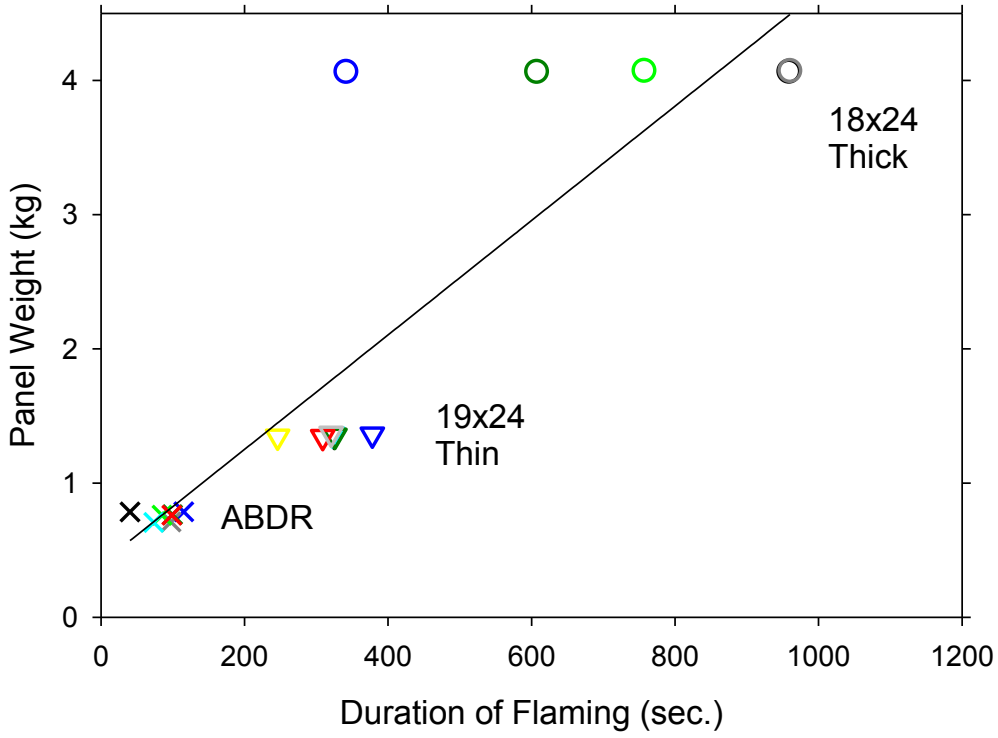


**Figure 98. Panel weight versus duration of flaming. Colors indicate type of loading (standard scheme).**

### 3.4.3 Panel Strength

Results indicate that there is not a simple way to predict beforehand the structural behavior of the panels. The thermal environment resulted in fairly reproducible behavior in the panels in terms of flaming initiation and termination. After performing the 18x24 thick panel and ABDR tests, it was expected that the 19x24 thin panels would distort under compression much like all others had, or perhaps more readily since they were thin, yet they did not.

The reason the 19x24 panels were apparently stronger in the fire environment merits some consideration. Besides the obvious difference in non-sandwich materials, the 18x24 panels were thicker and slightly narrower than the 19x24 panels. They flamed for a much longer time, perhaps due to the quantity of volatile in the thicker materials. This longer flaming period could create an increased damage state caused by a longer exposure to the flames, weakening the structural matrix sooner. It is also important to note that the 19x24 thin panels were made from a different binder material and from unidirectional fibers. The 18x24 thick panels were made from woven fabric. What effect this could have relative to the structural strength is not clear. One possibility is that the fabric because of the tighter weave makes a better gas seal, and that the decomposition deep in the layers creates higher and more destructive pressures. The width difference between the two panels was minor, but the 19x24 thin panels were able to distribute the weight in the compression tests around the holes that eventually formed, whereas the 18x24 thick panels grew weak at the edges. It is important to note that the 18x24 thick panels failed fairly early, which means that the fact that they failed had nothing to do with the extended time that the panels were exposed to the oven compared to the 19x24 thin panels.

A basic reason for development and use of composite materials is to generate a material that takes on characteristic behaviors of the components. Fibers exhibit almost zero strength in compression. The epoxy is not nearly as strong as the fibers in tension. By compositing the two materials, one achieves a material that exhibits a more functional structural behavior for engineering design that is a combination of the behavior of both constituencies. The compression strength variations are likely most attributable to the epoxy, since the fibers lack compressive strength. Residual compressive strength in the 19x24 thin panels is almost certainly due to a residual strength in the epoxy along the edges of the panel. Because the panel were nearly identical in width and the oven environment was reasonably identical, another feature is thought to contribute to the differences. A significant difference in the reaction rate of the epoxy might be a contributing factor. Variations in heat transfer might also be a factor. One can observe temperatures in the IR camera data that would suggest significant differences along the panel edges. The plots in Figure 69 and

Figure 91 are not sufficiently precise to be able to discern any significant difference between the temperatures of the two panels at the edges.

All this suggests a somewhat counter-intuitive finding, which is that there may be an intermediate material thickness that produces the best structural strength in a fire as a compromise between flaming off-gassing volatiles and bulk strength. Since there were many differences between the two panel types, this test series will not be able to fully explain if this is the driving factor, or if one of the other factors mentioned above is more significant. More work will need to be done to better understand the structural behavior found in these tests.

If one considers strength in fire on the basis of the weight of the panel, the ABDR panels performed well. Even with significant loading, they were able to hold the full compressive load for a couple of minutes, and retained residual strength for 20-30 minutes. In tension, these panels remained stout under the load for at least 20 minutes. Neither of the panels tested in torsion did particularly well with that type of force under fire conditions.

In the previous sections, a point has already been made that the ABDR and 18x24 thick panels resisted initial deformation best in tension, then compression, followed by torsion. Table 12 shows quantitative results of the remaining percent of initial force on the panel by the end of the test. In a fiber composite, one normally attributes tensile strength to the fibers. However, the failure mode was not ever seen to be related to the tensile failure of the fibers. Rather, the panels tended to fail at the point of attachment, which can ultimately be ascribed to a compressive failure.

**Table 12. Residual force in the panels at the end of the test.**

| Test | Panel | Remaining Force % |
|---|---|---|
| Comp24 | ABDR | 16.98 |
| Comp26 | 18x24 | 61.11 |
| Comp27 | ABDR | 35.37 |
| Tens29 | 18x24 | 11.76 |
| Tens31 | ABDR | 51.79 |
| Tens32 | ABDR | 21.82 |
| Comp34 | 18x24 | 33.33 |
| Tens35 | 18x24 | 1.54 |
| Tens41 | 19x24 | 17.07 |
| Tors42 | 19x24 | 50.00 |
| Tors43 | ABDR | 32.53 |

Examining these results by panel, the 19x24 thin panels supported at the end of the test on average 33.5% of the initial force, the ABDR panels supported 31.7% of the initial force, and the 18x24 thick panels supported 26.9% of the initial force. Given that repeat tests suggest low repeatability (on average different by 21.5%), this is insignificant. A more significant finding is that on average the tension tests had 20.8% of the original force

still supported by the panels at the end of the test. In compression, the value was much higher, 36.9%. This, like the rest of the results in this paragraph does not include the two compression tests for the 19x24 panel where 100% of the force was still supported at the end of the test. Including those data, the 36.9% figure would go up significantly (about 20%). Lack of repeatability prevents this from being a significant conclusion of this work, but it is something to continue to observe in future experiments. Also, due to the fact that three of the five tension tests lost strength around the mounting bolts, significant findings will not be made from these observations with respect to core panel behavior.

A couple of other observations in regard to the structural response of the panels are worth note. In no case did the panel yield abruptly. The failure was often times rapid, but never an instantaneous move from full strength position and shape to a final deformation. This was true regardless of the panel type or type of structural loading. As composites weaken in a fire, they deform gradually over a period of time. The imposed forces for these tests are probably representative of some of the forces on real transportation vehicles during normal operations. Such forces are significantly below the normal (room-temperature) structural failure point. We therefore hypothesize that a long-term fire involving a composite structure may cause the airframe to soften and droop with time like a plastic airplane in an oven, and not snap apart as many materials do near the stress yield limits. Real-time evaluations of the videos from these panels could not always detect the motion without careful and precise references on the monitor screens.

### 3.4.4 Broken Panel

One panel (Test 44) was broken prior to the test. This was a 19x24 thin panel, and the nature of the break was a line crack forming the shape of an X with the center near the peak point of thermal insult from the oven. This test was conducted without force. This test fell in line with the rest of the tests, and no observable differences were seen in the outcome of this test when compared with the others of the same panel type. This outcome is not a particularly conclusive finding. What it does suggest is that if previously damaged material behavior is investigated in future work, a more significant fracturing method should be used. Aircraft in a real crash might have materials damaged to a much greater extent. In this test, the initial exposed surface area did not change appreciably on account of the break. Real crashes may induce more dramatic panel fractures, increase the exposed surface area, which in turn might induce different reaction rates in a fire environment. The effect of pre-damage state on the burn rates probably relates most to the exposed surface area of the composite, a relationship that can be examined in more detail in future work.

### 3.4.5 Reflectometer

An obvious finding already discussed is that the ABDR panel back and front sides can be distinguished by the reflectometer. They are visibly different, which is not particularly revealing. More important is whether the instrument can tell what type of binder is used. To determine this, results from the different sections are re-plotted by material type. Furthermore, a down-select of the best comparison points from the full suite of data is made to evaluate the ability of the reflectometer to discriminate panels by material type.

The 19x24 thin panels were ostensibly the same on each side, so the 'front' side was chosen. The ABDR front side was smooth, and the same binder as the 18x24 thick panel. The 18x24 thick panel had texture on the front side, and was more smooth on the back. Data from the back side are compared to the ABDR front and the 19x24 data. Reflectivity at 20 degrees is found plotted in Figure 99 Figure 100 shows the same for 60 degrees angle. The band-range of 10.5-21.0 mm may be able to distinguish the ABDR material from the 19x24 material, as at that range the one standard deviation bounds do not overlap between the two materials at 20 degrees. The 18x24 thick panels had large uncertainty bounds at that same point, and could not be thus distinguished from the other panels. At 60 degrees, there is no such distinction.

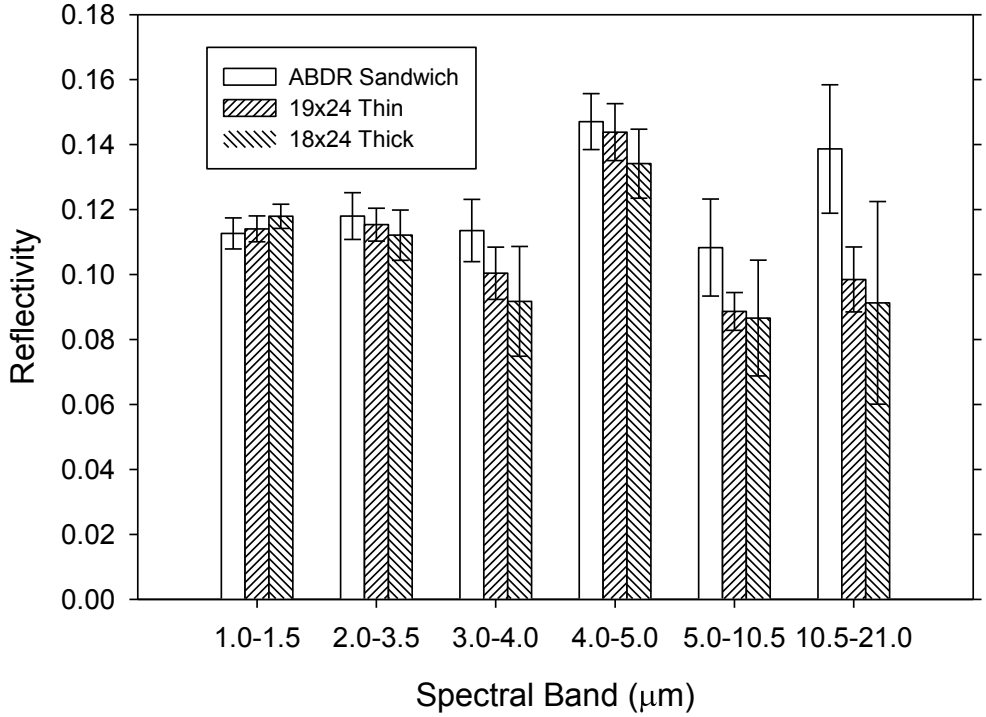


**Figure 99. Reflectometer comparison for the three panels at 20 degrees.**

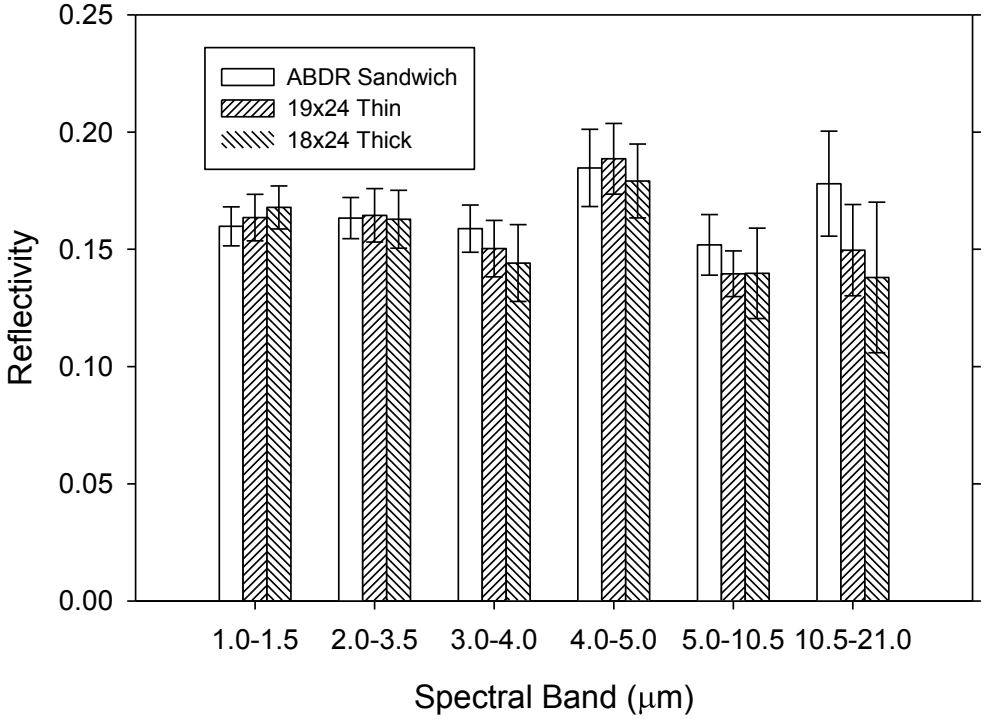


**Figure 100. Reflectometer comparison for the three panels at 60 degrees.**

A more significant comparison may be between panels with significantly different binders. The bismaleimide resin is also a common resin used in aviation transportation vehicles, and may be distinguishable by these methods. Other resins also exist. The value of an ability to distinguish parts by their spectral band reflectivity is in the ability to take an unknown part that visibly appears similar to a known part and to discriminate between the parts. We presently have a significant quantity of unknown materials, and could benefit from a simple method to classify the material. Data from this test series were used in a separate study with more material types to see if the reflectometer could be used to discriminate composite materials. This primary hypothesis failed, but there were interesting findings relating to the optical and spectral analysis of aviation composites (see Brown, 2013 for more detail).

### 3.4.6 Model Validation Challenges

One of the objectives of this work was to create a dataset that might be useful for future model validation work. There is an extent to which this work succeeded at that goal. There is also a degree to which the dataset will be found to be less than ideal. One challenge to this goal was that at the time the tests were being performed, there was not any known existing model that could adequately describe the dynamics of the test. Some models exist

for composite behavior in fire that include devolatilization, swelling, and surface reactions. Some models have been presented for thermal reactions combined with structural response. But the combination of fidelity between the two types of models has not been seen in any work discovered in the open literature. We did not have access to a model with fidelity of sufficient detail to provide much insight into the outcome of these tests. Efforts are underway to achieve improved modeling capabilities, but at the time at which the tests were being conducted the capabilities were still too immature to provide much insight. Because of a lack of maturity, modeling was not available to provide guidance to the test design effort.

Some positive aspects of this test series include the fact that there are a lot of conditions and types of panels with quality and repeatable data. Detailed modeling should be able to discriminate by panel type, and there were three types of panels with significantly different behavior for each panel type. A model that is able to capture the four hour and beyond resilience of the 18x24 thick panels, while correctly predicting the approximately one hour burn-through of the 19x24 thin panels without calibration parameters will be a good indication that modeling has reached maturity. This finding is expected to be difficult to replicate with the models, especially since at present the explanation for these differences is not obvious to the authors. The fact that this behavior is fairly repeatable lends confidence to the dataset and to the use of it as a comparison metric. There are other ways in which these tests are quite repeatable. Times at which flaming, smoking and movements occur were repeatable to a certain degree, and these can be also used as excellent target metrics for model validation. Some of the reaction rate data were also fairly repeatable. Another significant positive is that there should be enough data to make a detailed comparison for many points of interest during each test. This means that when making comparisons, the metric can include not just flaming time and reaction rate, but also radiometer readings as a function of time on both sides of the panel and panel motion due to imposed forces over the course of the whole test. It may thus be easier to distinguish model results that are deemed acceptable for the wrong reason from those that are acceptable because they are actually predicting the full dynamics of the test problem.

Aspects of the tests that were not particularly repeatable do not make as good of comparison points. The shape of the deforming panel in compression was not particularly repeatable. Since this feature has not yet been reported, these results are included from visual frames from video cameras in Figure 101. What may be discernable in these is that the ABDR panels under compression (Test 24 and 27) tended to separate, with the front face bending towards the heat source and the other two layers bending away. Mixed results were found from the 18x24 thick panels (Test 26 and 34), as in one case the panel wrinkled, and the other bent away from the heat source. The flaming reaction rate was also quite variable, and will be difficult to use as a comparison metric for model validation.

Test 24 at 10 min. 41 sec.:

Test 26 at 16 min. 31 sec.:

Test 27 at 5 min. 24 sec.:

Test 34 at 17 min. 17 sec.:

**Figure 101. Stills illustrating the shape of the deforming panels under compression.**

The apparent lack of consistency in the oven temperatures was not a desired feature of these tests; the steady-state oven thermocouple readings varied over about 200 °C from test to test. This lack of repeatability was somewhat surprising, as care was taken to provide a fairly constant power to the heating elements. The reason for this variability is believed to be from multiple sources. The oven boxes and the rods had finite lifetime, and were changed out periodically over the course of the tests. These changes were documented, but would require day-to-day detailed oven performance characterization to capture the variability caused by this. Rods were subject to performance degradation with time, manufacturing variability, and daily configuration. Ovens also had manufacturing variability. We suspect this to contribute partially to the findings. Another point that may not be particularly obvious at this point is that the oven thermocouples and oven temperature may be functionally related to the panel behavior. Take for example the 18x24 thick panel test in compression, Test 34. This test exhibited the lowest oven thermocouple temperatures. It also exhibited

significant bending away from the oven. Also, it can be seen that towards the end of the tests for ABDR and 19x24 panels where a hole is created that the oven temperatures drop off. Both of these are indications that the oven temperature (and consequently thermal boundary condition) was not just related to the daily variations, but also significantly influenced by the reaction of the panel. This feed-back between the thermal source and the panel response is not a desirable feature for modelers, because it creates an additional complication that may necessitate modeling the oven performance for a high-fidelity test comparison.

Our interpretation of the oven characterization can be checked by examining the radiometer and IR camera data. When a hole was fully open through the panel, the radiometer aimed ¼ of the panel height from the bottom would have a direct view to the oven. Peak flux from these openings were typically in the range of 120-160 kW/m$^2$ (see Figure 42 and Figure 67). Some obscuration with the panel back side may inhibit the radiometer from a full view of the oven in these cases. IR cameras suggest rod temperatures in the 1200-1400°C range, which can be seen in Figure 44 and Figure 69. Oven temperatures are in the range of 1000-1200°C. Black-body emission from 1000°C corresponds to about 150 kW/m$^2$, and emission from 1400°C corresponds to 440 kW/m$^2$. All this evidence can be viewed as consistent with the conclusions in regard to Figure 19, namely that the flux to the panels was oval in shape with peak flux in the range of 200-300 kW/m$^2$. The peak fluxes extracted from the analysis of the plate thermocouple data are likely higher than actual peaks, but the general magnitude is mostly consistent with the rest of the findings of the testing. IR images of the back-side of the panel also help confirm the shape of the thermal profile induced by the oven being similar to that found in Figure 15, but of higher magnitude. Even though oven characterization is not ideally represented, there should be enough information that the test results can still be used for model simulation comparison. The oven might be directly modeled using measured thermal data in a validation exercise, rather than applying directly a flux from a measurement as a boundary condition.

# 4 Conclusions

This report documents results from a composite panel decomposition test series. A unique aspect of the tests is the size of the panels tested, which is more characteristic of panel sizes that are typically found on aircraft. The tests were designed to explore the importance of structural loading on the fire behavior of decomposing composite panels. The data are presented in detail, so that they may be used in the future to help validate models for predicting this class of fire. Major findings include:

- During early phases of combustion that included flaming, some relationship was seen between the type of force imposed on the panels and the decomposition rate. This was most apparent in the 18x24 thick panels, as the tension tests were the only ones to exhibit back-side flaming that resulted in significantly higher decomposition rates.
- Panels deform differently depending on how they are loaded. The morphology of the deformation may play a role in how they react, although these tests did not find quantitative evidence.
- Two parameters governed post-flaming reaction rates. These were panel type and oven temperature. Structural loading had no discernable effect in this phase of the tests, despite the variations in deformation morphology (i.e., bending inward or outward).
- In the fire environment, a panel resists early deformation due to tension better than compression. Torsional forces imposed in these tests resulted in the earliest deformations due to the thermal environment, despite the fact that the torsional force imposed was a quarter that of the other two types of force.
- The glowing reaction rate was about a tenth of that of the flaming reaction rate for these tests.
- The ABDR sandwich panels exhibited significant flaming compared mass proportionally to the other panels, presumed to be due to the exposed edges and the flammable internal materials. The fact that the edges were not closed is an issue with these data, as most aircraft do not have exposed sandwich material edges.
- Structural force combined with fire induced motion that tended to be gradual with time given the force levels imposed in these tests, and not rapid or abrupt.
- The reflectometer provides data helpful for characterizing the radiation boundary condition for the panels.
- The three panel types tested each performed differently, suggesting that there are significant effects of panel variations (i.e., epoxy and fiber grades, lay-up, weave, etc.) on the behavior of composite panels in a fire. This dataset was not rich enough to be able to quantify these effects.

# 5 References


Bagot, K., and J. Hode, “Composite Material Fire Fighting Research,” Presentation from the ARFF Working Group, FAA presentation, 8 October, 2010.

Bai, Y.; Keller, T, 2009, “Pultruded GFRP tubes with liquid-cooling system under combined temperature and compressive loading,” Composite Structures, 90 (2), pp. 115-121.

Bai, Y.U. and Keller, T., 2009a, “Modeling of Strength Degradation for Fiber-reinforced Polymer Composites in Fire,” Journal of Composite Materials, 43 (21) pp. 2371-2385.

Boyd, S.E.; Lesko, J.J.; Case, S.W., 2007, “Compression creep rupture behavior of a glass/vinyl ester composite laminate subject to fire loading conditions,” Composites Science and Technology, 67 (15-16) pp 3187-3195.

Boyd, S.E.; Case, S.W.; Lesko, J.J., 2007a, “Compression creep rupture behavior of a glass/vinyl ester composite subject to isothermal and one-sided heat flux conditions,” Composites. Part A, Applied science and manufacturing, 38 (6) pp 1462-1472.

Brown, A.L., A.B. Dodd, and B.M. Pickett, “Enclosure Fire Tests for Understanding Aircraft Composite Fire,” Proceedings of the Sixth International Conference on Composites in Fire, CompositeLink Consultants (Limited), Newcastle upon Tyne, UK, 2011.

Brown, A.L., “Discriminating composite panels by use of a spectral reflectometer,” The 2013 ASME Summer Heat Transfer Conference, July 14-19, Minneapolis, MN, USA, 2013.

Brown, J. E., E. Braun, W. H, Twilley, “Cone Calorimeter Evaluation of the Flammability of Composite Materials,” National Bureau of Standards, NBSIR 88-3733, March 1988.

Burns, L.A., S. Feih, and A.P. Mouritz, 2010, “Compression Failure of Carbon Fiber-Epoxy Laminates in Fire,” Journal of Aircraft, 47, 2, pp. 528-533.

Cao S.; Wu Z.; Wang X., 2009, “Tensile Properties of CFRP and Hybrid FRP Composites at Elevated Temperatures,” Journal of Composite Materials, 43, (4), pp. 315-330.

Chelliah, H.K., Makino, A., Kato, I., Araki, N., and Law, C.K., (1996), "Modeling of Graphite Oxidation in a Stagnation-Point Flow Field Using Detailed Homogeneous and Semiglobal Heterogeneous Mechanisms with Comparisons to Experiments," Combustion and Flame, 104 pp. 469-480.

Delfa, G.L., J. Luinge, A. G. Gibson, "Next Generation Composite Aircraft Fuselage Materials under Post-crash Fire Conditions," Engineering Against Fracture: Proceedings of the 1st Conference, 2009, pp. 169-181.

Elmughrabi, A.E., M. Robinson, and A.G. Gibson, "Effect of stress on the fire reaction properties of polymer composite laminates," Polymer Degradation and Stability, 93, 1877-1883, 2008.

Fanucci, J.P., "Thermal Response of Radiantly Heated Kevlar and Graphite/Epoxy Composites," Journal of Composite Materials, Vol 21, 1987, p129-139.

Feih, S.; Mathys, Z.; Gibson, A.G.; Mouritz, A.P., 2008, "Modeling Compressive Skin Failure of Sandwich Composites in Fire," Journal of Sandwich Structures and Materials, 10(3), pp. 217-245.

Feih, S.; Mathys, Z.; Gibson, A.G.; Mouritz, A.P., 2008a, "Modelling the compression strength of polymer laminates in fire," Composites. Part A, Applied science and manufacturing, 38(11), pp.2354-2365.

Feih, S. ; Mouritz, A.P.; Mathys, Z.; Gibson, A.G., 2007, "Tensile Strength Modeling of Glass Fiber-Polymer Composites in Fire," Journal of Composite Materials, 41, 19, 2387-2410.

Gibson, A.G., Wright, P.N.H., Wu, Y.-S., Mouritz, A.P., Mathys, Z., and Gardner, C.P., 2004, "The integrity of polymer composites during and after fire," Journal of composite materials 38 (15) pp. 1283-1307.

Hubbard, J.A., A.L. Brown, A.B. Dodd, S. Gomez-Vasquez, and C.J. Ramirez, "Aircraft carbon fiber composite characterization in adverse thermal environments: radiant heat and piloted ignition flame spread," Sandia Report SAND2011-2833.

Incropera, F.P., and D.P DeWitt, "Introduction to heat transfer, 2nd ed.," John Wiley & Sons, 1990.

Jiang, G., S. J. Pickering, G. S. Walker, N. Bowering, K.H.Wong, C. D. Rudd, "Soft ionisation analysis of evolved gases for oxidative decomposition of an epoxy resin/carbon fibre composite," Thermochimica Acta V., 454, 2007, pp. 109-115.

Kawai, M., S. Yajima, A. Hachinohe, and Y. Takano, 2001, "Off-Axis Fatigue Behavior of Unidirectional Carbon Fibre-Reinforced Composites at Room and High Temperatures," Journal of Composite Materials, 35: 545-576.

Kawai, M., J.Q. Zhang, S. Saito, Y. Xiao, and H. Hatta, 2009, "Tension–Compression Asymmetry in the Off-Axis Nonlinear Rate-Dependent Behavior of a Unidirectional Carbon/Epoxy Laminate at High Temperature and Incorporation into Viscoplasticity Modeling," Advanced Composite Materials 18, 265-285.

Kandare, E.; Kandola, B.K.; Myler, P.; Edwards, G.; 2010, "Thermo-mechanical Responses of Fiber-reinforced Epoxy Composites Exposed to High Temperature Environments. Part I: Experimental Data Acquisition," Journal of Composite Materials, 44, 26, pp. 3093-3114.

Keller, T.; Bai, Y.; 2010, "Structural Performance of FRP Composites in Fire," Advances in Structural Engineering, 15, (5), pp. 793-804.

Kwon, S. W.; Smith, W.L.; Lee S.W.; 2006, "Thermo-viscoplastic modeling of composites exposed to fire or high temperature," Journal of composite materials, 40 (18), pp. 16-7-1624.

La Delfa G.; Luinge, J.; Gibson, A. G.; 2009, "Next Generation Composite Aircraft Fuselage Materials under Post-crash Fire Conditions," Engineering Against Fracture, 169-181.

Levchik, S. and E. D. Weil, "Review: Thermal decomposition, combustion and flame-retardancy of epoxy resins- a review of the recent literature," Polymer International, V. 53, 2004 p. 1901-1029.

Liu L.; Holmes J. W.; 2007, "Experimental investigation of the buckling of polymeric composites during simultaneous high heat flux exposure and compressive loading," Journal of Composite Materials, 41 (2) pp. 221-241.

Liu, J.; Zhou, Z.; Ma, L.; Xiong, J.; Wu, L.; 2011, "Temperature effects on the strength and crushing behavior of carbon fiber composite truss sandwich cores," Composites: Part B, 42, 1860-1866.

Lopez de Santiago, I., I. Saez de Ocariz Granja, A. Arbildi Fernandez, F. Fernandez Sanchez, A. Cortes Rueda, and K. Fernandez Horcajo, "Fire Penetration in a Aircraft Made in Composite," from the International Congress: Combustion and Fire Dynamics, Univeridad de Cantabria, Santander, Spain, 20-23 October, 2010, pp. 389-407.

Lua, J., 2011, “Hybrid Progressive Damage Prediction Model for Loaded Marine Sandwich Composite Structures Subjected to a Fire,” Fire Technology, 47, 851-885.

Makino, A., T. Namikiri, and K. Kimura, “Combustion rates of graphite rods in the forward stagnation field with high-temperature airflow,” Combustion and Flame 132, pp. 643-753, 2003.

Mouritz, A. P., “Fire Safety of Advanced Composites for Aircraft,” ATSB Research and Analysis Report B2004/0046, Australian Transport Safety Bureau, April 2006. ISBN 1 1921092432.

Mouritz, A.P.; Feih, S.; Kandare, E.; Mathys, Z.; Gibson, A.G.; Des Jardin, P.E.; Case, S.W.; Lattimer, B.Y., 2009, “Review of fire structural modeling of polymer composites,” Composites: Part A, 40, pp. 1800-1814.

Quintiere, J.G., Walters, R. N. and Crowley, S., “Flammability Properties of Aircraft Carbon-Fiber Structural Composite,” 2007, U.S. Department of Transportation, Federal Aviation Administration: Washington, DC. pp. 1-34.

Siegel, R. and J.R. Howell, “Thermal Radiation Heat Transfer, Third Edition,” Taylor and Francis, Washington DC, USA, 1992.

Sorathia, U.; Beck, C.; Dapp, T.; 1993, “Residual Strength of Composites during and after Fire Exposure,” Journal of Fire Sciences, 11, pp. 255-270.

Suo-Anttila, J.M. and Gritzo, L.A., “Thermal Measurements from a Series of Tests with a Large Cylindrical Calorimeter on the Leeward Edge of a JP-8 Pool Fire in Cross-Flow,” Sandia report SAND 2001-1986, July 2001.

Tyson, J.H., J. Childress, J.S. Fontenot, G.L. Wildman, “Carrier-Deck Fire Response of Graphite Epoxy Composite Materials,” NWC Technical Publication 6713, Naval Weapons Center, China Lake, CA, May 1986.

# 6 Appendix

## *6.1 Detailed Oven Characterization*

The raw thermocouple traces from the plate as described in Section 2.4.3 are plotted in Figure 102 through Figure 106. These raw readings were used to deduce the fluxes found in Figure 19. Horizontal positions (columns) were labeled with letters from A to F with A at the centerline, while vertical positions (rows) were numbered consecutively with 1 at the bottom. The oven was hottest at row 2, and showed as does the contour plot that column A has a lower temperature than column B or C. This suggests that the contours showing lower heat fluxes near the center of the panel are simply reflecting the findings of the raw experimental data. This also supports the notion that the panel distortions and the worn center of the panel lend to the finding of peak flux about ten centimeters from the center of the oven.

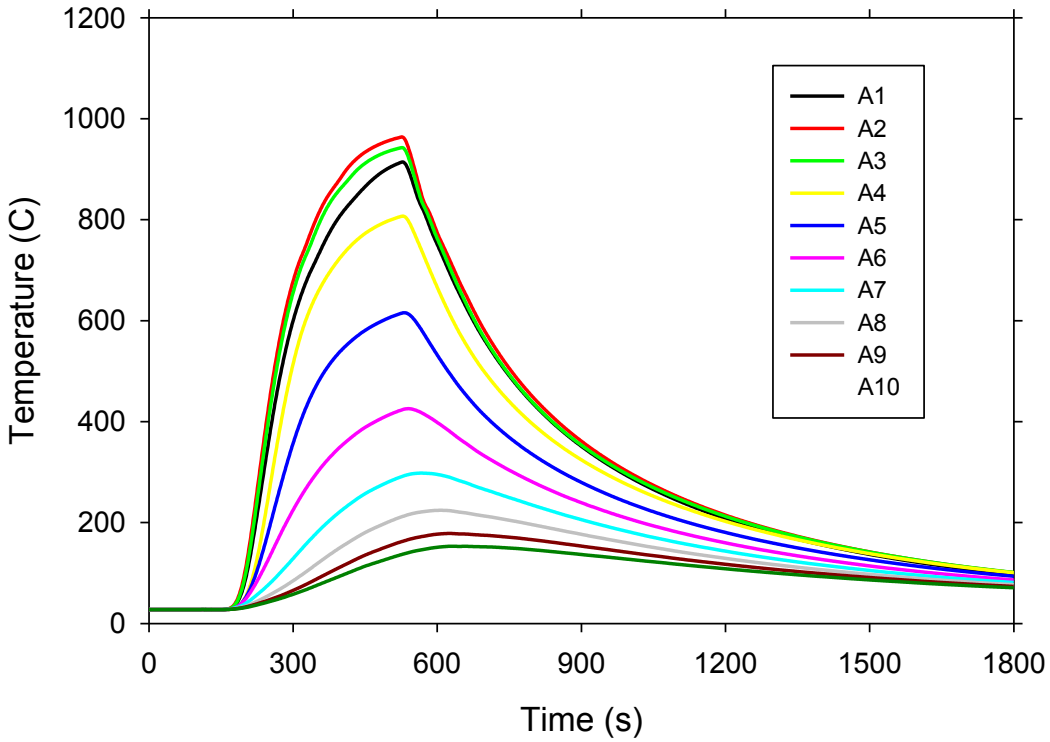


**Figure 102. Oven characterization column A temperatures.**

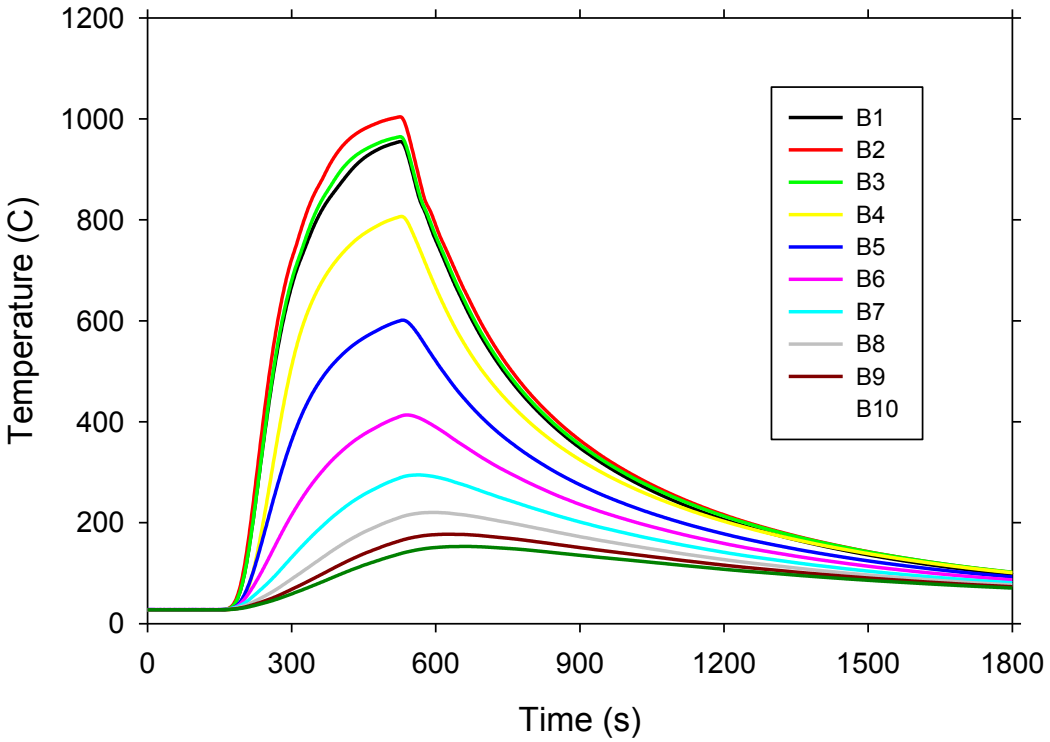


**Figure 103. Oven characterization column B temperatures.**

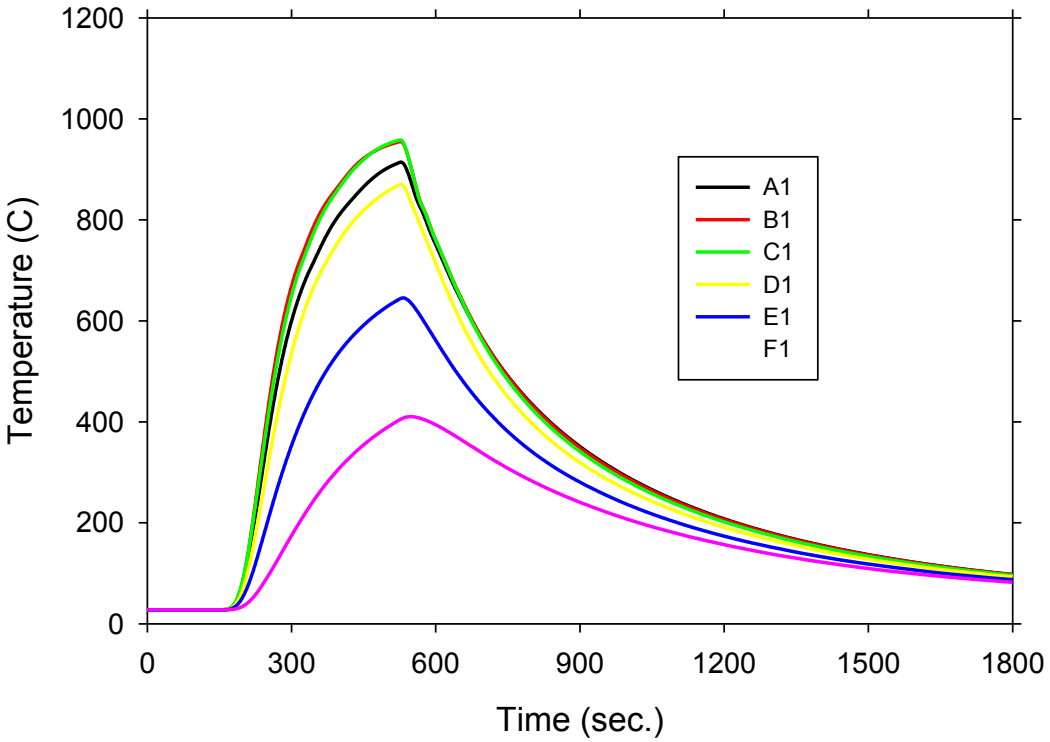


**Figure 104. Oven characterization row 1 temperatures.**

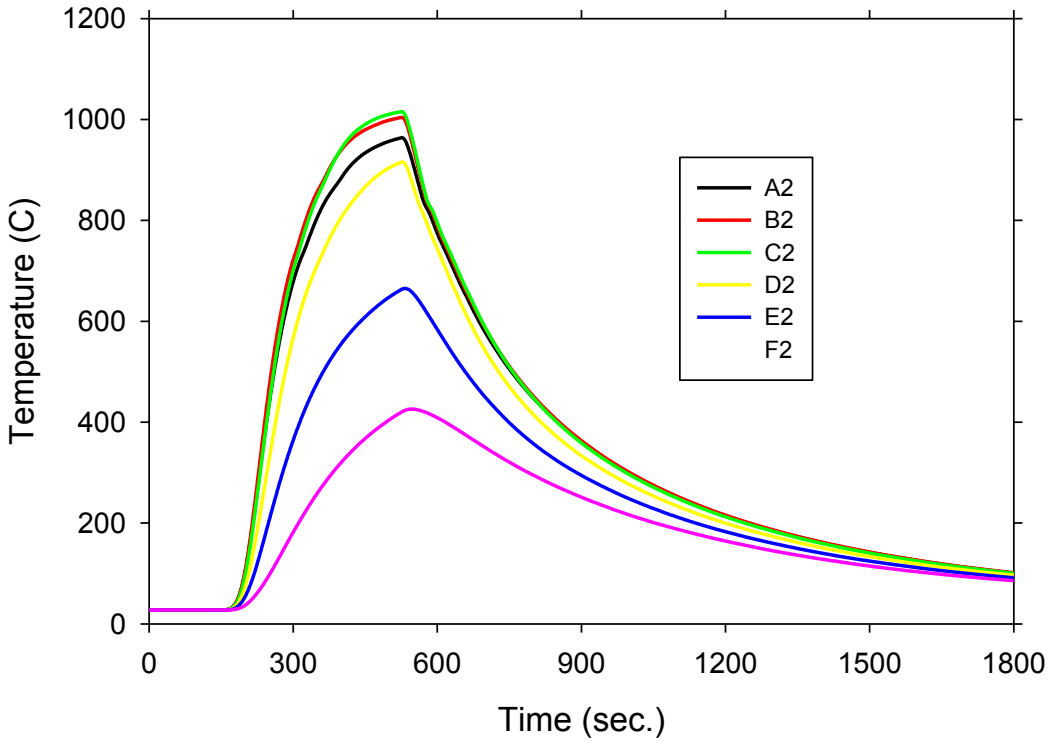


**Figure 105. Oven characterization row 2 temperatures.**

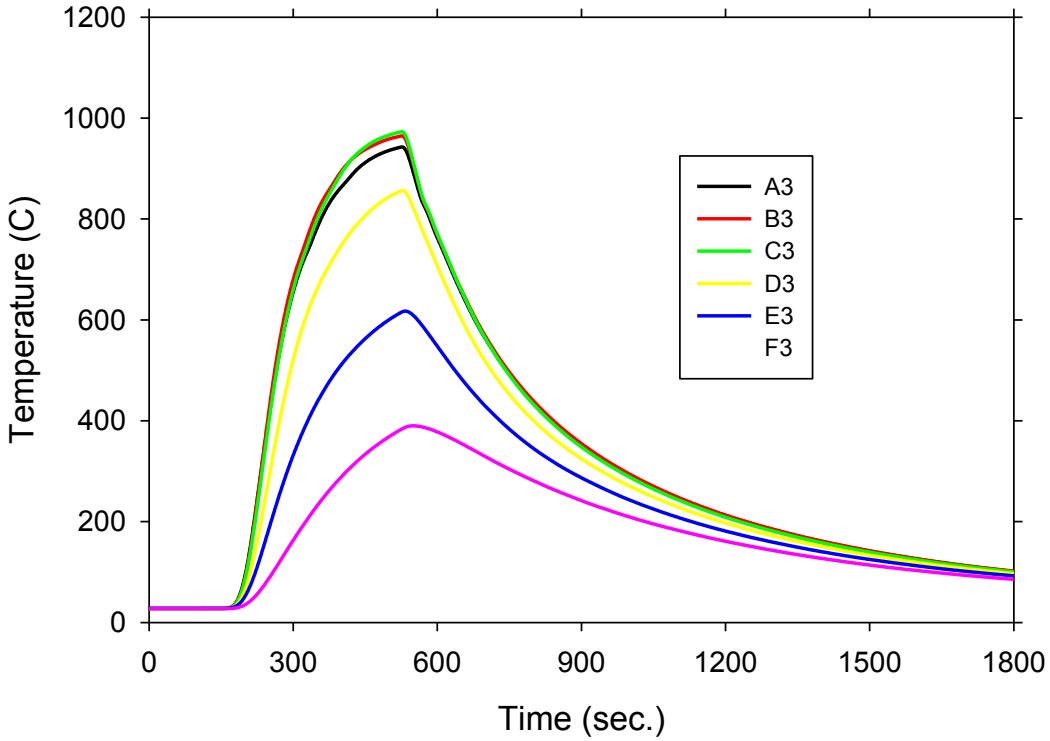


**Figure 106. Oven characterization row 3 temperatures.**

Some detailed output from the thermal model of the characterization panel are found in Figure 107 through Figure 112. Flux was averaged from 228 to 506 seconds to generate the plot found earlier in the body of the paper (Figure 19). The results plotted herein are a product of the model described previously. It can be seen that many of the thermocouple locations yielded fairly constant flux over the duration of the time where the oven was powered. Notice that for the most part, the predictions are moderately constant for the duration of the event, and that once power is turned off to the oven that the model appropriately shows flux decreasing back to ambient flux values.

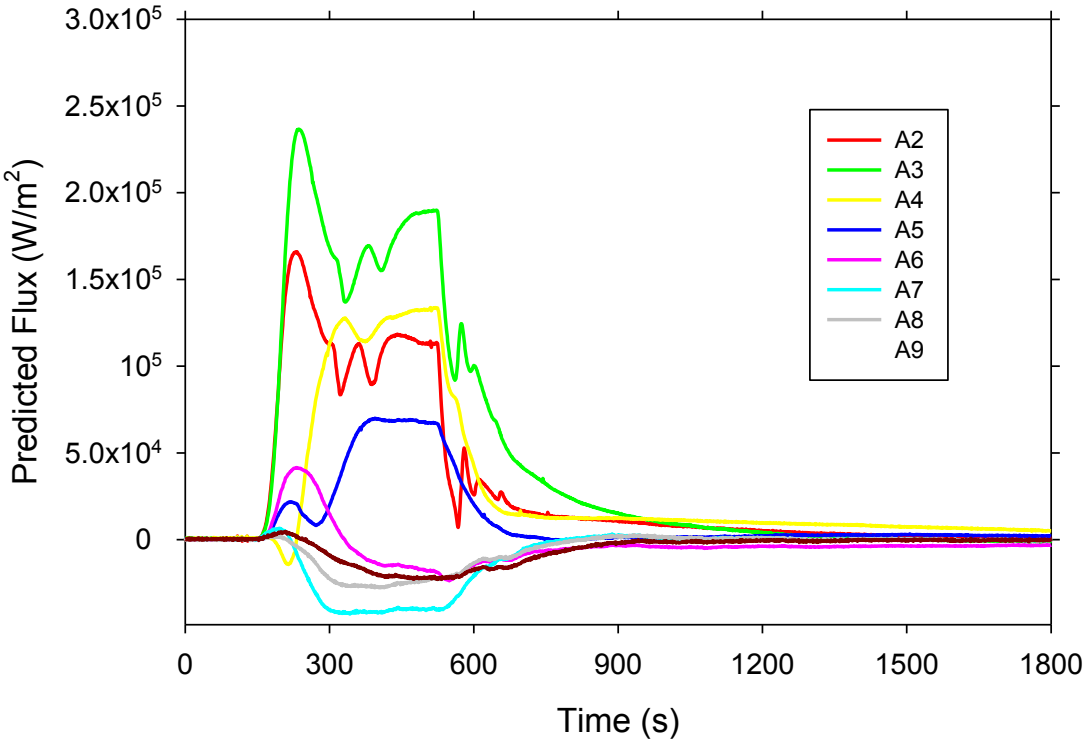


**Figure 107. Oven characterization column A fluxes.**

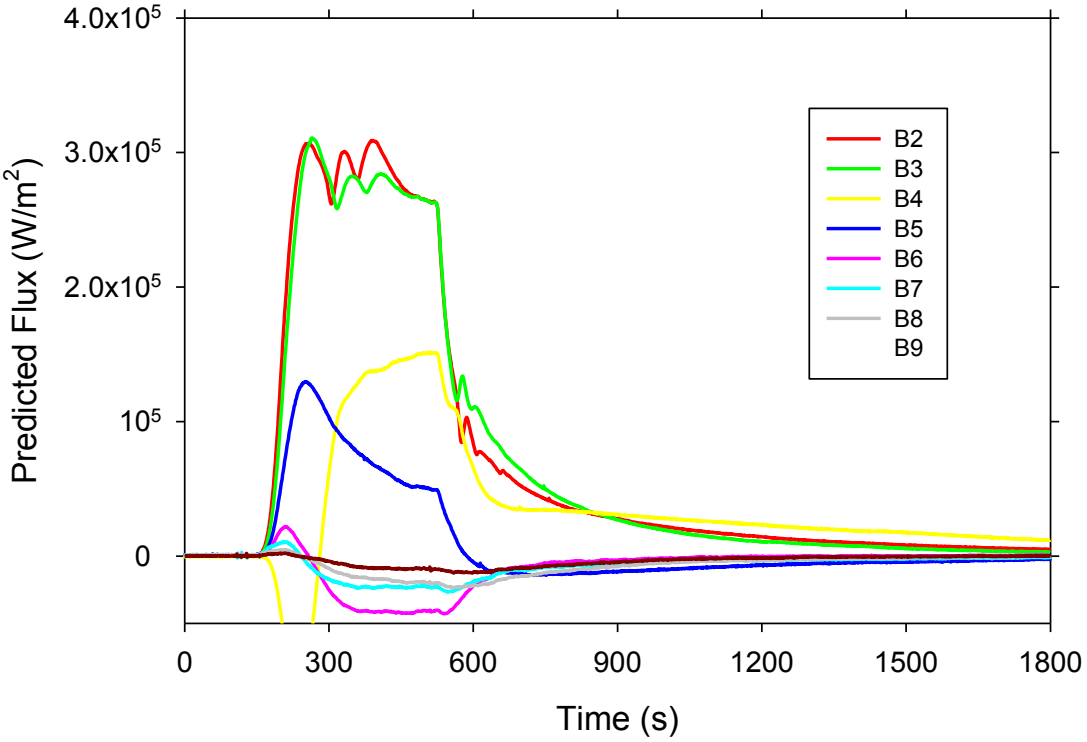


**Figure 108. Oven characterization column B fluxes.**

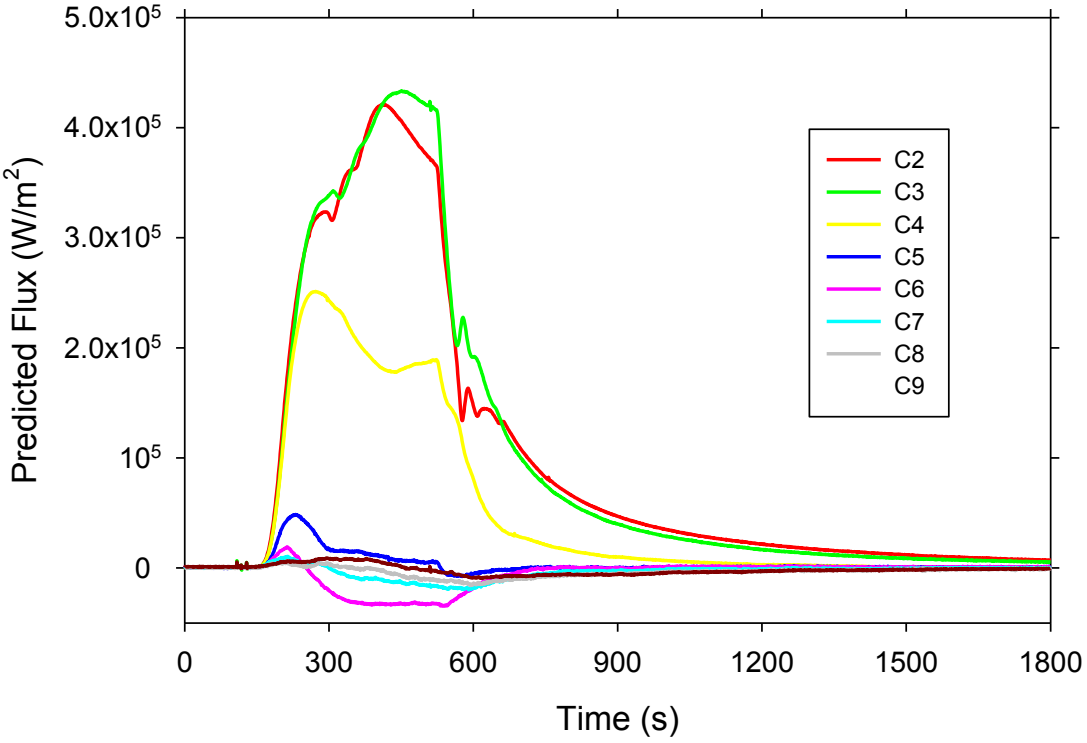


**Figure 109. Oven characterization column C fluxes.**

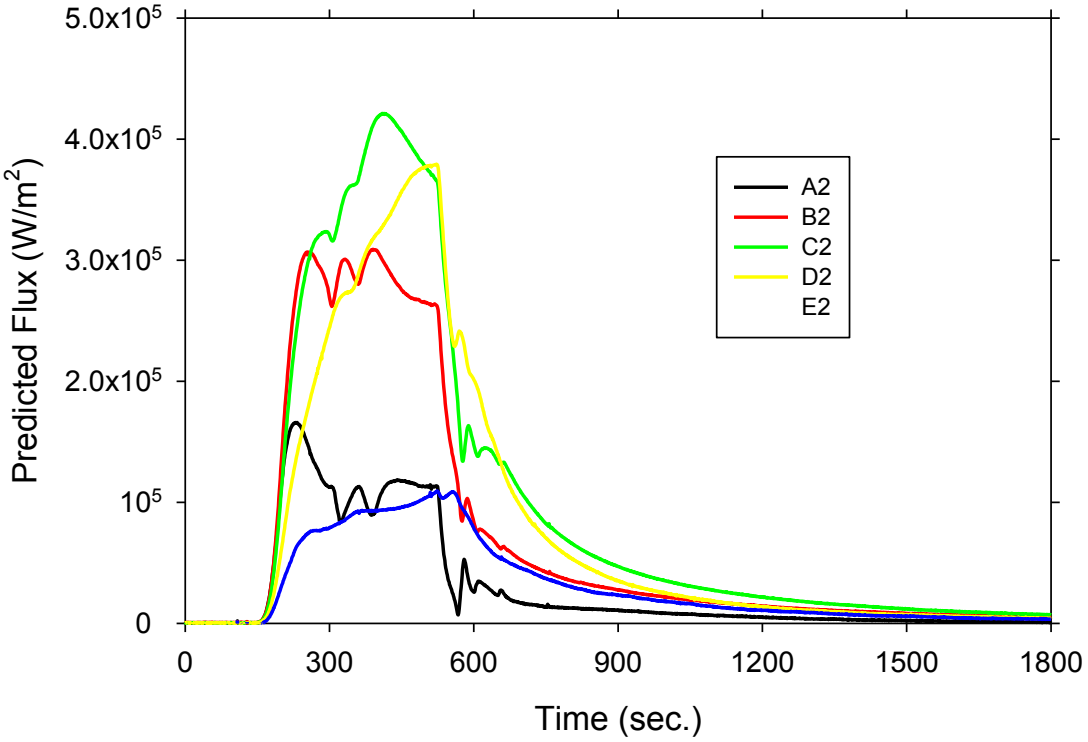


**Figure 110. Oven characterization row 2 fluxes.**

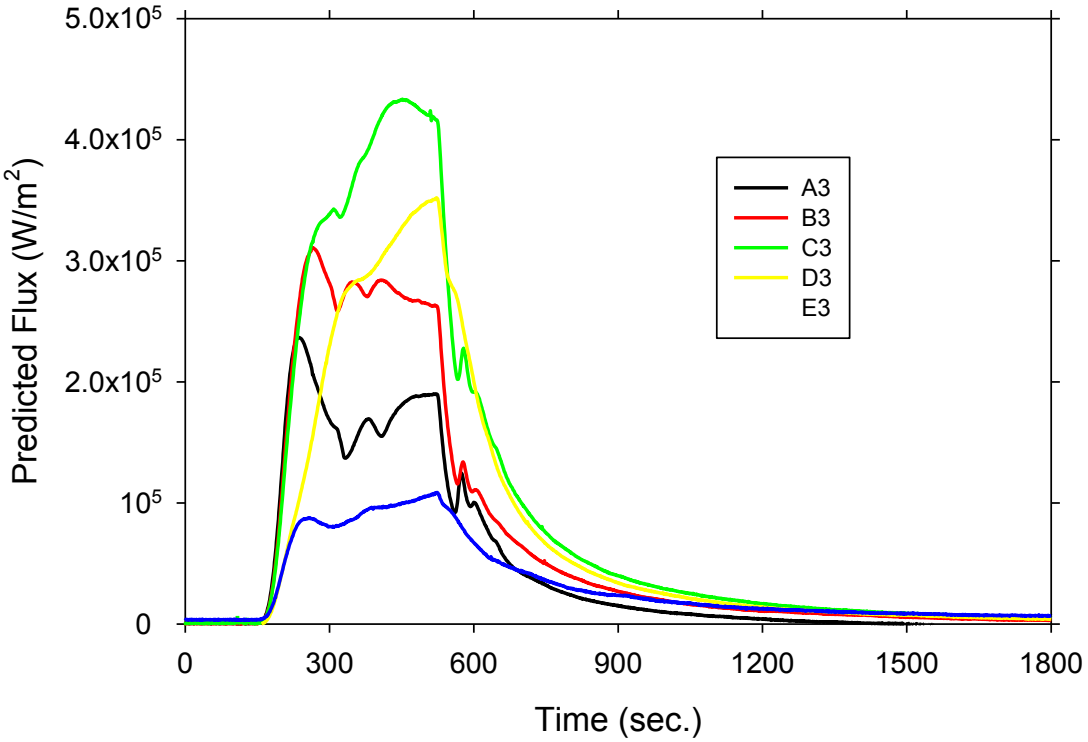


**Figure 111. Oven characterization row 3 fluxes.**

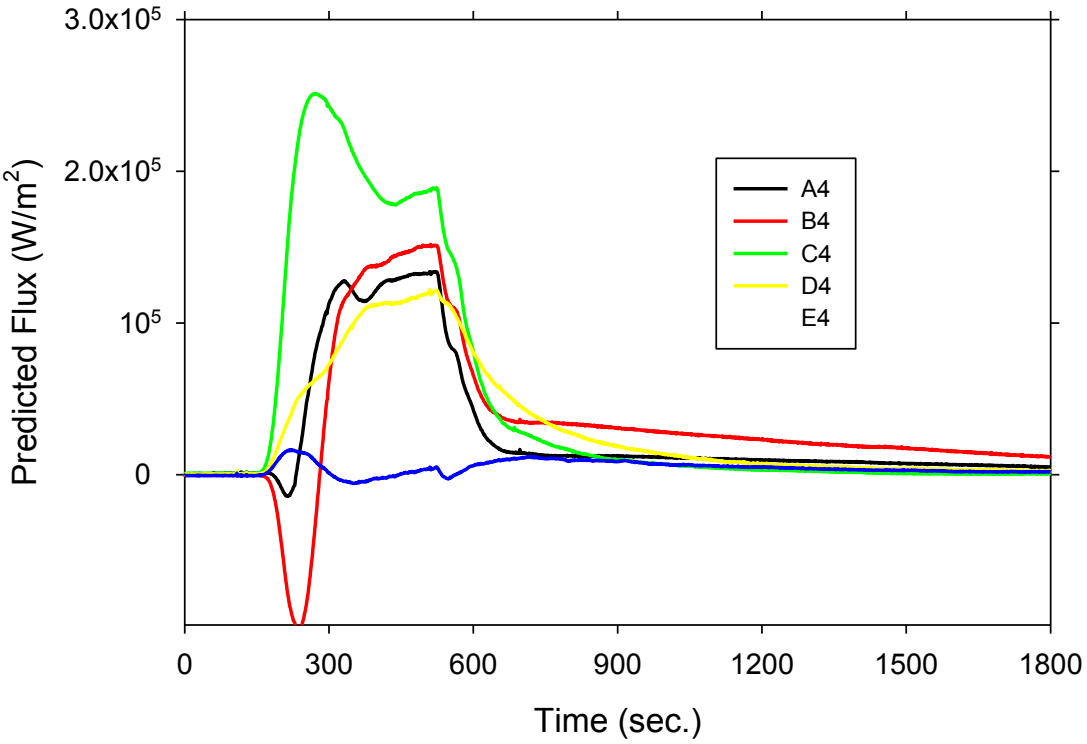


**Figure 112. Oven characterization row 4 fluxes.**

The model used to interpret these data provides a break-down of flux by mechanism. A detailed break-down of total flux by selected locations has been plotted, and these are found in Figure 113 through Figure 115. During heat-up, the sensible flux is high as the energy going into the panel is stored. Once power is turned off, it gives up the energy. Energy lost to radiation emission steadily increases during the temperature increase, and falls back afterwards. The conduction is a complex function of what neighboring material temperatures are, and exhibits less regular behavior. With the dynamics occurring in each sub-element class of flux, it is amazing how well the total flux appears to be flat over the duration of the test given the curved nature of the constituency fluxes. This provided confidence that the model had considered appropriately the important transport phenomena.

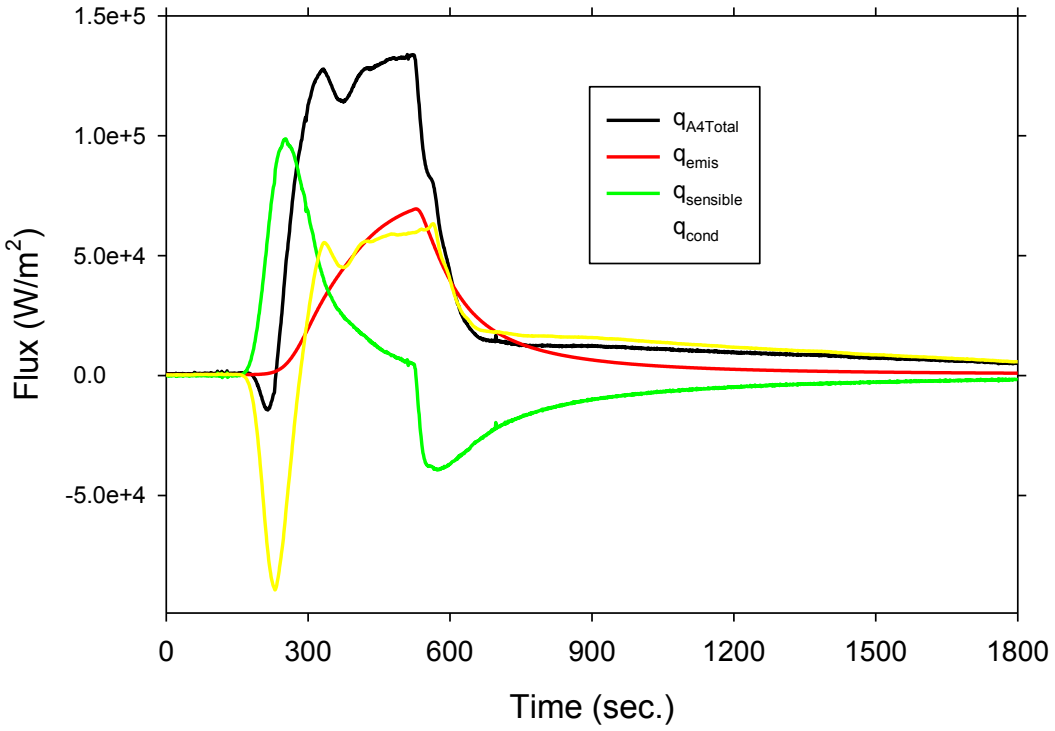


**Figure 113. Oven characterization A4 fluxes.**

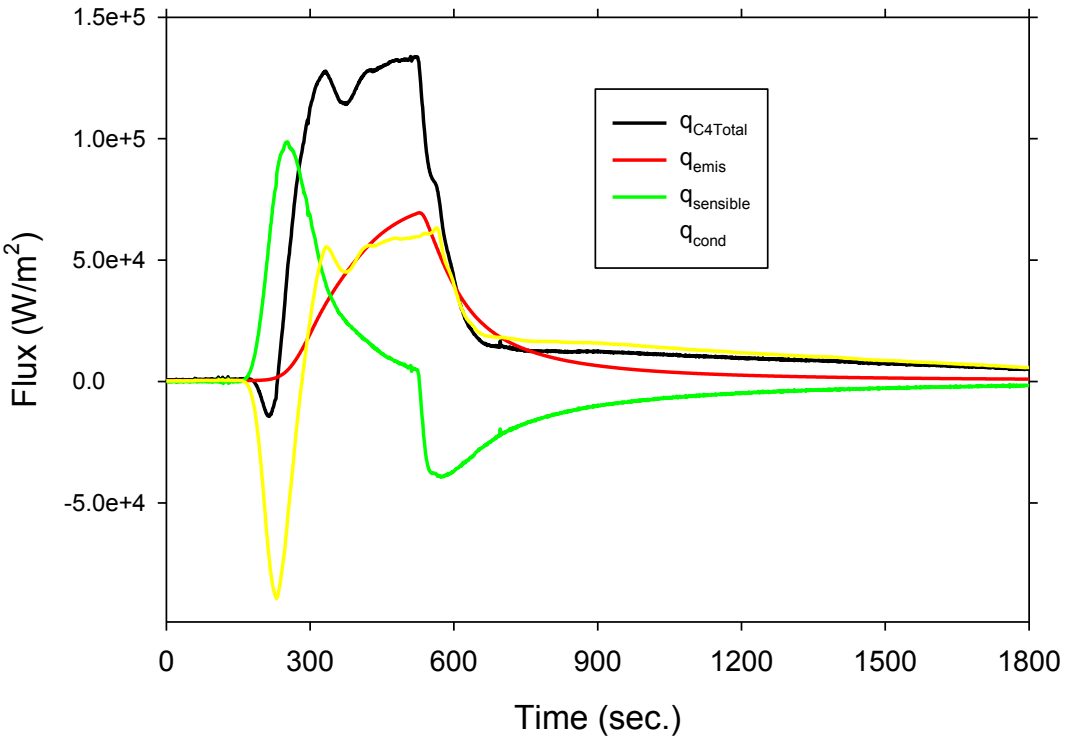


**Figure 114. Oven characterization C4 fluxes.**

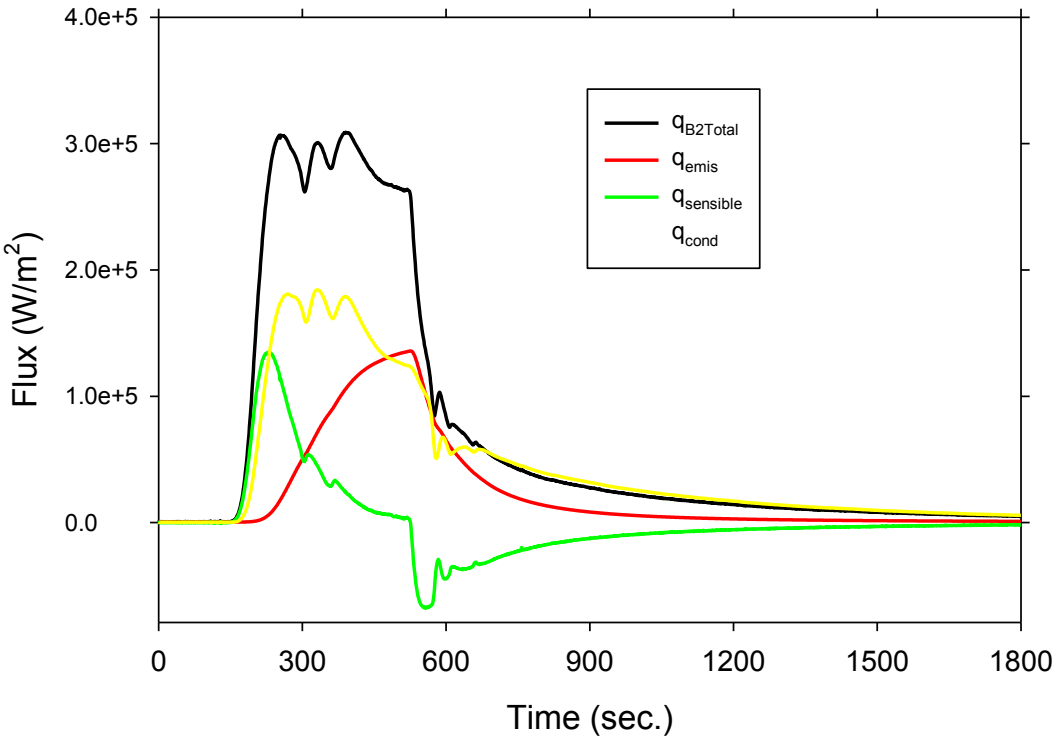


**Figure 115. Oven characterization B2 fluxes.**

## *6.2 Unused Heat Source Characterization*

In addition to the oven, two other heat sources were tested. These provided significant results, and resulted in the wear on the thermocouple plate. The details of the characterization are not presented herein, but there are two figures showing the burners shown in Figure 116 and Figure 117. They had several issues. One was that it is difficult at a significant burn rate to maintain a constant propane delivery rate. The other was that the oxygen as measured by a residual gas analyzer at the hot points was close to zero.

Notwithstanding the lack of oxygen and difficulty maintaining consistent flow for the propane burners, they were tested for performance. A thin wood panel pre-test took over an hour to burn through with the pipe burner. This was believed to be due to the insulative char layer formed and lack of oxidative reactions near this formed layer. Since wood consumes faster than composite generally speaking, the propane based burners were abandoned in favor of the oven that was detailed in the body of the report.

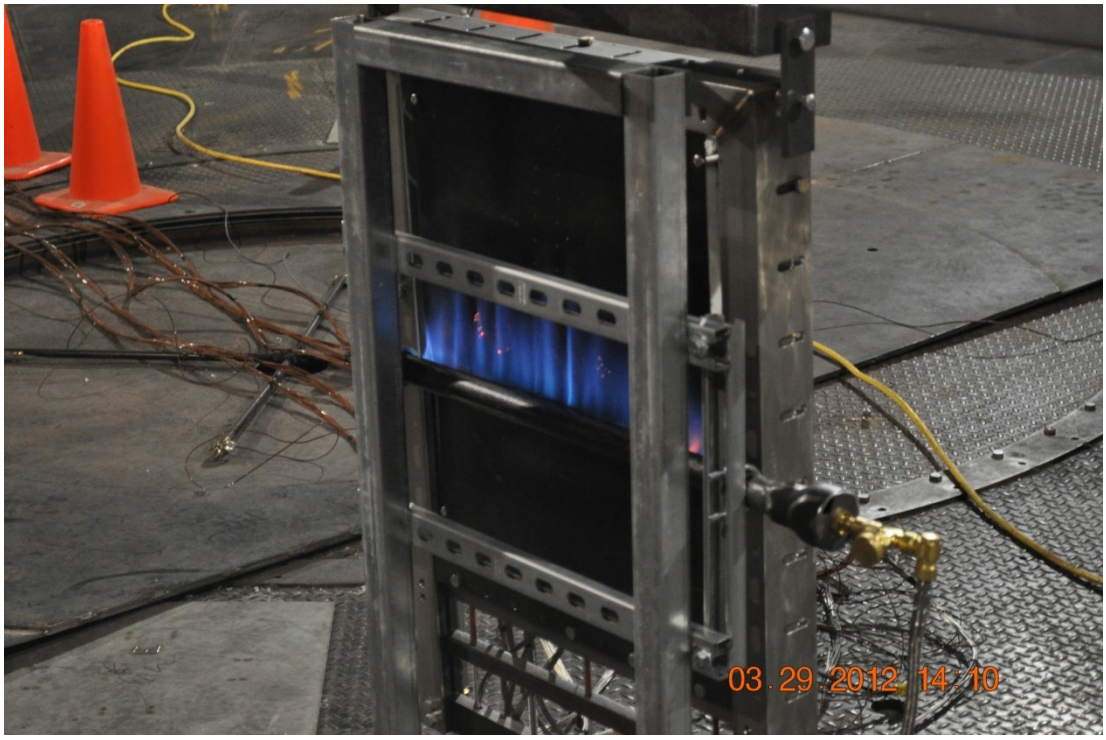


**Figure 116. A photograph of the pipe burner.**


**Figure 117. A photograph of the weed burner.**

## 6.3 Wood Pre-tests

Many of the pre-tests not fully documented herein were tests of wood panels, the purpose of which was to work out issues with the test system as a whole. In many cases, the data from these tests was not useful because the mass loss measurements were compromised by the panel touching the oven, or the frame impacting the ground. Three wood panel tests were successfully performed, and are reported here. Test 23 and 28 were with a mass-mock OSB panel for the ABDR sandwich panels. Test 36 was a mass mock for the 18x24 thick panels. Results are plotted in Figure 118. The bigger panel took longer to burn, but in none of these cases were burn times close to those of the composites.

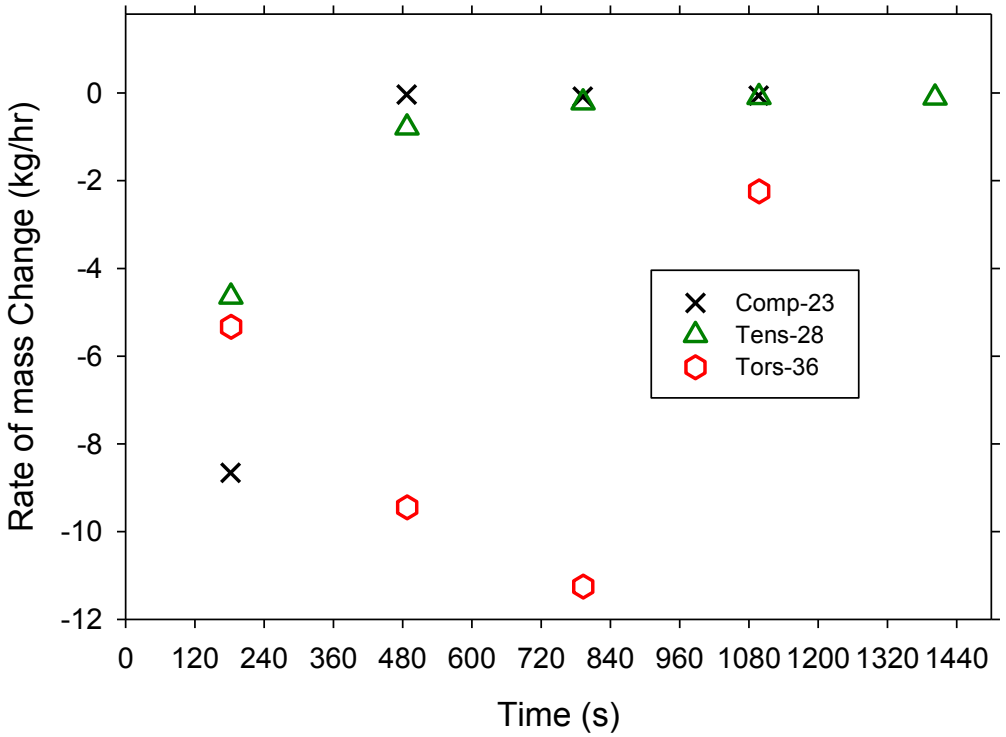


**Figure 118. Rate of mass change summary data for the OSB wood panels.**

Oven temperature data are plotted in Figure 119. Radiometer data are found plotted in Figure 120 through Figure 125. These are plotted for comparison to the composite data. Fluxes were generally higher for the wood, as the wood tended to burn with flames more readily than the composites.

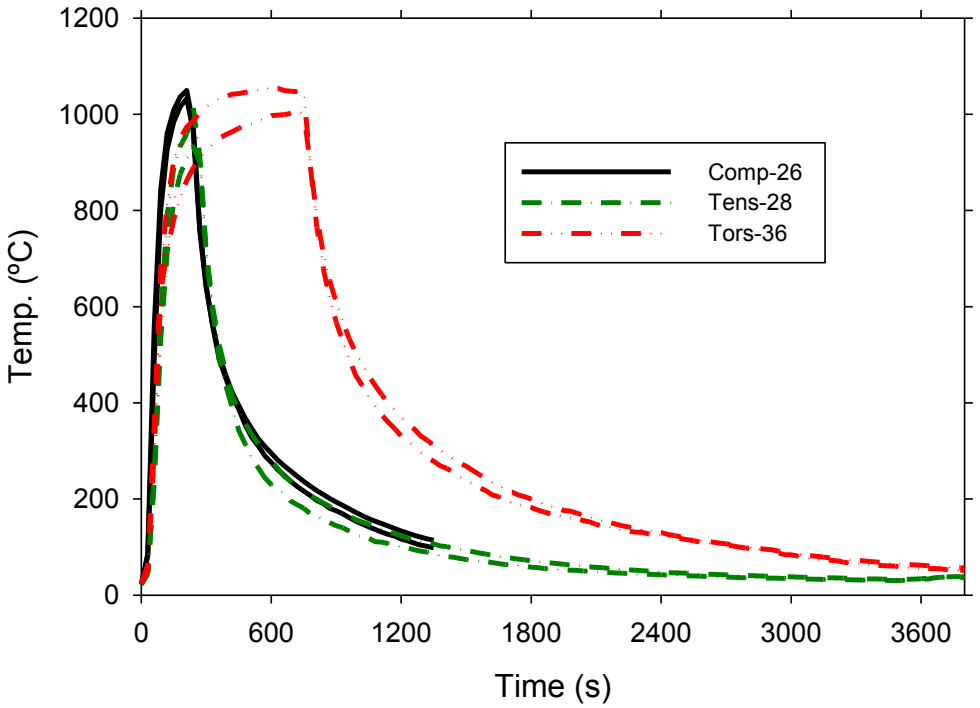


**Figure 119. Oven temperatures for the OSB wood panel tests.**

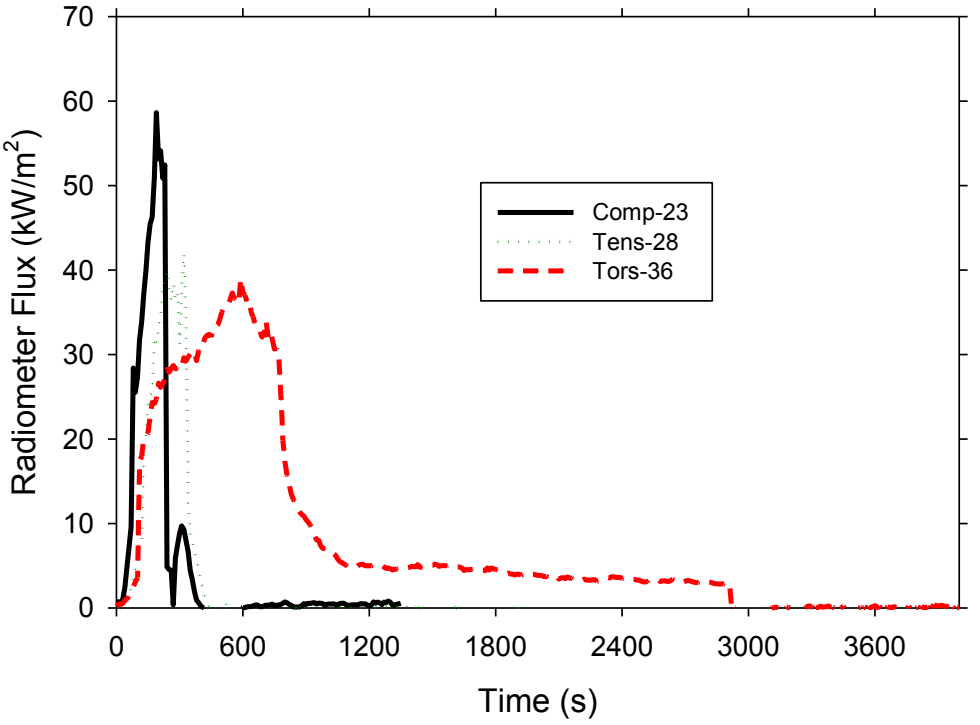


**Figure 120. Wood panel radiometer readings from the front of the panel at 0.5 from the bottom.**

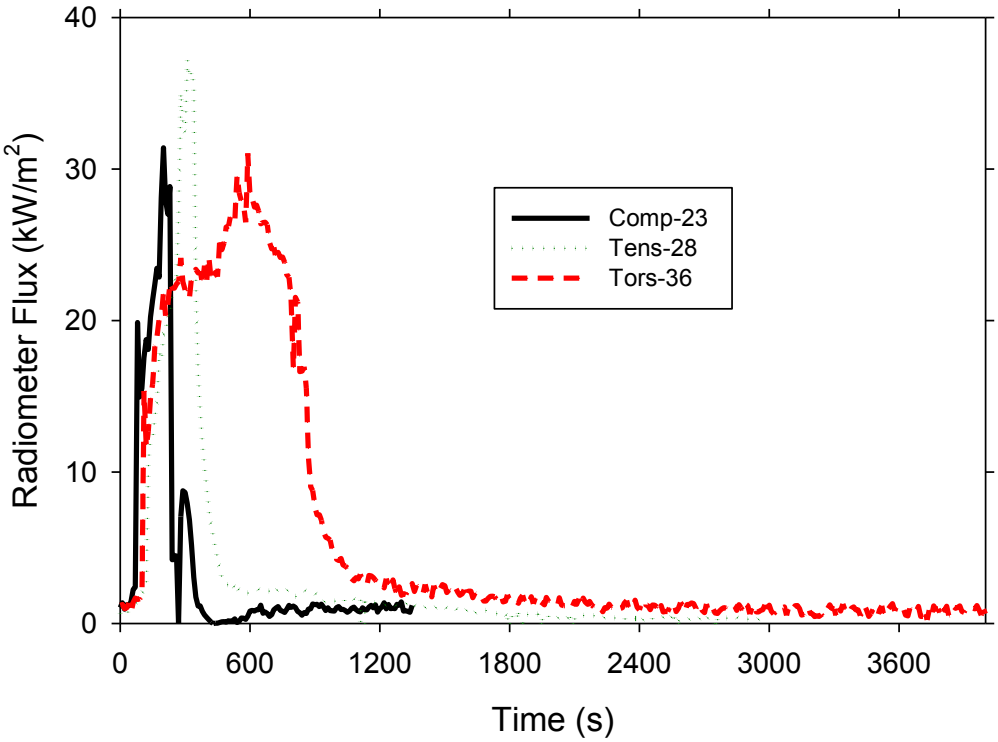


**Figure 121. Wood panel radiometer readings from the front of the panel at 0.75 from the bottom.**

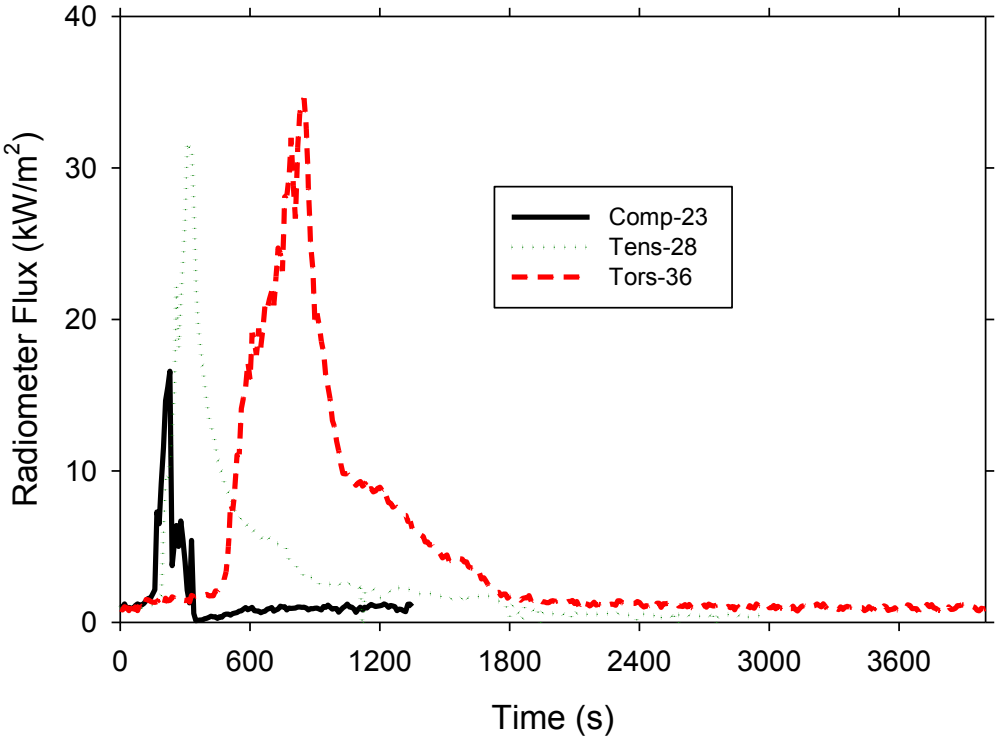


**Figure 122. Wood panel radiometer readings from the back of the panel at 0.75 from the bottom.**

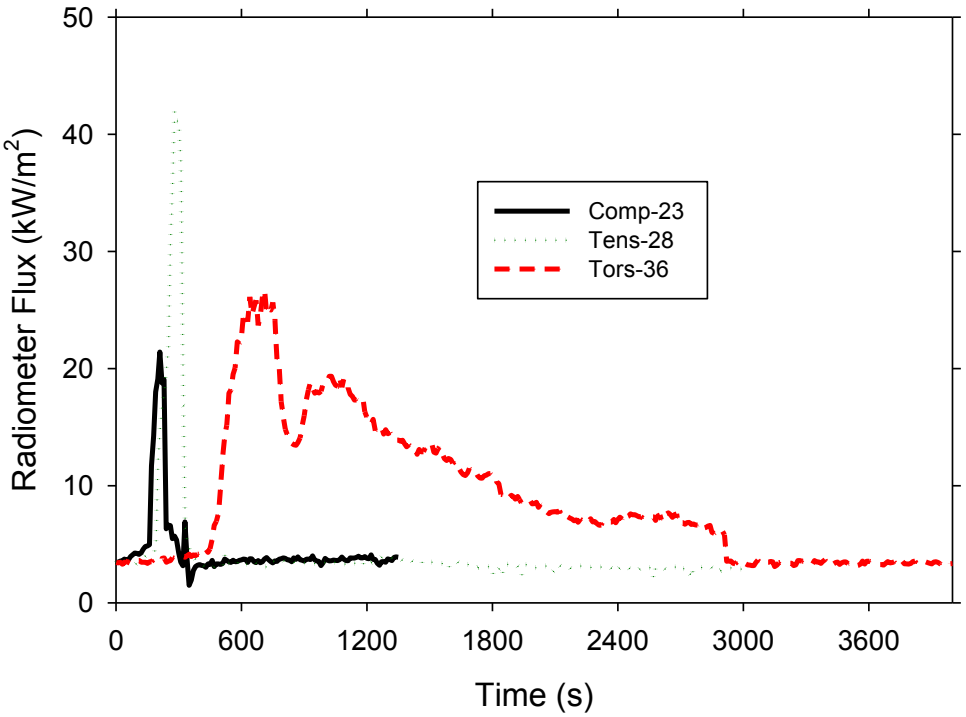


**Figure 123. Wood panel radiometer readings from the back of the panel at 0.5 from the bottom.**

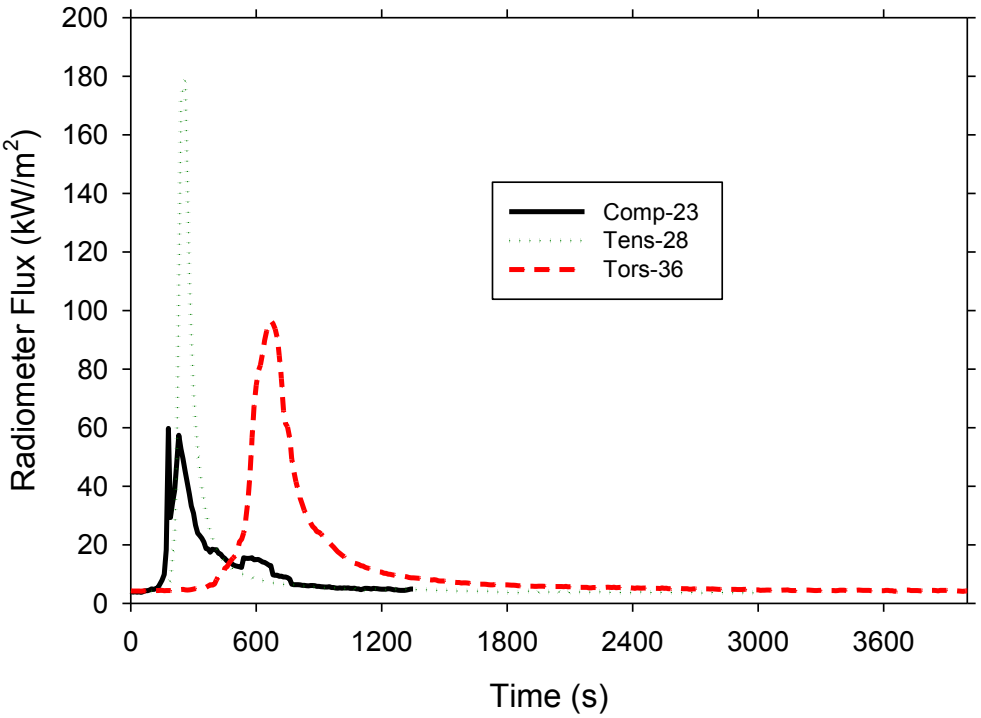


**Figure 124. Wood panel radiometer readings from the back of the panel at 0.25 from the bottom.**

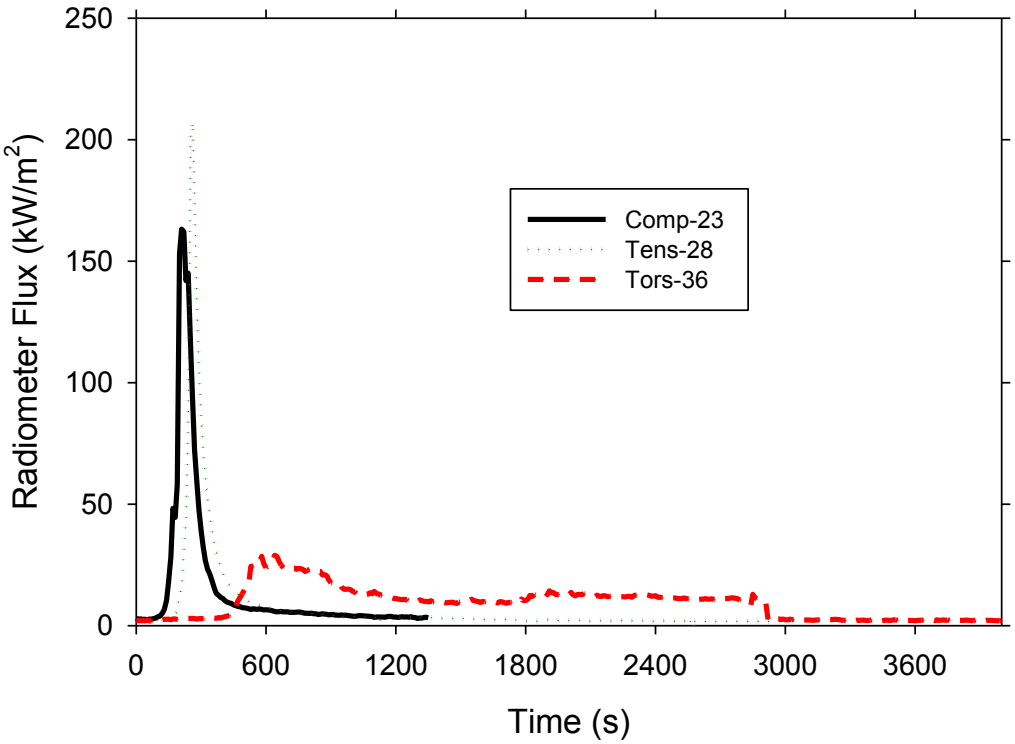


**Figure 125. Wood panel radiometer readings from the back of the panel offset at 0.25 from the bottom.**

## Distribution

1 MS 0899 RIM-Reports Management, 9532 (electronic copy)